STRATEGIES FOR HYDRAULIC FRACTURING IN NATURALLY FRACTURED SHALE GAS RESERVOIR

Ms. Duangkamon Jordnork

A Thesis Submitted in Partial Fulfillment of the Requirements
for the Degree of Master of Engineering Program in Petroleum Engineering
Department of Mining and Petroleum Engineering
Faculty of Engineering
Chulalongkorn University
Academic Year 2013

กลยุทธ์ในการทำไฮดรอลิคแฟรคเจอริงในแหล่งกักเก็บก๊าซธรรมชาติในหินดินดาน ที่มีรอยแยกตามธรรมชาติ

นางสาวดวงกมล จอดนอก

วิทยานิพนธ์นี้เป็นส่วนหนึ่งของการศึกษาตามหลักสูตรปริญญาวิศวกรรมศาสตรมหาบัณฑิต

สาขาวิชาวิศวกรรมปิโตรเลียม ภาควิชาวิศวกรรมเหมืองแร่และปิโตรเลียม

คณะวิศวกรรมศาสตร์ จุฬาลงกรณ์มหาวิทยาลัย

ปีการศึกษา 2556

Thesis Title	STRATEGIES FOR HYDRAULIC FRACTURING IN NATURALLY FRACTURED SHALE GAS RESERVOIR
By	Ms. Duangkamon Jordnork
Field of Study	Petroleum Engineering
Thesis Advisor	Assistant Professor Jirawat Chewaroungroaj, Ph.D.
Thesis Co-advisor	Kreangkrai Maneeintr, Ph.D.

Accepted by the Faculty of Engineering, Chulalongkorn University in Partial Fulfillment of the Requirements for the Master's Degree

…….....Dean of the Faculty of Engineering
(Professor Bundhit Eua-Arporn, Ph.D.)

THESIS COMMITTEE

.....…….. .Chairman
(Associate Professor Sarithdej Pathanasethpong)

…….…….....Thesis Advisor
(Assistant Professor Jirawat Chewaroungroaj, Ph.D.)

…….....Thesis Co-Advisor
(Kreangkrai Maneeintr, Ph.D.)

....…….....External Examiner
(Siree Nasakul, Ph.D.)

ดวงกมล จอดนอก: กลยุทธ์ในการทำไฮดรอลิคแฟรคเจอริงในแหล่งกักเก็บก๊าซธรรมชาติในหินดินดานที่มีรอยแยกตามธรรมชาติ. (STRATEGIES FOR HYDRAULIC FRACTURING IN NATURALLY FRACTURED SHALE GAS RESERVOIR) อ.ที่ปรึกษาวิทยานิพนธ์หลัก: ผศ.ดร.จิรวัฒน์ ชีวรุ่งโรจน์, อ.ที่ปรึกษาวิทยานิพนธ์ร่วม: อ.ดร.เกรียงไกร มณีอินทร์., 114 หน้า.

แหล่งกักเก็บก๊าซธรรมชาติในหินดินดานได้ดึงดูดความสนใจมากขึ้นในอุตสาหกรรมปิโตรเลียมเนื่องจากมีปริมาณสำรองของก๊าซธรรมชาติเป็นจำนวนมาก จากลักษณะของหินดินดานซึ่งมีความสามารถในการซึมผ่านน้อยมากในอัตราการวัดเป็นนาโนดาร์ซี่ ในทางทฤษฎี ก๊าซธรรมชาติไม่สามารถไหลผ่านจากแหล่งกักเก็บเข้ามาในหลุมผลิตในอัตราการผลิตที่คุ้มค่าในทางเศรษฐกิจได้ การทำไฮดรอลิคแฟรคเจอริงเป็นวิธีการกระตุ้นการผลิตที่ใช้กันอย่างแพร่หลายในปัจจุบันซึ่งคือการสร้างรอยแยกเพื่อเพิ่มช่องทางการไหลของก๊าซธรรมชาติ ทั้งนี้ทั้งนั้นก็เพื่อให้ก๊าซธรรมชาติไหลเข้ามาในหลุมผลิตได้ง่ายขึ้น และเพื่อเพิ่มอัตราการผลิต

จุดประสงค์ในการศึกษาครั้งนี้คือการออกแบบการทำไฮดรอลิคแฟรคเจอริงเพื่อเพิ่มประสิทธิภาพการผลิตโดยใช้หลุมผลิตแบบแนวนอน ตัวแปรที่มีผลกระทบต่อการผลิตและใช้ศึกษาในแบบจำลองแหล่งกักเก็บประกอบด้วย อัตราการซึมได้ของหินดินดาน, ความพรุนของหินดินดาน, ระยะห่างระหว่างรอยแยก, จำนวนรอยแยกที่สร้างขึ้นจากการทำไฮดรอลิคแฟรคเจอริง, และความกว้างของรอยแยก รูปแบบการจัดวางรอยแยกและอัตราการดูดซับไฮโดรคาร์บอนของหินดินดานรวมอยู่ในการศึกษาการวิเคราะห์ความไว

จากผลการศึกษาพบว่าความพรุนของแหล่งกักเก็บมีผลน้อยมาก แต่พบว่าอัตราการซึมได้ของหินมีผลต่อการผลิตค่อนข้างมาก จำนวนรอยแยกมีนัยสำคัญมากเช่นกันและมีความสัมพันธ์เชิงเส้น ความกว้างของรอยแยกเป็นตัวแปรสำคัญและเป็นตัวชี้วัดความสามารถในการไหลได้เป็นอย่างดี อย่างไรก็ตามความกว้างของรอยแยกมีค่าจำกัดอยู่ที่จุดจุดหนึ่งซึ่งจะไม่สามารถเพิ่มการผลิตได้มากขึ้น ก๊าซธรรมชาติจึงสามารถผลิตได้สูงสุดที่ความกว้างของรอยแยกค่านั้น ๆ การออกแบบการทำไฮดรอลิคแฟรคเจอริงในกรณีศึกษาพบว่าจำนวนรอยแยกที่สร้างขึ้นและความกว้างของรอยแยกมีผลอย่างมากต่อประสิทธิภาพการผลิตก๊าซธรรมชาติในแหล่งกักเก็บหินดินดาน

ภาควิชา วิศวกรรมเหมืองแร่และปิโตรเลียม ลายมือชื่อนิสิต.....

สาขาวิชา วิศวกรรมปิโตรเลียม ลายมือชื่ออ.ที่ปรึกษาวิทยานิพนธ์หลัก.....

ปีการศึกษา 2556 ลายมือชื่ออ.ที่ปรึกษาวิทยานิพนธ์ร่วม.....

5371603821 MAJOR PETROLEUM ENGINEERING
KEYWORDS: SHALE GAS/HYDRAULIC FRACTURING

DUANGKAMON JORDNORK. STRATEGIES FOR HYDRAULIC FRACTURING IN NATURALLY FRACTURED SHALE GAS RESERVOIR. ADVISOR: ASST. PROF. JIRAWAT CHEWAROUNGROAJ, Ph.D., CO-ADVISOR: KREANGKRAI MANEEINTR, Ph.D., 114 pp.

Shale gas reservoirs have become more attractive for the petroleum industry because of the huge amount of reserves. Nanodarcy permeability can be characteristic of shale reservoirs. For this condition, natural gas does not flow economically from the reservoir to the wellbore. Hydraulic fracturing is a common stimulation approach to provide conductive paths through the reservoir so that the gas is allowed to flow more easily hence gas productivity can be improved.

Therefore, the objective of this study is to design the hydraulic fracturing strategies in order to improve gas productivity. A horizontal-wellbore production is utilized and the effects of several parameters on the reservoir performance are investigated. These parameters include reservoir porosity, reservoir permeability, fracture spacing, number of fractures, and fracture width. Hydraulic fracturing pattern and gas desorption are also included in sensitivity analysis.

The results of this study showed insignificant effect of reservoir porosity but are greatly influenced by reservoir permeability. Increasing the number of fractures can develop gas productivity significantly expressed in linear relationship. Fracture width is another essential factor indicating gas flow ability. However, there is certain point that fracture width cannot further enhance gas productivity. Maximum gas productivity will then be reached at that point. Both the number of fractures and fracture width are the important factors used to design hydraulic fracturing strategies to achieve significant gas productivity improvement.

Department Mining and Petroleum Engineering Student's Signature…….....…...
Field of Study Petroleum Engineering Advisor's Signature…....…….....
Academic Year 2013 Co-advisor's Signature…....…..

Acknowledgements

First of all, I would like to thank Asst. Prof. Jirawat Chewaroungroaj, my thesis advisor and Ph.D. Kreangkrai Maneeintr, my co-advisor for giving me knowledge of petroleum engineering and invaluable advices throughout my study.

Secondly, I would like to express my special thankful to faculty members in the department of Mining and Petroleum Engineering for giving me Petroleum Engineering knowledge and provide excellent suggestions. I also want to thank the thesis committee members for their comments and recommendations. That could direct me to accomplish this work.

Thirdly, I would like to thank Schlumberger for providing ECLIPSE reservoir simulation to the Department of Mining and Petroleum Engineering which was used in this study. I am sincerely grateful to Mr. Nattaphon Temkiatvises who gave me excellent instructions and great advices on the ECLIPSE software.

Fourthly, I sincerely appreciate the scholarship I received from Siam Moeco that encourages me to study hard on this program. I am also very thankful to PTT Exploration and Production for providing financial support to this study.

Eventually, I appreciate all the supports from my family members, friends and classmates for encouragements and warm supports.

Contents

Page

Page

List of Tables

Page

Page

List of Figures

Page

Page

Page

Page

Page

List of Abbreviations

BHP	Bottom Hole Pressure, psi
BSCF	Billion Standard Cubic Feet
cP	Centipoises
DEM	Discrete Element Model
lb/ft^3	Pound per cubic feet
LGR	Local Grid Refinement
mD	MilliDarcy
MMSCF	Million Standard Cubic Feet
MSCF/D	Thousand Standard Cubic Feet per Day
OGIP	Original Gas In Place
PL	Langmuir Pressure
PR	Poisson's Ratio
psi	Pounds per square inch
psia	Pounds per square inch absolute
PVT	Pressure, Volume, Temperature
PVDG	Gas PVT functions
PVTW	Water PVT functions
rb/Mscf	Reservoir barrel per thousand standard cubic feet
SCAL	Special Core Analysis
SRV	Stimulation Reservoir Volume
UF	Unstructured Fracture
VFP	Vertical Flow Performance
VL	Langmuir Volume
YMS	Young's Modulus

Nomenclatures

K_n	Knudsen number
b	Fracture half-width (mm)
b_f, w	Frature width (m)
C_{fD}	Dimensionless conductivity
Δp_1	Pressure drop in the natural fracture between intersection and position 1, psi
Δp_{nf}	Pressure drop in the natural fracture, psi
g	Acceleration due to gravity
H	Thickness or depth
h_f, X_f	Fracture half length (m)
k	Matrix permeability (Darcy, Millidarcy)
k_f	Fracture permeability (Darcy, Millidarcy)
k_{rg}	Gas relative permeability
k_{rw}	Water relative permeability
Λ	Mean free path of gas molecule
L	Length of the channel
p	Pore (reservoir) pressure (psi)
$p_i(t)$	Pressure in the fracture at the intersection with the natural fracture (psi)
p_{tip}	Pressure at fracture tip, psi
p_{wf}	Well Flowing pressure (psi)
S_g	Gas Saturation
S_w	Water saturation
t	Time (s)
T_o	Tensile strength of the rock, psi
$T_{o,i}$	Tensile strength of the rock at the intersection, psi
$T_{o,l}$	Tensile strength of the rock at location 1, psi
$T_{o,tip}$	Tensile strength of the rock at the natural fracture tip, psi

α	Biot's poroelastic constant (dimensionless)
ρ	Density of the formations (lb/ft3)
σ_3	Minimum in-situ principal stress, psi
σ_H	Maximum horizontal stress (psi)
σ_h	Minimum horizontal stress (psi)
σ_n	Stress acting perpendicular to the natural fracture plane, psi
F_g	Gas flow
DIFFMF	Matrix-fracture diffusivity
D_c	Diffusion coefficient
GC_b	Bulk gas concentration
GC_s	Surface gas concentration

CHAPTER I
INTRODUCTION

1.1 Background

Shale gas reservoirs have become more attractive for the petroleum industry recently due to the increasing prices of gas and the advancement in oilfield technologies [3]. Nanodarcy permeability can be characteristic of shale reservoirs. The nanodarcy permeability means there will not be sufficient permeability to allow natural gas to flow from the reservoir to the wellbore at an economic rate. Therefore, there has been an emphasis on improving gas extraction from this type of reservoir using hydraulic fracturing. Hydraulic fracturing is a common stimulation approach to achieve economical gas production rates by providing a conductive path through the reservoir which would otherwise have permeabilities measured in a nanodarcy range. Without hydraulic fracturing in shale reservoirs, gas flow would be almost impossible.

The hydraulic fracturing treatment aims to increase the stimulation reservoir volume (SRV) and improve matrix connection so that gas can flow in the matrix and eventually flow through the main created conductive paths towards the wellbore.

Therefore, the objectives of this study are to evaluate gas production performance based on reservoir parameters and to obtain optimum hydraulic fracturing strategies utilizing horizontal-wellbore production. In general cases, hydraulic fracturing is typically propagating through existing fractures or natural fractures as a result increasing in SRV which delivers significant improvement of gas flow in the matrix rocks enhancing gas recovery factor.

Shale gas is an organic-rich shale formation which simultaneously is a source rock and reservoir rock. Natural gas is stored in the pore space which can be varied from 2-8% [10]. Some fractions of gas are adsorbed on the organic material or shale surface which will then be released once the pressure declines. Generally, adsorbed gas has some effects on gas productivity especially in late-time production when reservoir pressure reaches a certain point which allows adsorbed gas to be liberated

and acts as free gas. Shale permeability varies from tens to hundreds nano-darcy and the typical thickness of the reservoir is 50 – 500ft [3] so it would be more beneficial to produce the gas through horizontal well bore to obtain maximum contact volume into the shale reservoir. In some cases, hydraulic fracturing in shale gas reservoirs utilize low-viscosity fluid typically water as well as placing a small concentration of proppants to promote the complexity and creating fracture network. The complexity of fracture network is impacted by natural fractures. Therefore, it is not possible to accurately predict the fractures growth. The only way to monitor fracture propagation into the rock is the use of microseismic mapping. Microseismic mapping is now an important tool to measure the size of the fracture network real-time providing a more understanding of stimulation performance results in more effective hydraulic fracturing design in future projects.

This study aims to obtain optimum hydraulic fracturing strategies in order to improve gas productivity in naturally fractured shale gas reservoir. The results from this study can be used as guide to optimize the hydraulic fracturing design in the most effective way. A reservoir simulator, ECLIPSE100 is used to construct the reservoir simulation model exhibiting production performance analysis based on various reservoir parameters.

1.2 Objectives

1. To study gas production performance by accounting for the following parameters;
    - Reservoir porosity
    - Reservoir permeability
    - Presence of natural fractures
    - Presence of induced fractures from hydraulic fracturing
    - The effect of natural fracture width, number of fractures, fracture spacing, and gas adsorption.
2. To determine optimum strategy in designing hydraulic fracturing based on fracture width, fracture spacing, and number of fractures.

1.3 Outlines of Methodology

1. Study related published papers and gather necessarily input information for reservoir simulation model.
2. Construct a base case of shale gas reservoir with the presence of natural fractures.
3. Construct reservoir simulation models with altering interested parameters in order to study the effect of reservoir properties include matrix permeability and porosity, number of natural fractures and spacing, and fracture width.
4. Vary hydraulic fracturing design based on number of fractures, spacing, and fracture width. Analysis on each case in this study is performed include;
   - Production performance versus time.
   - Pressure and saturation profile in the reservoir.
5. Discuss all results from simulation model on each case to define the optimum strategy in designing hydraulic fracturing.
6. Perform sensitivity analysis to study the effect of matrix permeability, hydraulic fracturing pattern, and gas adsorption.
7. Provide conclusions and recommendation for future study.

1.4 Review of Chapters

This report is divided into five chapters. The outlines of each chapter are described below.

Chapter II elaborates related literature reviews studying on hydraulic fracturing in shale gas reservoir which includes the background of rock mechanics, modeling of shale gas reservoir simulations, and gas flow behavior. The studies show the previous works done to improve gas production and demonstrate the successful case studies of carefully design the hydraulic fracturing strategies.

Chapter III presents the detail of the related concepts and theories applied on this study.

Chapter IV describes the reservoir simulation model and demonstrates the processes of work.

Chapter V discusses the reservoir simulation base case results and evaluates the effects of reservoir parameters include matrix porosity, matrix permeability, number of fractures (also with different matrix permeabilities), fracture width (also with different matrix permeabilities). This chapter elaborates the selection of the optimum hydraulic fracturing strategy. Furthermore, sensitivity analysis is also performed.

Chapter VI provides conclusions and recommendation for future study.

CHAPTER II

LITERATURE REVIEWS

This chapter presents the detail of the previous studies which are related to hydraulic fracturing in shale gas reservoir. It describes shale fracturing mechanism, reservoir simulation model, and experimental model. Potential parameters that have effects on production performance are discussed. This chapter is divided into three parts, 1) Shale fracturing and rock mechanics 2) shale gas reservoir simulation models 3) gas flow behavior.

2.1 Shale Fracturing and Rock Mechanics

There are many paper publications evaluating on hydraulic fracturing in the shale gas reservoir. The most challenge as such is hydraulic fracturing in shale reservoir with the presence of natural fractures. Murphy and Fehler [1] pointed out some specific behavior in shale gas application; first, microseismic mapping does not show perfect matching of the bi-planar fractures or conventional fractures. Second, shear slippage is more easily induced along natural fractures than inducing tensile failure in the matrix and third, shear slippage can generate more branching and the creation of a complex stimulation pattern.

In 2011, Nagel et al [2] extended a study of fluid injection into naturally fractured shale using Discrete Element Model (DEM). The study aimed to investigate the effect of stress orientation, fluid viscosity, and rock mechanics. They presented the shear failure evaluation as a result of the creation of a hydraulic fracture as a function of fracture length within two different fracture networks. The reservoir simulations were modeled by accounting for fracture strength, different fracture network orientation within the stress field, stress ratio (the ratio of the maximum horizontal stress relative to minimum horizontal stress), Poisson's ratio of the shale, and Young's modulus of the shale. They concluded that the degree of fracture shear was directly linked to fracture friction angle. An importance factor which affected to fracture stability was the orientation of the fracture network within the in-situ stress

field. It appeared that stress ratio, Poisson's ratio and Young's modulus had a second order effect on the shearing and the stimulation of the natural fracture system.

Moos [3] wrote a report regarding an improving shale gas production using geomechanics. He reported that the relative magnitudes of the three principle stresses and consequent orientation of the fracture defined the stress regime to be normal faulting, strike slip faulting or reverse faulting. It is now generally accepted that the horizontal stresses are highest relative to the vertical stress in a reverse faulting regime and lowest relative to the vertical stress in a normal faulting regime. Hydraulic fractures will be vertical and propagated in the direction of the greatest horizontal stress in a strike-slip or normal faulting regime. In a reverse faulting stress regime in which vertical stress is the minimum stress, fractures will be horizontal. Most but not all, shale gas plays are in either a normal faulting or a strike-slip faulting regime. The Barnett shale has very low horizontal stresses relative to the vertical stress.

In 2010, Potluri et al [4] presented the effect of the fractures interaction between the natural fractures and the induced fractures from hydraulic fracturing. They used the approach of Warpinski and Teufel [5] to evaluate the fracture propagation that would occur after the hydraulic fractures intersect the existing natural fractures. The study demonstrated the effect of differential stress, angle of interaction, and fracture toughness for which dilation of natural fractures would occur. The approach of Warpinski and Teufel was applied by the three possible modes of propagation include

1. Crossing of the hydraulic fracturing on pre-existing occurs when normal stress on natural fracture is high relative to the fracture toughness of the rock.

2. Dilation of the natural fracture then continuously propagates from the natural fracture tip.

3. Dilation of the natural fracture then break out occurs from the natural fracture.

The above scenarios were based on the horizontal stress contrast, the angle of interaction, the fracture toughness and the pressure drop within the natural fractures.

In 2011, Zhou and Zue [6] performed the experiment of fracture interaction between natural fractures and hydraulic fractures to observe fracture propagation

behaviors derived from a series of tri-axial experiments. Three types of geometry were observed in their tests. The first was a vertical dominating fracture with multiple branches at high horizontal stress contrast, in this case the fracture propagate in a preferred direction which is in the direction of maximum horizontal stress. The second was radial net-fractures around wellbore at low horizontal stress contrast. The third was partly vertical fracture (one wing) with random branches. From the results; it could be concluded that the hydraulic fracture would propagate in the direction of maximum horizontal stress with creating small branches from natural fracture interaction.

Du et al [7] developed a modeling hydraulic fracturing induced fracture networks in shale gas reservoir as a dual porosity system. This approach decoupled complex reservoir characteristics and geomechanical factors from production response. Microseismic responses were used to delineate stimulated volumes from hydraulic fracturing treatment. The following procedures were used in their study to obtain induced fracture network including 1. estimating an average fracture width for an ideal network system based on rock mechanics and hydraulic fracturing treatment pressure data 2. characterizing microseismic events intensity and/or natural fracture intensity 3. establishing the relationship among hydraulic fracturing induced fracture intensity, average fracture width and hydraulic fracturing treatment volume data 4. calibrating microseismic intensity or natural fracture intensity to hydraulic fracturing intensity 5. calculating dual porosity reservoir properties directly or create discrete fracture network and upscale it to dual porosity model and then run reservoir simulation. Their study presented the detail of uncertainty analysis and history matching of production data for calibrating the model. The results of this study illustrated the impact of rock mechanics, hydraulic fracturing and microseismic parameters on cumulative gas production consist of Poisson’s ratio, fracture height, pressure difference, shear modulus, fracture conductivity, water holding coefficient, and microseismic intensity grid cell size.

2.2 Shale Gas Reservoir Simulation Models

Hydraulic Fracturing was first introduced in the late 1940s [8] and was first used by Stanolind Oil company to a well in Grant County, Kansas [9] involving to injected fluid at the sufficient pressure to overcome formation strength in order to generated fractures. Hydraulic fracturing is now considered one of the most important and enduring technologies ever developed in petroleum industry.

In 2009, Cipolla et al [10] developed reservoir models in shale gas reservoirs using the production data histories from Barnett and Marcellus Shales to estimate reservoir properties. They studied the effect of gas adsorption on gas productivity and ultimate gas recovery in the shale reservoirs. Their paper observed the significant change when closure stress distribution is increased could reduce fracture conductivity; hence, significantly reducing ultimate gas recovery. According to their simulation model, it could be drawn the conclusions that gas desorption is not a significant component of production in many moderate to deep shale gas reservoir. Even though the gas is adsorbed on the shale surface can make up the gas content up to 40-50% of the original gas in place but to be able to retrieve the adsorbed gas is limited to the ultra-tight matrix with the high bottom hole pressure. However, the desorbed gas can be produce 5-15% of ultimate gas production during the later life of the well. The effect from gas desorption showed similar results for both Barnett and Marcellus Shale. Apparently closure stress distribution had more effect on gas recovery for the Marcellus Shale which Young's modulus was much lower (softer rock) than that of the Barnett Shale. The simulation model showed that with closure stress included in the model could significantly reduce gas recovery in softer rock but may not be evident in the initially 1-2 years of production life.

Freeman et al [11] studied production performance on tight reservoirs and shale gas reservoir systems which accounted for ultra-tight matrix permeability, hydraulically fractured horizontal wells, multi-porosity and permeability fields and gas desorption which were relevant to this system. They examined various tight/shale gas systems and determined the various flow regimes which progressively occurred over time. They concluded that the pressure gradient was the main driving force for

fluid flow. It rapidly lost its ability to contribute productivity to the fracture as it moved away from the fracture. They also observed an effective no-flow boundary was formed when the pressure transient from the individual fracture reached the pressure transient of the adjacent fracture. Once the pressure transients were sufficiently coincided, this could appear as a boundary-dominated flow regime feature in production data analysis.

Mirzaei et al [12] developed a work flow for modeling and simulation of hydraulic fractures in unconventional gas reservoir which combined discrete fracture network (DFN) and unstructured fracture (UF) in order to improve the stimulation design. They constructed two model methods in this study. First, simple method which assumed fractures laid in the single plane of local grids placed around them. The local grids were constructed in each stage of the treatment. Second, fracture geometries were complex and unstructured grid model was used to evaluate both effect of propped and unpropped hydraulic fracture using the well information from Barnett shale play. For the simple model and unstructured model, they studied the effect of adsorbed gas; fracture spacing and length, number fracture per stage, conductivity and production performance which accounted for propped and unpropped hydraulic fracturing. Their study discovered that the more reservoirs could be effectively drained if the more complex hydraulic fractures could be created. That could reduce the number of stages stimulation if high conductivity can be achieved.

Gong et al [13] created the discrete fracture model of natural and hydraulic fractures in shale gas reservoirs by applying the geologic interpretation and micro-seismic mapping to enable realistic modeling of hydraulic and pre-existing fracture networks. The studied model used highly resolved unstructured grids building with low, medium, and high density fractured constrained by micro-seismic mapping results. Based on two months production history, it can simply match to the low fracture density case. The studies parameters consisted of adsorption/desorption, matrix-fracture transfer, non-Darcy effect and porosity and permeability. According to the simulation results, they found that the highest fracture density case showed declined simulated production became slower in the early-times but steeper in the

later -times. Also the highly connected fracture network helped to maintain pressure in the early stage; therefore, the gas desorption become less effective.

Uleberg et al [14] developed a numerical simulation for dual porosity, dual permeability formulation for fractured reservoir. The study reviewed key physical mechanisms and calculation methods for modeling of fluid flow in North Sea fractured reservoirs. The main matrix fracture fluid exchanges and mechanisms descriptions were gravity drainage, capillary imbibitions, and molecular diffusion. From the study; it could be concluded that all major flow mechanisms and flow processes must be incorporated in a model for fractured reservoirs. These included gravity, capillary forces, gravity drainage, diffusion, capillary continuity and refiltration. Also a multiple grid concept was recommended to improve the model for sufficient detail in the calculation so that all these flow mechanisms were represented.

Aboaba et al [15] presented a new approach to determine the fracture properties for multi-stage hydraulic fracturing in shale gas reservoir. The method evaluated the history production data which include production rate and pressure data for estimating the fracture half-length and reservoir permeability. The method first converted variable rate-pressure data into equivalent constant-rate pressure drawdown test and then pressure transient analysis techniques were applied for fracture properties estimation.

2.3 Gas Flow Behavior

Sakhaee-Pour and Bryant [16] proposed an analysis of gas permeability in shale reservoir by evaluating the effect of adsorbed layer of CH_4 and of gas slippage at pore walls on the flow behavior in individual conduits of simple geometry and in networks of such conduits. The effects of adsorption and slip depended on pressures and on conduit diameters. The hydraulic conductance that determined gas flow regimes was determined based on the Knudsen number (Kn) criterion. It was used to distinguish flow regimes at micro and nanoscale. Knudsen number was defined as $K_n = \lambda/\Lambda$ where λ represents the mean free path of gas molecule and Λ represents the length of the channel. The regime changed from continuum flow to discrete particles as the Knudsen number increased. They analyzed the conductance of a single-sized

throat to study the effects of adsorbed gas and slippage then built a network model to evaluate these effects when the connected throats exhibited a distribution of sizes. Their study could be concluded that the large pressure at initial shale gas reservoir pressures, the effect of slip gas had no effect as the system was dominated by the effect of the adsorbed layer. Slip would have an effect after longer period production consequently the reservoir permeability was predicted to increase over the life of the producing well.

In 2011, Cheng [17] analyzed pressure transient characteristics of hydraulically fractured horizontal shale gas well. They investigated the pressure transient characteristics responded under a number of factors and flow mechanisms including matrix permeability, conductivity of hydraulic fractures, cluster spacing and size/enhanced permeability of stimulated zone. The study classified the flow regimes into five flow regimes including Radial Flow/Linear Flow, Bilinear Flow, Inner Linear Flow, Quasi-steady state flow and late time outer linear flow, respectively. Each of which occurred for a different period of time. It was noticed that in the Quasi-steady flow period, pressure interference between fractures were dominated when the flow across the boundary between the inner and outer reservoirs started. It was worth to note that due to the nature of ultralow permeability of shale matrix, the drainage was unable to feel the outer no-flow boundary and therefore it would not develop Boundary-Dominated-Flow over the life-time of the well. According to the simulation results, the matrix permeability significantly affected to pressure transient especially during the inner linear flow period. Fracture conductivity effected mostly at the early times to pseudopressure derivative response but it effected on pseudopressure lasts much longer as much as in the inner linear flow regime. Fracture spacing dictated how long the inner linear flow lasts. It affected significantly to both pseudopressure drop and derivative at both early and intermediate times.

Cinco-Ley and Samaniego [18] presented for analyzing pressure transient data for finite conductivity vertical fracture. This method was based on the bilinear flow theory, which considered transient linear flow in both fracture and formation. It demonstrated that a graph of p_{wf} Vs $t_{1/4}$ produced a straight line whose slope was inversely proportional to $h_f(k_f b_f)_{1/2}$. Based on the material presented in this work, they

concluded that transient flow behavior of a vertically fractured well may exhibited four flow regimes a) fracture linear flow b) bilinear flow c) formation linear flow and d) pseudo-radial flow.

After reviewing several previous studies, no work has been done on designing the strategies of hydraulic fracturing in naturally fractured reservoir with accounting for the combination of fracture width, spacing and number of fractures. The motivation of this work is to gain an understanding of the parameters that have effects on the gas production performance in order to provide an optimum hydraulic fracturing design based on three parameters as stated.

CHAPTER III

THEORY AND CONCEPT

This chapter elaborates fundamental of shale rock mechanics and shale rock characterization based on rock stress, Young's modulus and Poisson's Ratio to gain an understanding of shale fracturing mechanism as well as discusses the related theories and concepts of hydraulic fracturing in tight gas reservoir, its flow behaviors in the ultra-low permeability system, and parameters those have effects to shale gas production such as fracture conductivity, fracture width, fracture half length, fracture spacing, adsorbed gas concentration, closure stress and stimulated reservoir volume as well as multi-stage hydraulic fracturing. Gas production efficiency is described in this section as this factor will be used as a technical judgment to specify the hydraulic fracturing optimum design.

3.1 Shale Rock Mechanics

An improved understanding of hydraulic fracture geometry and shale rock mechanics enables reservoir engineering teams to improve stimulation performance, well productivity, and hydrocarbon recovery. Many researchers have been studying hydraulic fracture propagation in the presence of natural fractures. As stated in Economides and Martin [19] “Fractures will always propagate along the path of least resistance. In a three-dimensional stress regime, a fracture will propagate so as to avoid the greatest stress and will create width in a direction that requires the least force. This means that a fracture will propagate parallel to the greatest principal stress and perpendicular to the plane of the least principle stress. This is a fundamental principle; therefore, the key to understanding fracture orientation is to understand the stress regime”. In general applications where the reservoir is deeper than 1,000ft which the maximum principle stress will be likely in the vertical direction as the rock stress relies on the overburden stress, the fracture will be in vertical direction. For some shallow reservoirs or in reverse fault regimes, the fracture can be in horizontal direction since the minimum stress is horizontal. The azimuth orientation of the

vertical fracture depends on the differential stress between the minimum and maximum horizontal stresses.

3.1.1 Vertical Stress

The absolute vertical stress, σv, is the weight of overburden above that point per unit area; the typical unit is in pounds per square inch (psi) which is a function of density of rock and the vertical depth. The equation is expressed by [20]

$$\sigma_v = \rho g H \quad (3.1)$$

where ρ is the density of the formations (lb/ft3)
g is the acceleration due to gravity
H is the thickness or depth

In a porous medium, not only weight of rocks that are carried but it is actually included the fluid within pore space therefore an effective stress (σ_v') is expressed by

$$\sigma_v' = \sigma_v - \alpha p \quad (3.2)$$

where α is Biot's poroelastic constant (dimensionless),
p is pore (reservoir) pressure (psi).

3.1.2 Horizontal Stress

The vertical stress is translated horizontally through Poisson's ratio (ν) [21]

$$\sigma_H' = (\nu/(1-\nu))\ \sigma_v' \quad (3.3)$$

where σ_H' is effective horizontal stress (psi).

The absolute horizontal stress is defined by adding the αp term to the effective horizontal stress. Due to tectonic components, the horizontal plane stress varies with direction. The above equation defined minimum horizontal stress; the maximum horizontal stress is

$$\sigma_{H,max} = \sigma_{H,min} + \sigma_{tect} \quad (3.4)$$

where σ_{tect} is tectonic stress contribution (psi)

3.1.3 Fracture Geometry

For simplicity, classical bi-wing fracture geometry is applied onto this study as the injected fluid flow along the perforation channels, the fractures extend away from the horizontal wellbore. Figure 3.1 shows bi-wing fracture geometry.

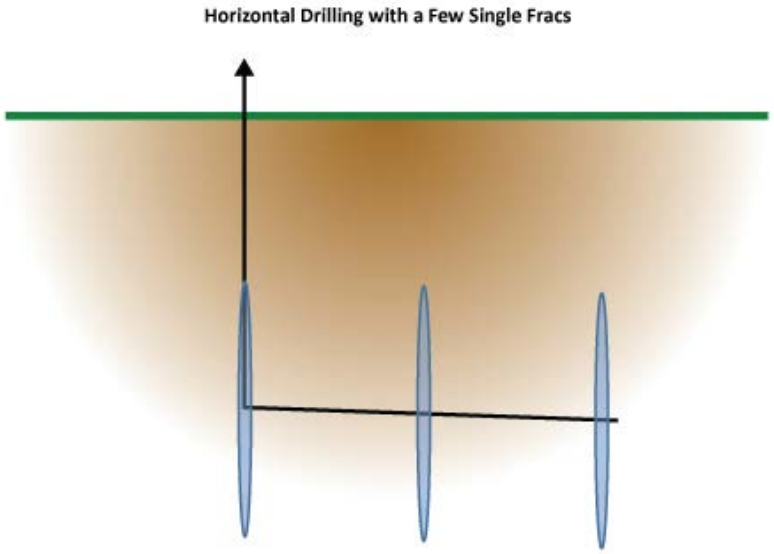

Figure 3.1 Horizontal drilling with a few single fracs

In general, hydraulic fracturing treatment, a horizontal well is drilled along the minimum horizontal stress direction in order to generate transverse fractures to obtain the maximum contact inside the shale reservoir as a result the higher gas production rate can be achieved. Figure 3.2 depicts transverse and longitudinal fractures.

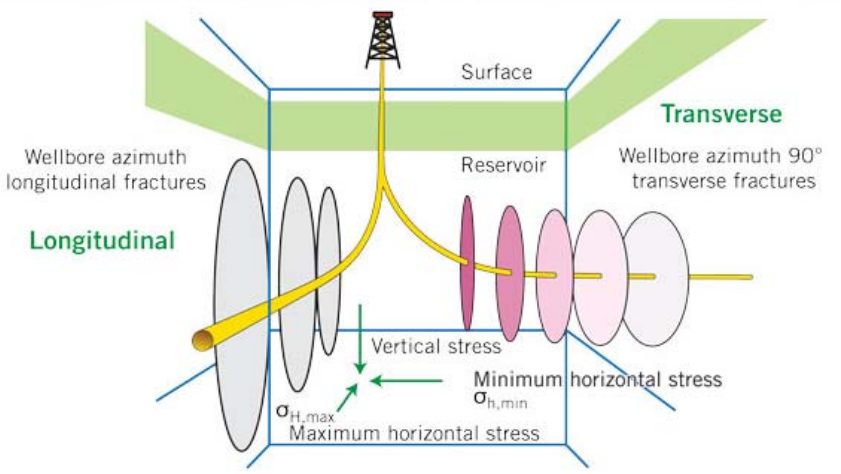

Figure 3.2 Fracture developments as function of wellbore orientation

3.1.4 Effect of Natural Fracture on Hydraulic Fracture Propagation

Experimental investigations have shown the propagation of hydraulic fracturing which sometime it crosses the natural fracture, turns into the natural fracture, or in some cases turns into the natural fracture for a short distance, and then breaks out again to propagate in the more favorable direction. Application of fracture interaction can be defined as the following possible interaction criterions [4];

If the pressure in the propagating hydraulic fracture is greater than the normal stress on the natural fracture, the natural fracture will immediately expand. As the natural fracture opens, the pressure in the natural fracture will increase. As the pressure in the natural fracture increases, three modes of fracture growth can possibly occur as follows;

a) The pressure at the interaction point exceeds the threshold pressure to initiate a fracture along the original path of the propagating hydraulic fracture, hence hydraulic fracture crosses natural fracture can be a result;

$P_i(t) > \sigma_3 + T_{o,i}$.

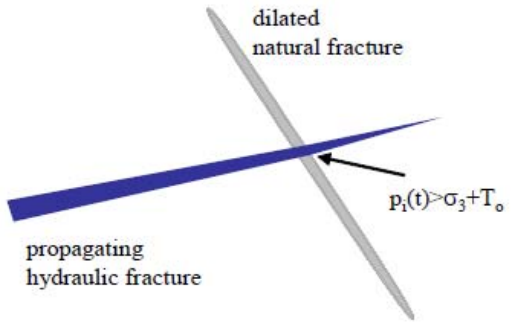

Figure 3.3 Hydraulic fracture crosses natural fracture

b) The pressure at one of the tips of the natural fracture exceeds the net pressure required to begin propagating from the natural fracture tip, hydraulic fracture extends natural fracture tip;

$P_i(t) > \sigma_n + T_{o,tip} + \Delta p_{nf}$

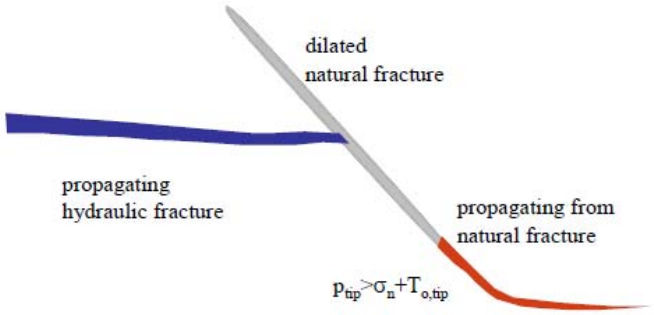

Figure 3.4 Hydraulic fracture propagates
from the tip of natural fracture

c) The pressure somewhere in the natural fracture is high enough to overcome the local fracture toughness and the fracture breaks out of the natural fracture somewhere between the interaction point and fracture tip.

$T_{o,l} < T_{o,i} - \Delta p_l$

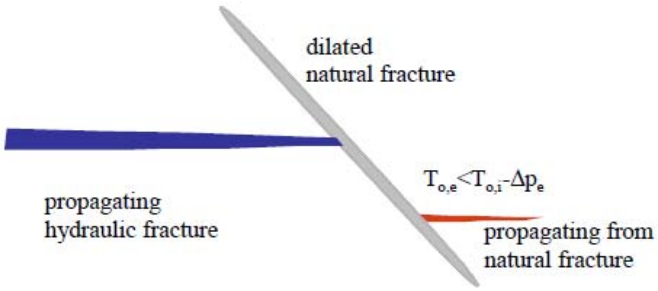

Figure 3.5 Hydraulic fracture propagates from
weak point along natural fracture

3.1.5 Shale Characterization

It is important to note before a stimulation treatment can be designed for shale reservoir is to aware of shale brittleness. The concept of rock brittleness combines both Poisson's ratio and Young's modulus. These two components are indicating the

rock's ability to fail under stress (Poisson's ratio) and maintain a fracture (Young's modulus). Even though, ductile shale is not a good reservoir because the formation will want to heal any natural or hydraulic fractures; there are still some areas that shale have this characteristic such as Haynesville shale which Shale is “soft” with a low Young’s Modulus and higher Poisson’s Ratio. Figure 3.6 shows an example of calculating brittleness from Poisson's ratio and Young's modulus. The concept is that the ductile shale points fall to the north-east quadrant, and the more brittle shale fall to the south-west quadrant.

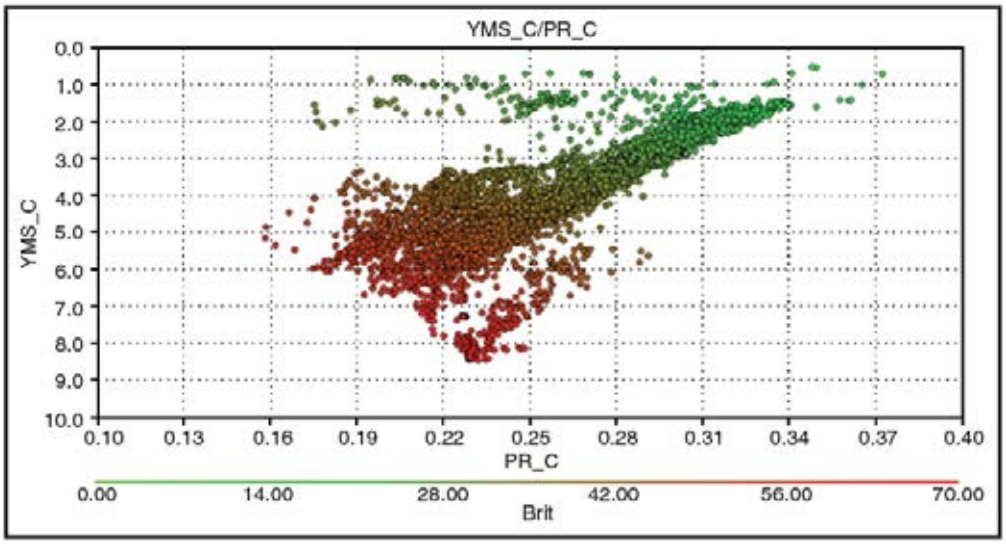

Figure 3.6 Cross Plot of Young's modulus and Poisson's Ratio

Fracture Model Assumptions Based on Shale Rock Mechanics

In this work, the assumptions applied on the reservoir simulation model are as follows;

1) Shale reservoir in-situ stress is homogeneous which means the stress regime is evenly distributed within the shale reservoir.

2) Fractures occur in the vertical direction assuming the maximum stress is in the vertical direction. Providing the top of reservoir is at 8,000ft, the maximum stress mostly relies on overburden pressure.

3) Induced hydraulic fracturing reactivates the natural fracture in the direction of an existing maximum stress or no in-situ stress changes after hydraulic fracturing is conducted.

4) Existing natural fracture height and half-length are extended for entire reservoir thickness and length so the hydraulic fracturing is propagating throughout the reservoir thickness and length.

5) A horizontal well is drilled along the minimum stress regime so the hydraulic fracturing initiated is transverse fracture.

6) Fracture width is assumed to be constant from the top throughout the bottom of the reservoir.

7) Ductile shale is assumed in this study so the bi-wing hydraulic fracturing is initiated.

3.2 Hydraulic Fracturing in Tight Gas Reservoirs

The hydraulic fracturing is the most common stimulation method that has been applied on ultra-low permeability formation. Its permeability is measured in nano-darcy range especially in shale gas formation where pores irregularly distributed throughout reservoir which has poor connection by very narrow capillaries. Since the permeability in this formation is too low for economically production therefore hydraulic fracturing treatment is needed to create the passageways through the reservoir in order to increase connectivity and for better communication between reservoir and production well in order to increase gas production rates. Hydraulic fracturing begins by injecting a large volume of a suitable fluid at a pressure exceeding the tensile strength of rock. Fracturing of formation matrix has initiated along a plane perpendicular to the minimum compressive stress (minimum principle stress). Fluid has been continuously injected until the fractures are open enough to accept proppants. Proppants then are added to keep the fractures open when the pump stops and pressure reduces.

In shale gas system, many complexities are much more than hydraulic fracturing in tight sand due to the unique characteristic of shale. This kind of reservoir has unique properties which are;

1) Nanodarcy matrix permeability, which makes flow almost impossible.
2) Narrow, calcite-sealed natural fractures reactivated during hydraulic fracturing, which is reducing fluid flow capability.
3) Complex fracture network distributions because of the presence of both natural and hydraulic fractures.
4) Adsorbed gas in organic materials, making up nearly 50% of the gas content in some shale gas reservoirs

Figure 3.7 illustrates processes of hydraulic fracturing in tight gas reservoir.

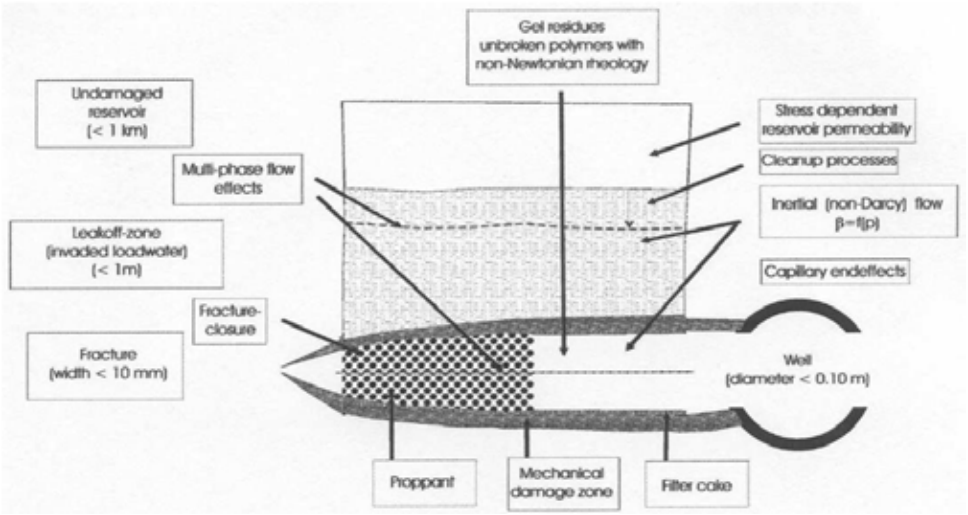

Figure 3.7 Process Specification in Hydraulically Fractured Wells in Tight Gas Reservoir [18]

3.3 Gas Flow Behaviors

Studies of gas flow regime in shale reservoir have been appeared on many published papers. Cinco-Ley et al [22] identified four flow regimes for gas flow in shale reservoir; four flow regimes are 1) Fracture linear flow, 2) bilinear flow, 3) Linear flow in the formation and 4) Pseudo-Radial flow. Fracture linear flows take place relatively short period of time, most of the fluids entering the wellbore come from fluid expansion in the fracture. The flow regime is linear; it may be dominated by well bore storage effects. Bilinear flow will be developed only in finite-conductivity fractures as fluid in the surrounding formation flows linearly into the fracture and into the well bore. Finite-conductivity can be defined as the fractures

with significant pressure drop along its axis. Linear flow in the formation is evolved afterward. Duration of formation linear flow increases with higher fracture conductivities, mostly the fluid come from the formation. Pseudo-radial flow occurs after a sufficiently long production period. The fractures appear to the reservoir as an expanded well bore. Drainage area appears around fracture length and gas flow radically through the drainage area. Figure 3.8 illustrates the four flow regimes of gas flow into the hydraulic fractured well.

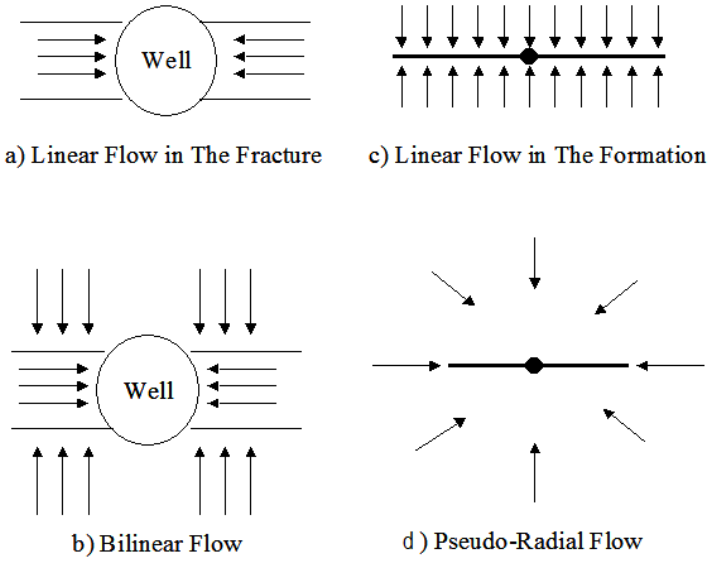

Figure 3.8 Fracture Flow Regime Cinco-Ley et al [22]

3.4 Parameters Effect on Gas Production

Parameters that have effects on gas production in hydraulic fracturing in shale gas well are discussed in this section.

3.4.1 Fracture Conductivity

Fracture conductivity is a key parameter in hydraulic fracturing and represents the ability to transmit the fluid from the fracture to production well. The dimensionless conductivity C_{fD} is a function of fracture permeability, fracture width, matrix permeability, and fracture half length.

Dimensionless fracture conductivity can be defined as

$$C_{fD} = \frac{k_f w}{k x_f} \qquad (3.5)$$

The fracture conductivity may be increased by enlarging the propped fracture width by using high proppant concentration. In this model, the fracture half-length is constant and is equal to reservoir half-length; therefore, fracture conductivity corresponds to variable fracture width.

where k_f is fracture permeability
w is fracture width
k is matrix permeability
x_f is fracture half length

In this model, because the fracture half-length is constant and is equal to reservoir half length; fracture permeability is corresponded to fracture width therefore the fracture conductivity is solely based on fracture width.

3.4.1.1 Fracture Width

Fracture width is the perpendicular width of an open fracture. The fracture width corresponds to fracture permeability and fracture conductivity. However, this definition does not take into account of fracture roughness, gouge, degree of mineral infill and lateral continuity. For these reasons, it is difficult to accurately determine a fracture aperture within a rock body. Typical hydraulic fracture width is 3.00mm which the proppant size of 30/50 mesh would be used [30]. Fracture permeability is defined by using a cubic function of the fracture half-width [11] which is given by

$$k_f = \frac{1}{12} b^3 \qquad (3.6)$$

where b is fracture half-width, mm
k_f is effective fracture permeability, m^2

3.4.1.2 Fracture Half Length

Fracture half-length is defined as a radial distance from the wellbore to the outer tip of a fracture penetrated by the well or propagated from the well by hydraulic fracturing. Fracture half-length is individually developed as each treatment further progressed. As seen in Figure 3.9, the total fracture network system continued to grow as the fluid pumped volume increases.

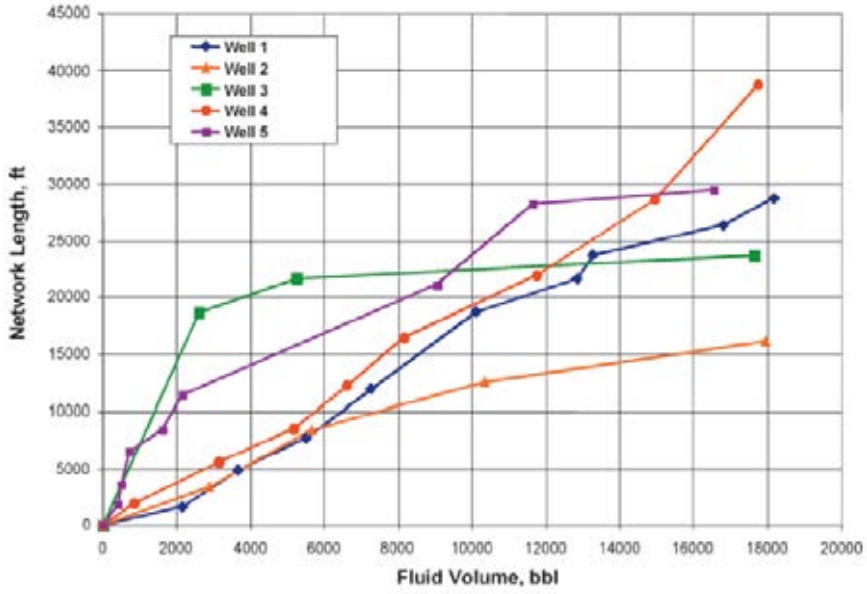

Figure 3.9 Relationship of total fracture network length corresponds to fluid volume pumped [25]

3.4.2 Fracture Spacing

Fracture spacing is one of the key factors in hydraulic fracturing optimization design. When hydraulic fractures are close to each other, a small reservoir area is in contact with the hydraulic fractures. If the spacing is increased, more contact surface within the reservoir will be a result and gas will be drained more effectively. Increasing fracture spacing can bring more reservoir matrix into contact with fractures, leading to earlier production and much improved gas recovery. Figure 3.10 shows the effect of fracture spacing on gas drainage area.

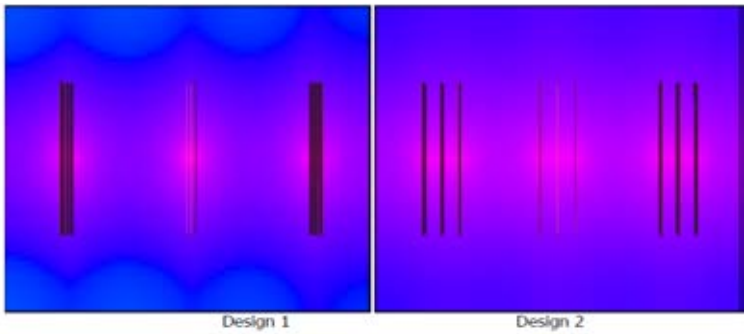

Figure 3.10 Gas drainage correspond to fracture spacing [12]

3.4.3 Number of Fractures

It is important to note that a higher number of fractures would develop the gas productivity in ultra-tight gas shale as it represents more flow channels are created, penetrating through the rock and increasing surface contact in the shale reservoir. In other words, this increases the stimulated reservoir volume (SRV) result in improve productivity.

3.4.4 Closure Stress

The impact of increasing closure stress on hydraulic fracture conductivity has been brought into more attention to many researchers recently. There is a likelihood that large stimulation treatment may be un-propped or ineffectively propped [3]. Fredd et al [28] investigated the effect of closure stress on un-propped and partially propped fracture conductivity to evaluate stress sensitivity. Figure 3.11 shows an estimation of the impact of closure stress on un-propped fracture conductivity, illustrating the dramatic decreases in fracture conductivity when closure stress increases.

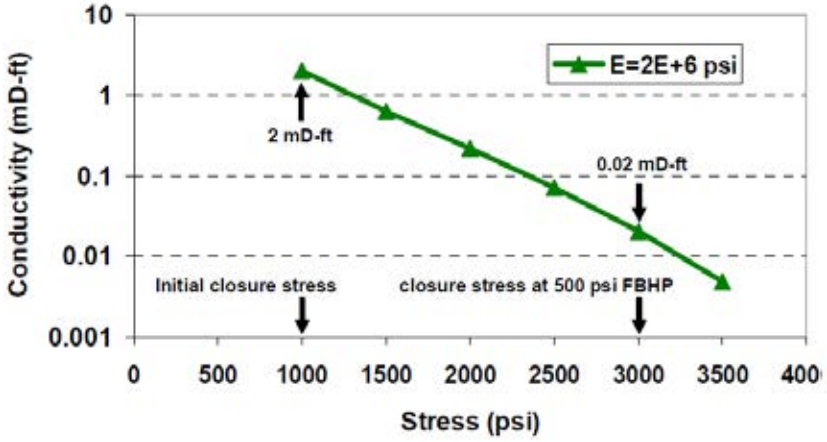

Figure 3.11 Effect of closure stress un-propped fracture conductivity [10]

3.4.5 Stimulated Reservoir Volume

Stimulated Reservoir Volume defines 3D size of created fracture network in the reservoir. This factor is a direct driver of well performance [32]. Figure 3.12 represents the effect of SRV on the production performance. It appears in the work of

Cipolla [10] that the SRV is generated as a result of the complexity and conductivity of the fracture network which are the key components that control well productivity in shale gas reservoirs. With respect to the limitation of constructing the complexity, the investigation of multi-stage bi-wing hydraulic fracture is examined. Therefore, stimulated reservoir volume in this study is a function of fracture width, fracture half length, and fracture height.

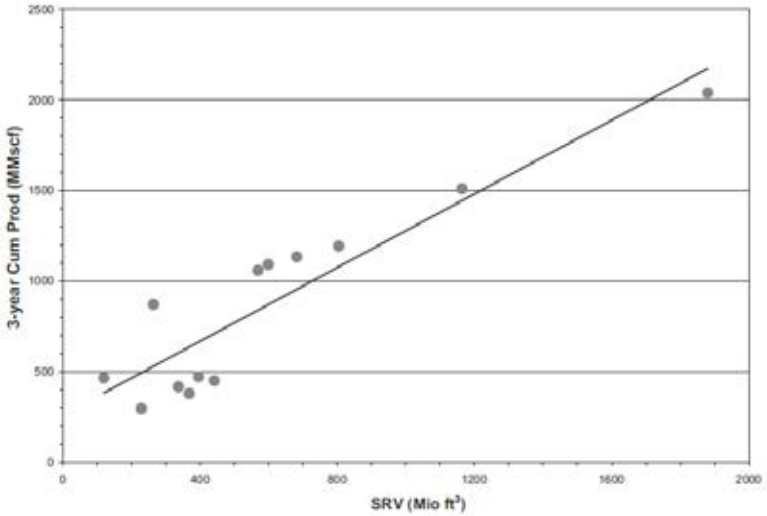

Figure 3.12 SRV trend vs cumulative horizontal-well production [32]

3.4.6 Adsorbed Gas

Gas is stored in shale in three different ways. Some of the gas is held in natural fractures; some in the pore spaces; and some are adsorbed onto the organic material. The gas in the fractures is produced immediately, and gas adsorbed onto organic material is released as the formation pressure declines. Gas is usually generated in place from shale with high total organic carbon content. The Langmuir isotherm is used to specify the amount of stored gas in the matrix in a range of reservoir pressure. The maximum storage capacity for gas is referred to as the Langmuir volume constant and the pressure corresponding to one-half this value is referred to as the Langmuir pressure constant [12]. The example of desorbed gas in relation to pressure schematically shows in Figure 3.13 for the two shale types, rich and lean shale.

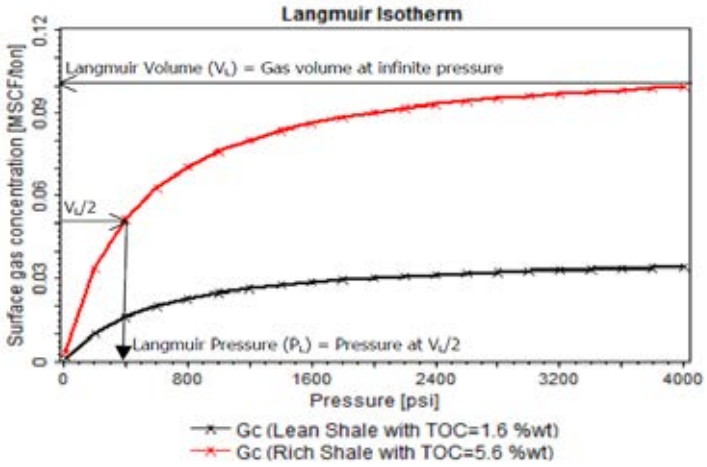

Figure 3.13 Langmuir Isotherm for gas adsorption [12]

The diffusive flow of gas from the shale matrix is given by [27]:

$$F_g = DIFFMF \times D_c \times (GC_b - GC_s) \qquad (3.7)$$

where

	F_g	is gas flow
	DIFFMF	is matrix-fracture diffusivity
	D_c	is diffusion coefficient
	GC_b	is bulk gas concentration
	GC_s	is surface gas concentration

3.5 Production Efficiency

Production efficiency is defined as the ratio of the amount of output relative to the amount of input. The production efficiency can be used to show improvement area in a technical aspect.

The change of input is defined as the enhancement of stimulated reservoir volume (SRV). The change of output can be expressed as the improvement of gas recovery factor. Therefore production efficiency can be defined as;

$$\text{Production Efficiency} = \frac{\text{Improved Gas Recovery Factor}}{\text{Improved Stimulated Reservoir Volume}} \qquad (3.8)$$

In this model, four parameters as described above are investigated to understand their effects on the gas production performance; these parameters include fracture width, fracture spacing, number of fracture, and gas adsorption. The closure stress and stress heterogeneity are also important factors. However, there is the limitation of the available reservoir information so it is unable to construct the completed model based on these factors.

CHAPTER IV

RESERVOIR SIMULATION MODEL

The reservoir model is constructed using ECLIPSE100 simulation software to analyze gas production performance. This chapter is divided into four main sections which consist of reservoir grid, fluid properties section, SCAL section and well model section. These four sections detail on processes of constructing the reservoir simulation model. The reservoir grid section elaborates grid geometry as well as specifies porosity and permeability. The fluid property section describes gas properties and initial reservoir conditions. The SCAL section provides a data table showing relative permeability generated by the simulation software. The last section, well model explains the details of constructing a horizontal well.

4.1 Reservoir Grid

4.1.1 Gridding

The reservoir grid is 65 x 65 x 11 with the total dimensions of 50ft x 20ft x 10ft in the x-, y- and z- direction, respectively. The reservoir is built by using Cartesian grid block with two phase fluids consisting of water and gas. The top of reservoir is at 8,000ft depth with the total thickness of 110ft. The horizontal well is placed in the middle of z-layer as well as in the middle of both x- and y- direction. Table 4.1 lists the reservoir properties which are input in the base case of the reservoir simulation model.

Table 4.1 Reservoir properties

Parameter	Value
Top of reservoir, ft	8,000
Reservoir grid	65 x 65x11 50ftx20ftx10ft
Reference reservoir pressure, psi	3,500
Net pay, ft	110
Porosity, %	8

Matrix permeability, mD	0.0002
Water saturation, %	30
Reservoir temperature, ^{0}F	260
Horizontal length, ft	3,050
Well bore diameter, inches	6 ½
Tubing size, inches	3 ½
Tubing head pressure, psi	450

4.1.2 Local Grid Refinement (LGR)

The local grid refinement (LGR) is used in this model to enhance grid definition near the well bore and the fractures for accurate calculation. This is to allow individually specify the reservoir properties in the local grid blocks. Grid blocks those represent the fractures are replaced by a number of the small grid blocks with variable sizes as well as reservoir properties. In this case study, the local grid blocks are assigned with the fracture properties consisting of fracture permeability and porosity.

4.1.2.1 Wellbore LGR

At the grid blocks laid by the well bore are replaced with the local grids. It is virtually useful for hydraulic fracturing model as it is necessary to concentrate the changes in pressure profile and gas saturation around the well bore.

To simply construct the reservoir model, the number of parent grid for X, Y and Z axis is defined as an odd number; 65, 65 and 11 grid blocks, respectively. It allows the horizontal well to be placed in the middle of the reservoir layer; at coordinate's I-33, J-33 and K-6 along the X-axis. In this model, 9 LGRs are placed in the parent grid blocks those represented the well bore. The length of 50ft parent grid is refined equally into 9 grid blocks providing the grid size of 50/9ft. Table 4.2 represents wellbore local grid refinement defines on each coordinate.

Table 4.2 Horizontal well local grid refinement

LGR Name	Coordinate			Number of refined grid cell		
	I	J	K	X	Y	Z
HZ WELL	3-63	33	6	549 (61 x 9)	9	9

4.1.2.2 Fracture LGR

In this study, fractures are constructed based on Herge [25] suggested to specify small grid cell near fractures and gradually increase the size away from the fracture. In this model, 9 local grids are placed into the parent grid that represents fractures and modified logarithm grid size is used. For the base case, fracture width is 0.0001ft (0.03mm) hence the 50-ft parent grids are refined into small size local grid cells. The lengths of the local grid cell are 0.0001ft (fracture grid), 0.00995ft, 0.09ft, 0.9ft and 24ft in the x-axes outward to the border grid for both wings. In this model, 9 LGRs are selected because it gives an acceptable run time and reasonable result. Figure 4.1 illustrates number of LGR grids comparison. Table 4.3 represents local grid refinement for 7 LGR, 9LGR, 11LGR and 13 LGR respectively.

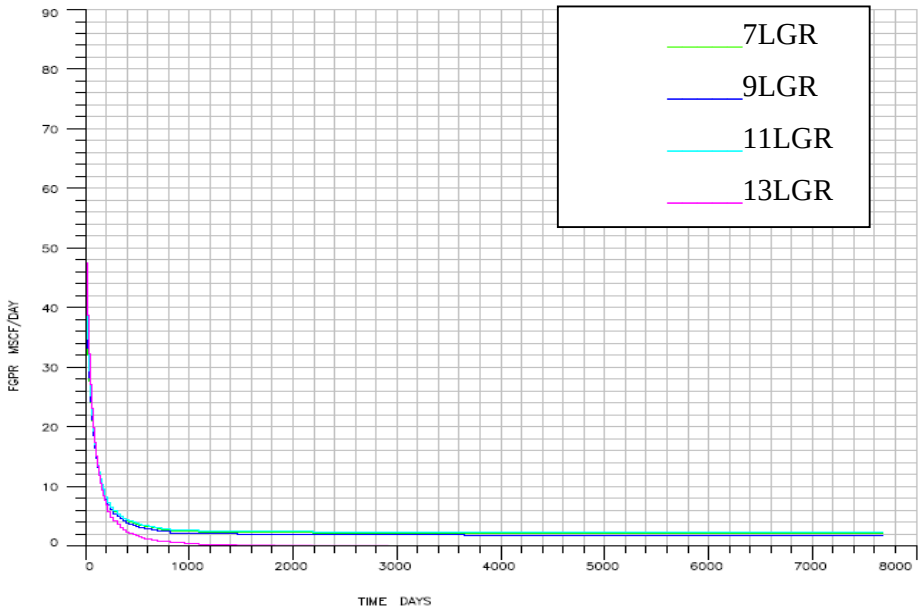

Figure 4.1 Number of LGR grid comparisons

Table 4.3 Sizes of locally refined fracture grid blocks for fractures

No.	**Local Grid Size (ft)**												
LGR	L#1	L#2	L#3	L#4	L#5	L#6	L#7	L#8	L#9	L#10	L#11	L#12	L#13
7				24.9	0.09	0.00995	0.0001	0.00995	0.09	24.9			
9			24	0.9	0.09	0.00995	0.0001	0.00995	0.09	0.9	24		
11		15	9	0.9	0.09	0.00995	0.0001	0.00995	0.09	0.9	9	15	
13	7.5	7.5	9	0.9	0.09	0.00995	0.0001	0.00995	0.09	0.9	9	7.5	7.5

Figure 4.2 through Figure 4.5 show the areal grid view for fracture girds, areal view for the middle reservoir layer illustrating wellbore grid structure, magnified fracture grid, and 3D grid of the reservoir model, respectively.

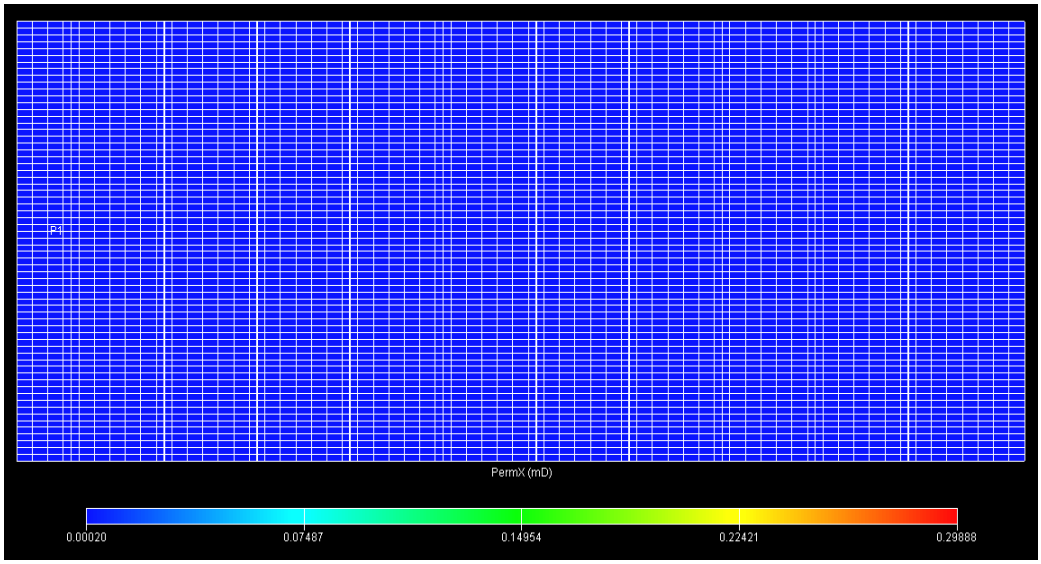

Figure 4.2 Areal view of the reservoir model with ten natural fractures

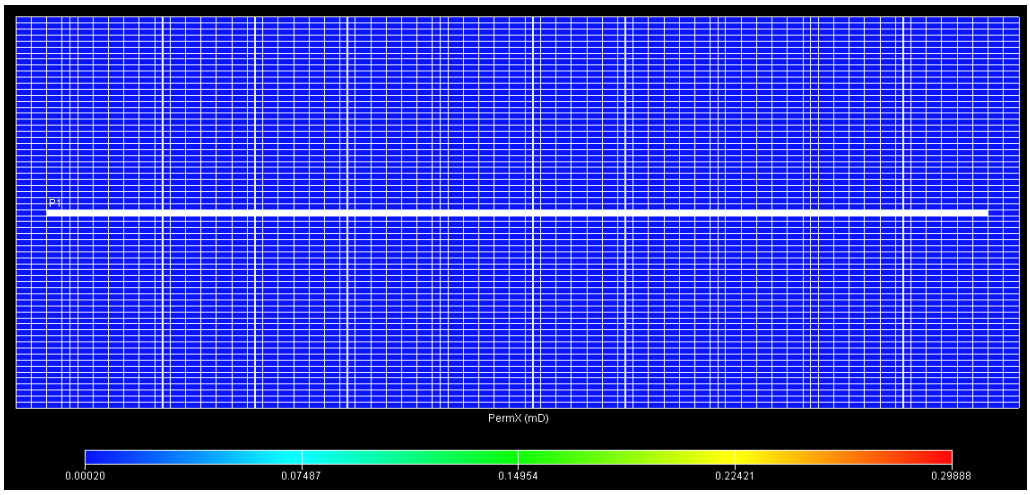

Figure 4.3 Areal view of the reservoir model at
the middle layer showing wellbore grid structure

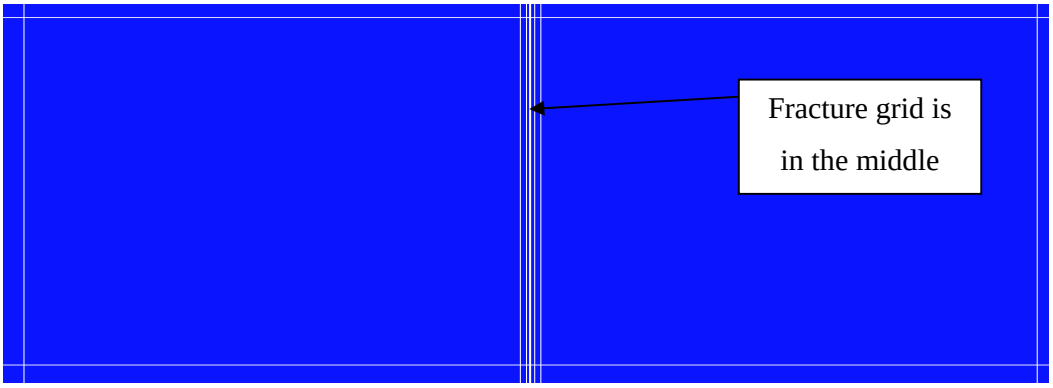

Figure 4.4 Magnified view of fracture grid

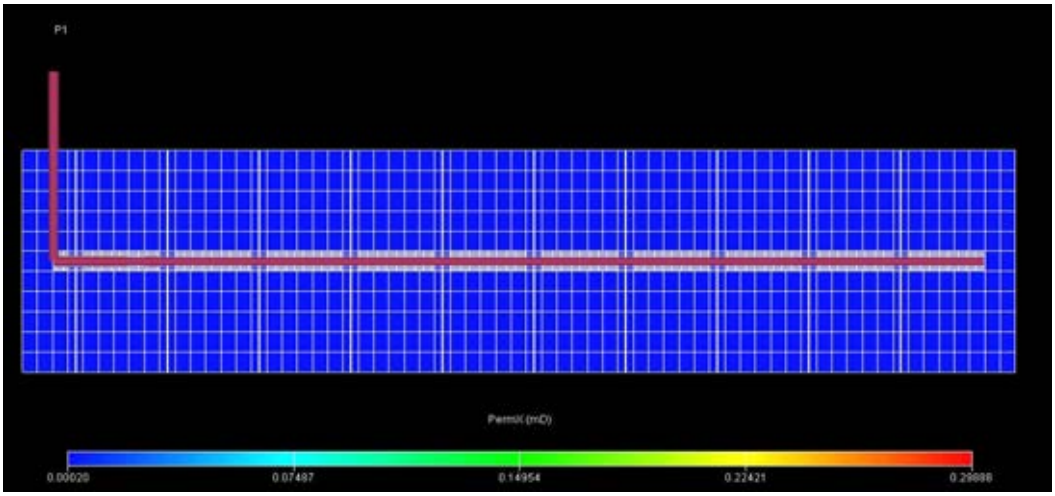

Figure 4.5 Side view of the reservoir model

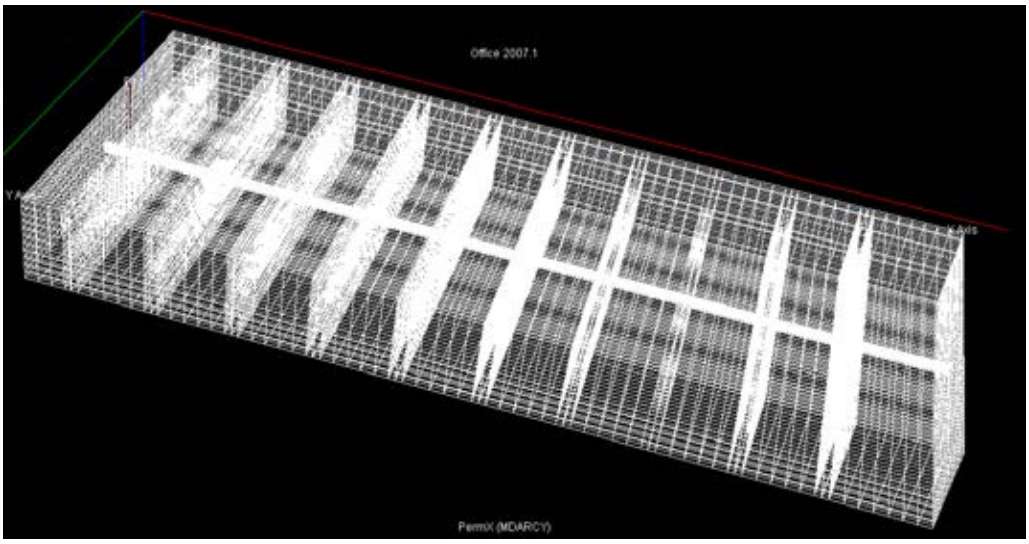

Figure 4.6 3D view with transparent grid of the reservoir model

4.2 Fluid Properties Section

In this model, the reservoir temperature is constant of 260 °F. PVT properties are generated by ECLIPSE using keywords PVTW and PVDG which represent the properties of water and that of dry gas, respectively. The tables 4.4 and 4.5 present the PVTW and PVDG properties. Table 4.6 shows fluid densities and rock properties calculated by the ECLIPSE reservoir simulator.

Table 4.4 Water PVT properties

Properties	**Value**
Reference pressure, psi	3,500
Water FVF at the reference pressure, rb/stb	1.045
Water compressibility, psi^{-1}	3.53×10^{-6}
Water viscosity at the reference pressure, cP	0.225

Table 4.5 Dry gas properties

Gas phase pressure (psia)	Gas FVF (rb/Mscf)	Gas viscosity (cP)
14.7000	245.5998	0.0142
224.4526	15.8915	0.0143
434.2053	8.1219	0.0146
643.9579	5.4190	0.0148
853.7105	4.0486	0.0151
1063.4630	3.2225	0.0155
1273.2160	2.6720	0.0159
1482.9680	2.2803	0.0163
1692.7210	1.9885	0.0167
1902.4740	1.7638	0.0172
2112.2260	1.5861	0.0177
2321.9790	1.4428	0.0183
2531.7320	1.3253	0.0188
2741.4840	1.2277	0.0194
2951.2370	1.1455	0.0200
3160.9890	1.0757	0.0206
3370.7420	1.0159	0.0212
3590.2510	0.9620	0.0219
3790.2470	0.9192	0.0225
4000.0000	0.8798	0.0231

Table 4.6 Fluid densities and rock properties

Parameter		Value
Fluid densities at surface conditions	Oil density, lb/ft^3	49.999
	Water density, lb/ft^3	62.428
	Gas density, lb/ft^3	0.0436
Rock properties	Reference Pressure, psia	3500
	Rock compressibility, psi^{-1}	6.654×10^{-6}

4.3 SCAL (Special Core Analysis) Section

The gas and water saturation function is illustrated in Table 4.7. This model is built with two phase fluids consisting of water and gas. Two types of relative permeability, k_{rg} and k_{rw} are used; k_{rg} is gas relative permeability and k_{rw} is water relative permeability. The data is generated by ECLIPSE simulator using Corey correlation.

Table 4.7 Gas/water saturation and gas/water relative permeability

S_w	k_{rw}	S_g	k_{rg}
0.3000	0.0000	0.0000	0.0000
0.3700	0.0001	0.0700	0.0010
0.4400	0.0016	0.1400	0.0080
0.5100	0.0081	0.2100	0.0270
0.5800	0.0256	0.2800	0.0640
0.6500	0.0625	0.3500	0.1250
0.7200	0.1296	0.4200	0.2160
0.7900	0.2401	0.4900	0.3430
0.8600	0.4096	0.5600	0.5120
0.9300	0.6561	0.6300	0.7290
1.0000	1.0000	0.7000	1.0000

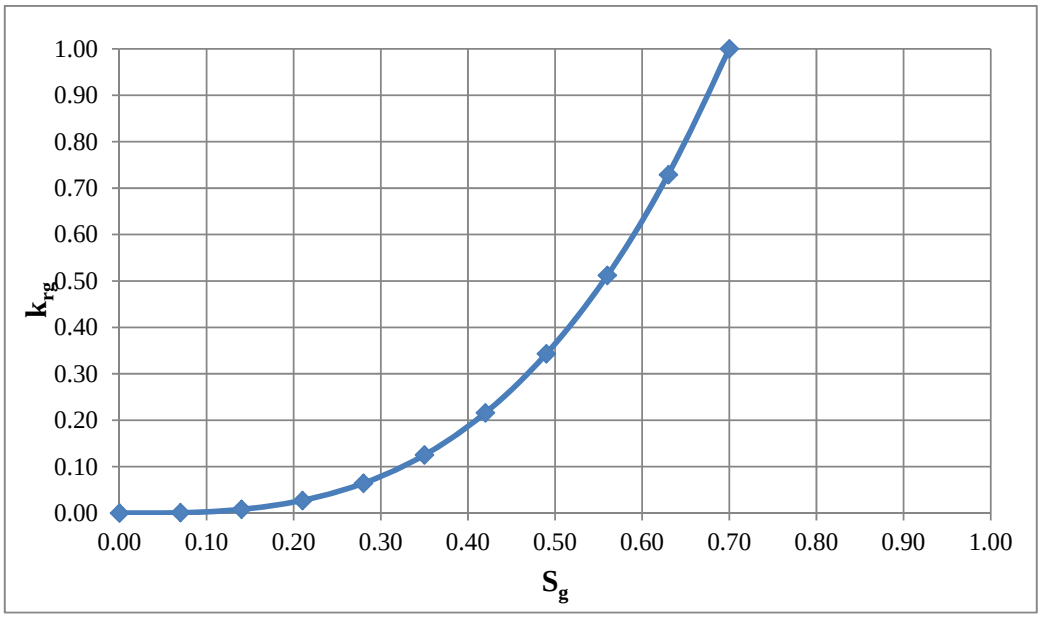

Figure 4.7 Gas relative permeability versus gas saturation

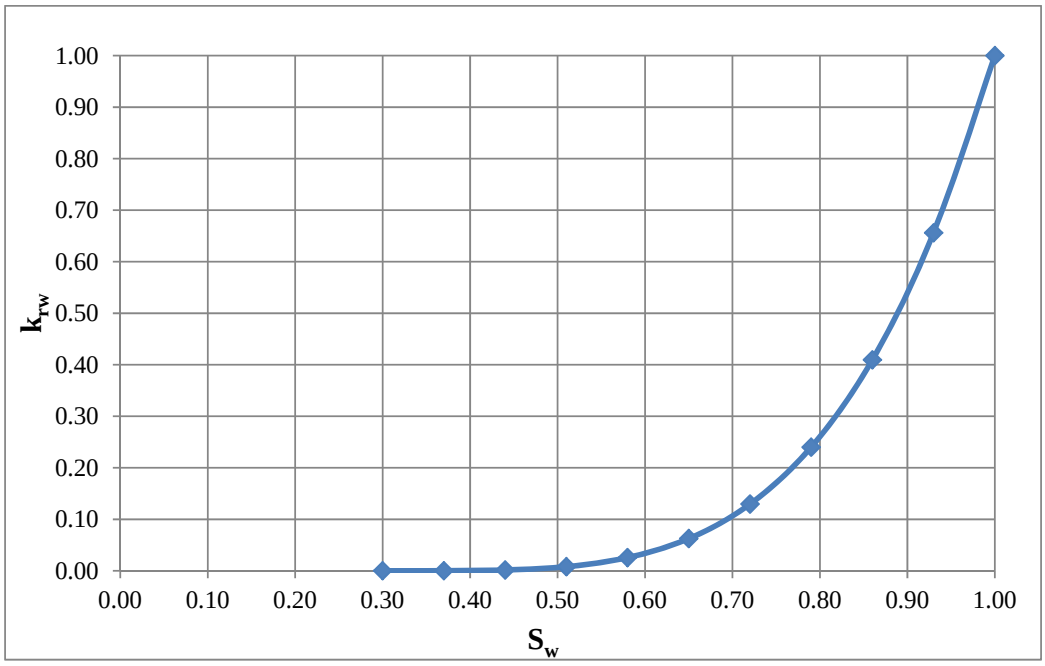

Figure 4.8 Water relative permeability versus water saturation

4.4 Well Model

In this model study, a production horizontal well is constructed using a well diameter of 6 ½ inches and is located at the depth of 8,055ft. The length of the horizontal well is 3,050ft. 3½ inches production tubing is run into the production zone. In this well model, tubing head pressure is defined at 450 psi. Pressure losses along the tubing string are calculated using VFP table. The VFP table offers the most flexible, and potentially the most accurate, means of determining the pressure drop across each segment. In this study, it uses a PROSPER software [26] to generate the VFP table.

Multi-Segment well function is utilized in this study. Multi-Segment Well function provides a detailed description of fluid flow in the well bore. The facility is specifically designed for horizontal and multi-lateral wells; this case is used in the horizontal well. The detailed description of the fluid flow conditions within the well is obtained by dividing the well bore into a number of 1-dimentional segments.

There are four variables per segment which are the fluid pressure, the total flow rate, the flowing fractions of water and gas. Each segment describes the local fluid conditions. In this model, open hole production is used. The variables within each segment are evaluated by solving material balance equations for each phase or component and a pressure drop equation that takes into account the local hydrostatic, friction, acceleration pressure gradients. The pressure drop is calculated using homogeneous flow model where all phases flow within the same velocity that allows slip between the phases. Figure 4.9 shows the multi-segment well diagram.

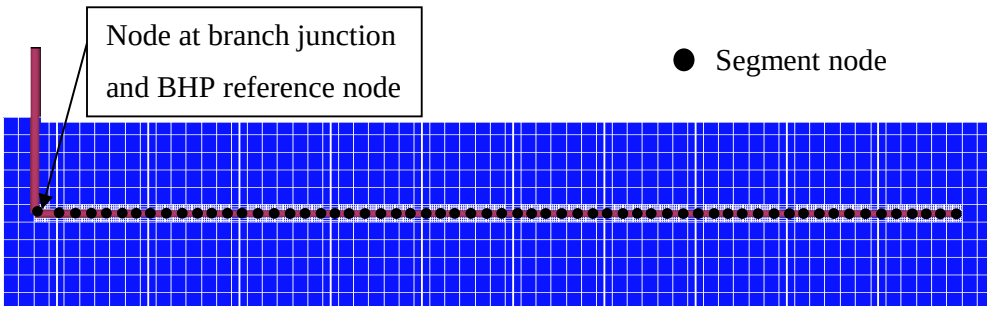

Figure 4.9 A multi-segment well

CHAPTER V

RESULTS AND DISCUSSION

The base case is modeled with 10 natural fractures using the reservoir properties as described in the chapter IV. Succeeding that, reservoir performance is evaluated by accounting for the following parameters.

- Matrix porosities
- Matrix permeabilities
- Number of fractures (also with minimum and maximum matrix permeability)
- Fracture widths (also with minimum and maximum matrix permeability)

Each case study reveals reservoir performance versus time, reservoir pressure and gas saturation profile in the reservoir. The objective is to examine the effects of each parameter on gas productivity in order to understand production performance of shale gas reservoir. Production period is set at 20 years as shale gas production rate drastically declines in early-time then gradually decrease and eventually is stable in later-time. Therefore, observing 20 years production is sufficient for hydraulic fracturing strategy assessment. Table 5.1 shows the reservoir parameter variations applied on this study.

Table 5.1 Variable parameters used in the reservoir simulation models

Parameter	**Value**							
Matrix Porosity (%)	4	8	12					
Matrix Permeability (mD)	0.00007	0.0001	0.0002	0.0003	0.0004	0.0005		
Number of Fractures	10	20	30	60				
Fracture Width (mm)	0.015	0.03	0.15	0.30	0.60	1.20	2.40	3.00

5.1 Gas Production Performance Producing from Natural Fractures

The base case is built utilizing a horizontal well bore production. The well is drilled through the shale reservoir penetrating through natural fracture planes perpendicular to the well bore. Gas reservoir is produced through 10 natural fractures. A tubing head pressure is controlled at 450psi. Figure 5.1 illustrates the gas production rate from 10 natural fractures with 0.0002mD matrix permeability, 8% porosity, and 0.03mm natural fracture width. Gas production rate is initially produced at 140 MSCF/day then quickly declines to 3 MSCF/day at the end of 2 years production. Afterward, the production rate gradually decreases and is stable at 2.5 MSCF/day throughout 20 years production. Figure 5.2 illustrates cumulative gas production showing a straight line after 2 years production. Gas recovery factor for producing gas from natural fractures is 0.49% given the original gas in place (OGIP) of 4.78 BSCF. Figures 5.3 and 5.4 represent reservoir pressure and gas saturation profiles. Reservoir pressure almost remains unchanged throughout 20 years production. The reservoir pressure drops from 3555psi to 3536psi which is only 19psi depletion. Since reservoir fluid is modeled as dry gas, it is technically not affecting much in terms of gas saturation change as gas expansion always occurs.

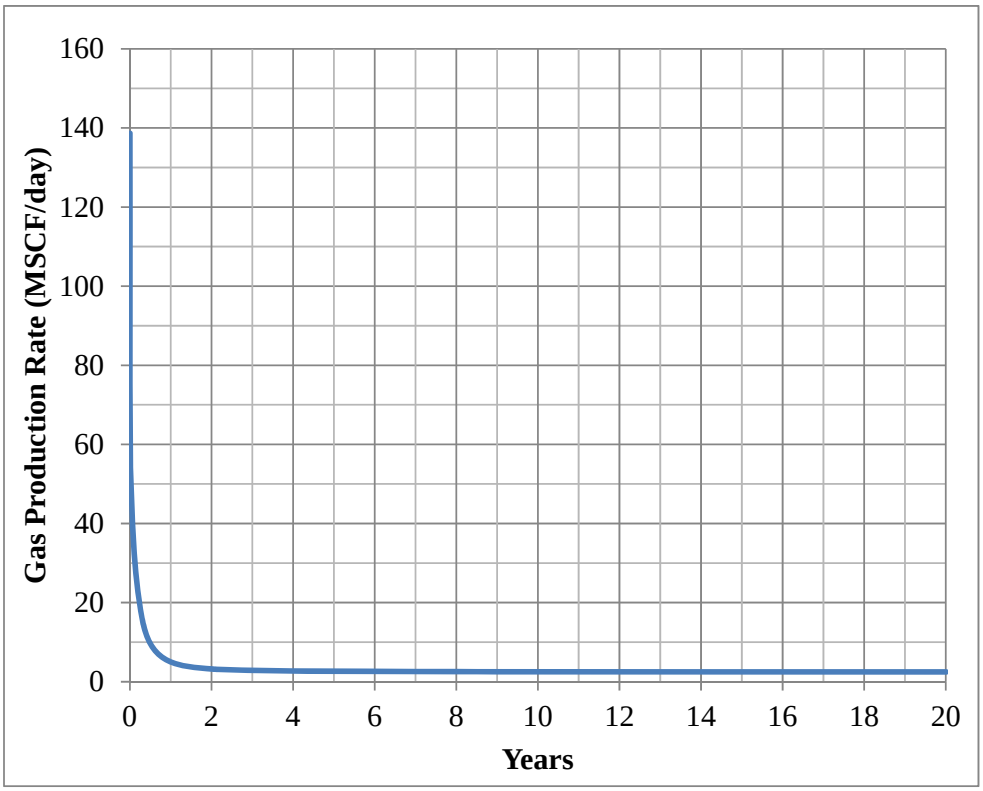

Figure 5.1 Gas production rate of the base case

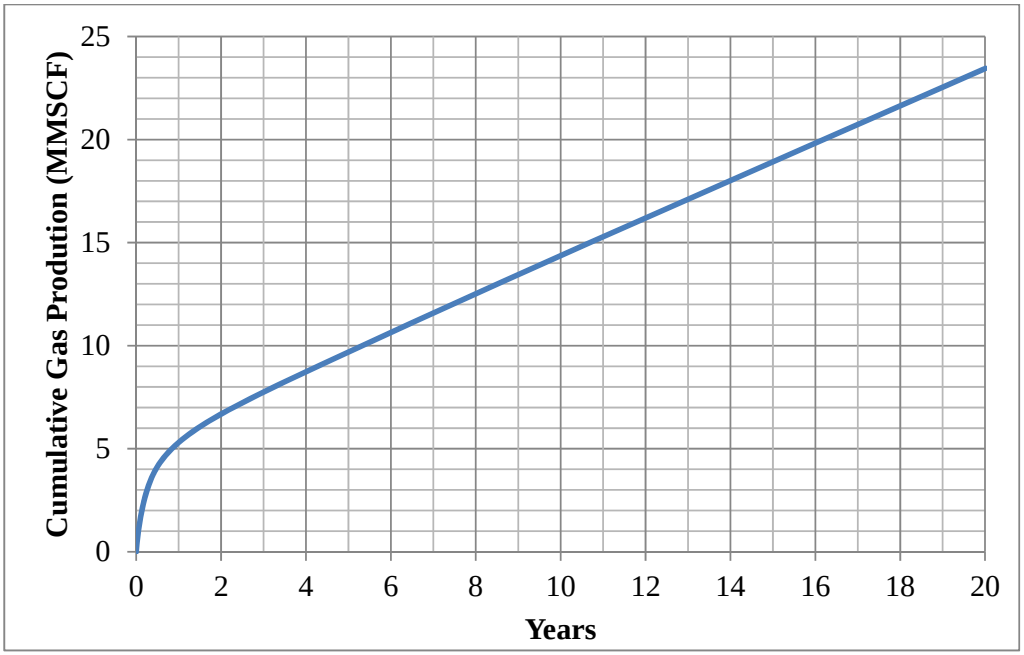

Figure 5.2 Cumulative gas production rate of the base case

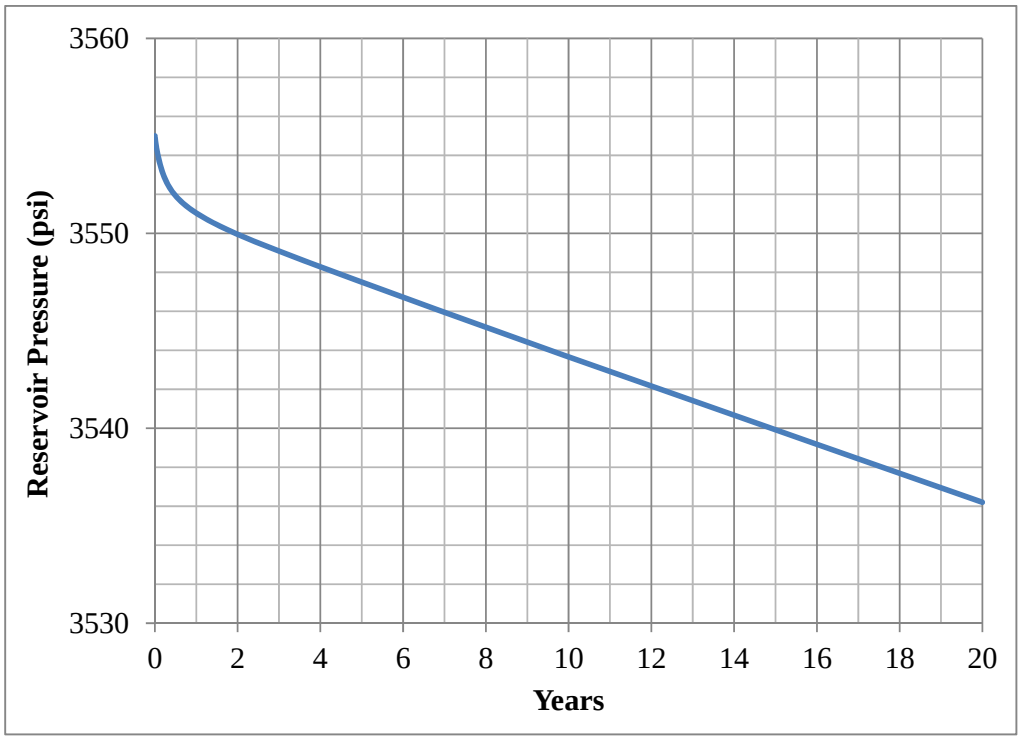

Figure 5.3 Reservoir pressure profile of the base case

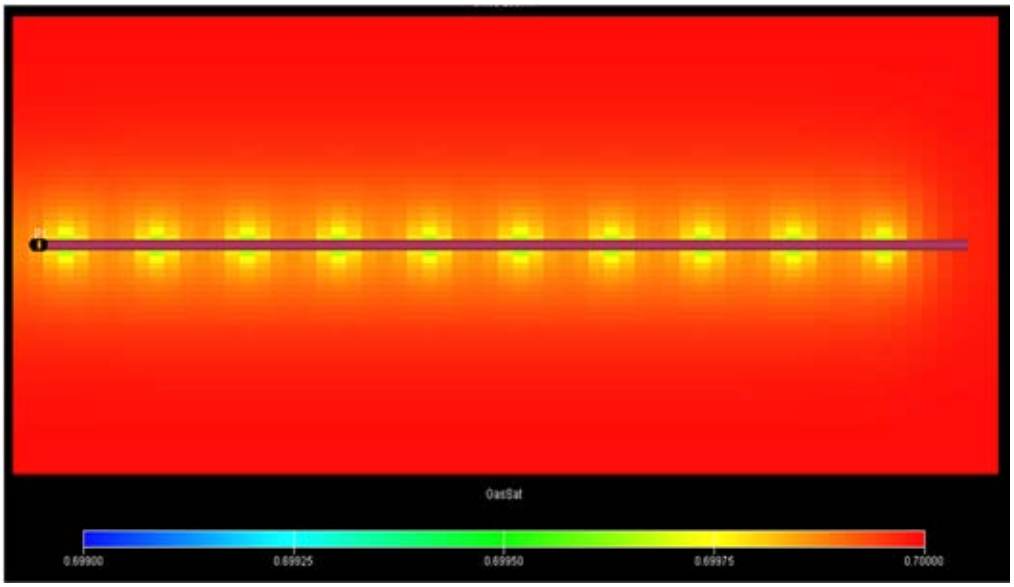

Figure 5.4 Gas saturation at the end of production of the base case

5.2 Effect of Reservoir Properties

This section investigates the effect of reservoir properties to assess gas production performance. Two parameters are evaluated which are matrix porosity and matrix permeability. The other input parameters are maintained constant same as in the base case.

5.2.1 Matrix Porosity

Matrix porosity of 4%, 8%, and 12% are used in the reservoir simulation model. Figures 5.5 and 5.6 represent gas production rate and cumulative gas production for different porosities. The results apparently show insignificant effect on gas production in the late-time but it affects in the first two years production. Higher porosity seems to aid the production rate in early-time due to the larger gas storage in the reservoir near the fractures. This gas is initially produced when the production starts. Therefore, the higher gas production rate can be observed in the first two years for the higher matrix porosity cases. Figure 5.7 shows reservoir pressure profile. The pressure drop for higher porosity case is less than the lower porosity case. It can be described that when the gas is being produced, the higher gas expansion occurs in the higher storage or higher porosity cases thereby less pressure drop can be a result. This concept can be applied on the gas saturation profiles show in Figures 5.8 through 5.10. Table 5.2 shows the summary of gas recovery factor for different porosities.

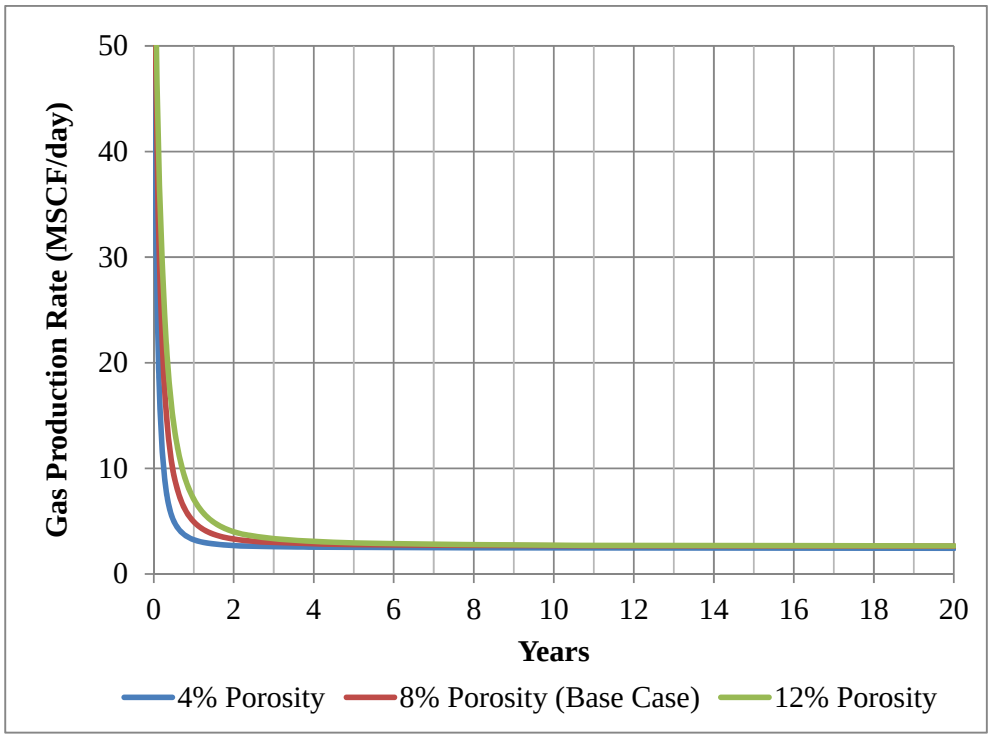

Figure 5.5 Gas production rate for different porosities

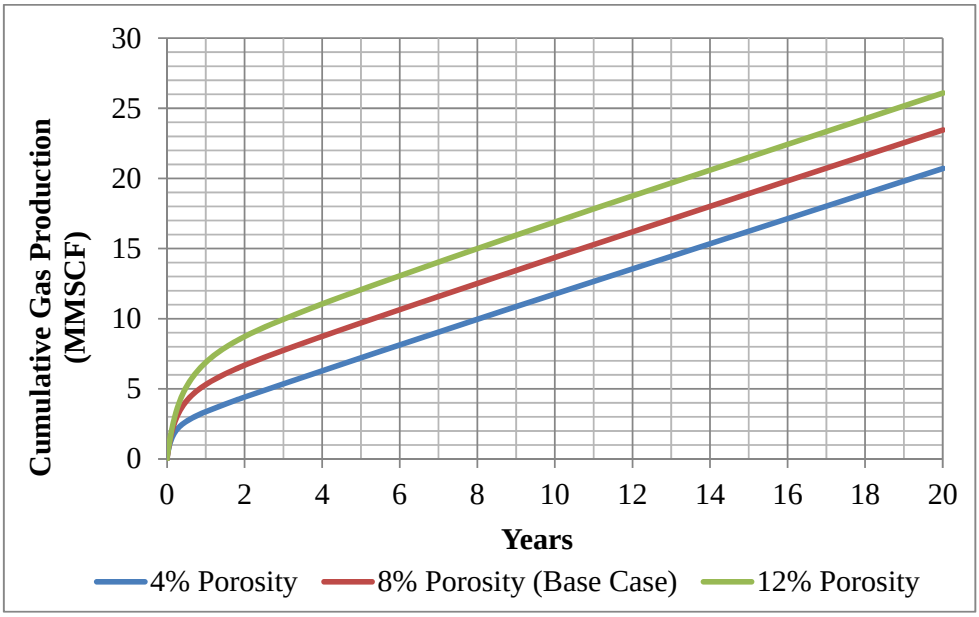

Figure 5.6 Cumulative gas production for different porosities

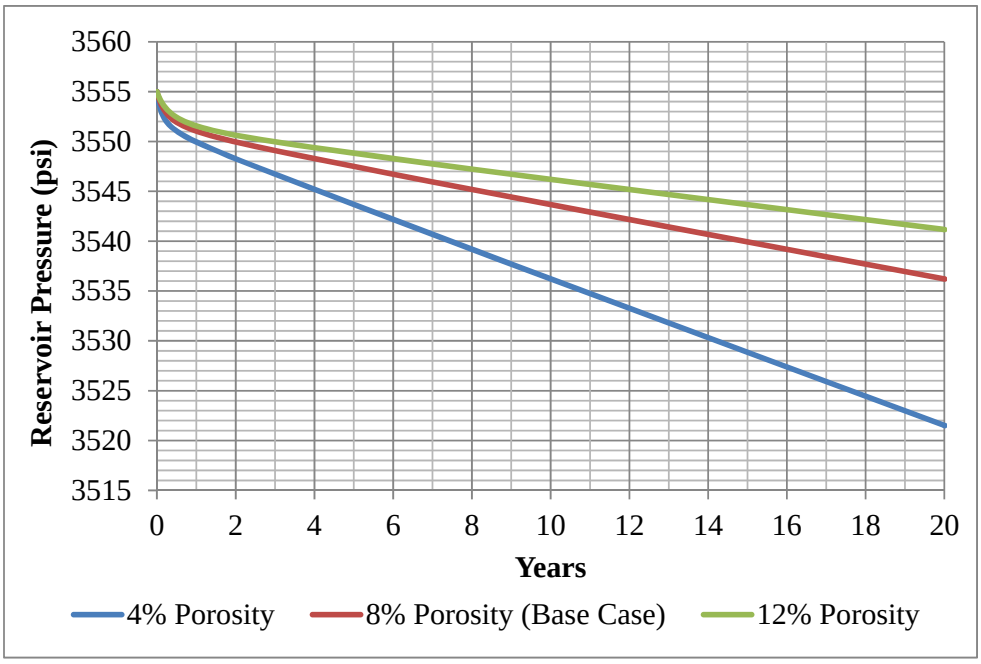

Figure 5.7 Reservoir pressure for different porosities

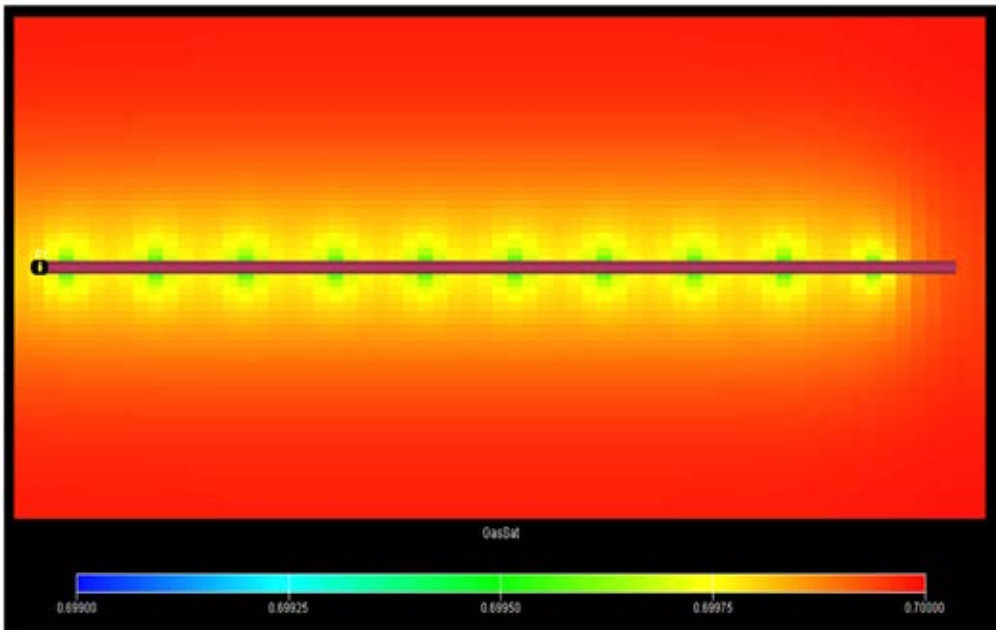

Figure 5.8 Gas saturation profile for 4% porosity

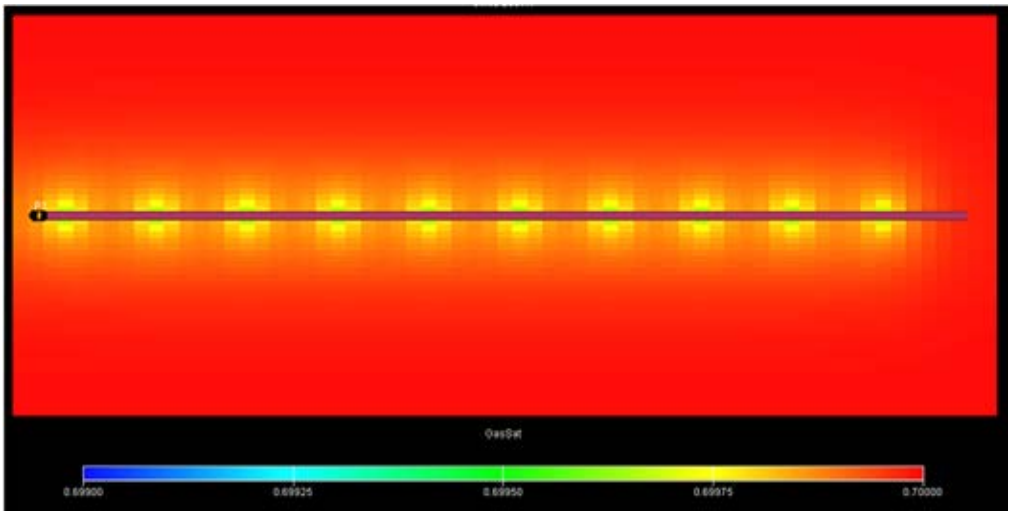

Figure 5.9 Gas saturation profile for 8% porosity (Base Case)

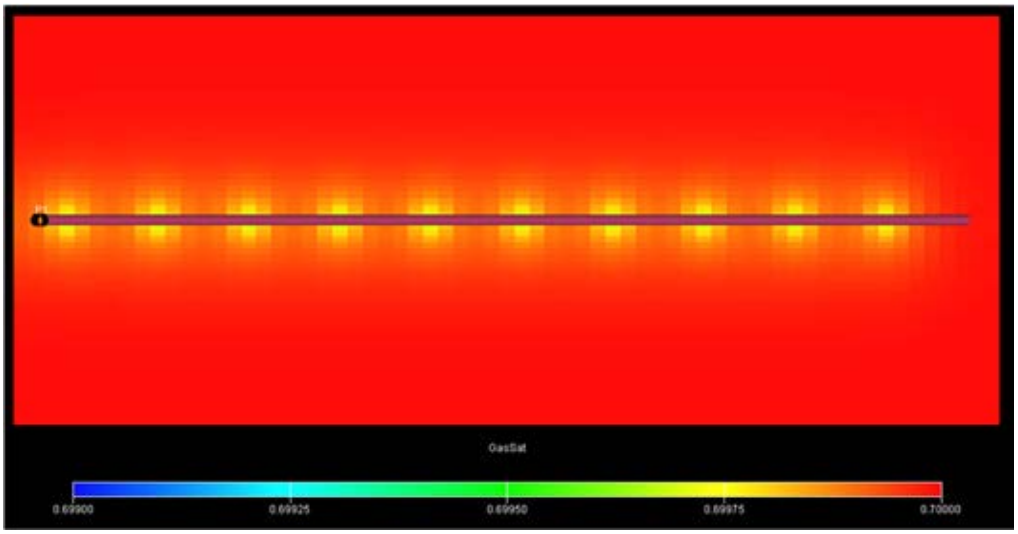

Figure 5.10 Gas saturation profile for 12% porosity

Table 5.2 Summary of gas recovery factor for different matrix porosities at the end of production

Matrix Porosity (%)	**OGIP (BSCF)**	**Cumulative Gas Production (BSCF)**	**Gas Recovery Factor (%)**
4	2.39	0.0207	0.87
8	4.78	0.0235	0.49
12	7.17	0.0261	0.36

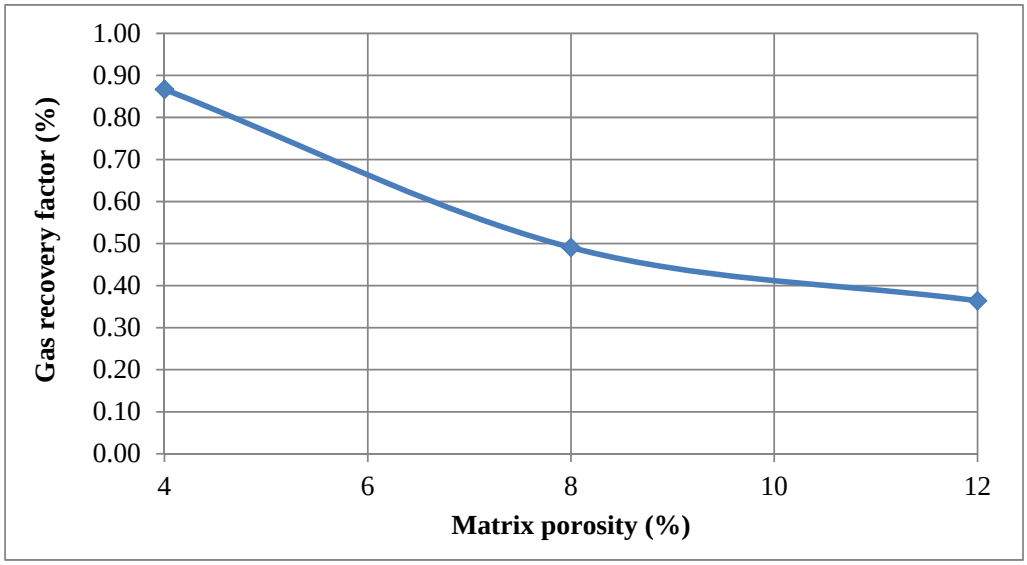

Figure 5.11 Porosity and gas recovery factor relationship

From Table 5.2, cumulative gas productions for all three cases are 0.0207BSCF, 0.0235BSCF and 0.0261BSCF for matrix porosity of 4%, 8% and 12%, respectively. With respect to similarity of gas productivity indicates that porosity does not have much effect on production performance. Figure 5.11 shows the relationship between matrix porosity and gas recovery factor. Gas recovery factor of 12% porosity case is lowest as a result of produced gas relative to OGIP is smallest compare to the lower porosity cases.

5.2.2 Matrix Permeability

Matrix permeabilities of 0.00007mD, 0.0001mD, 0.0002mD, 0.0003mD, 0.0004mD and 0.0005mD are evaluated. Figure 5.12 and Figure 5.13 illustrate the production performance for various matrix permeabilities. The production rate drastically decreases and is gradually stable after 2 years production for all cases. Gas recovery at 20 years production of 0.13%, 0.13%, 0.49%, 0.68%, 0.89% and 1.09% can be achieved for matrix permeabilities of 0.00007mD through 0.0005mD, respectively.

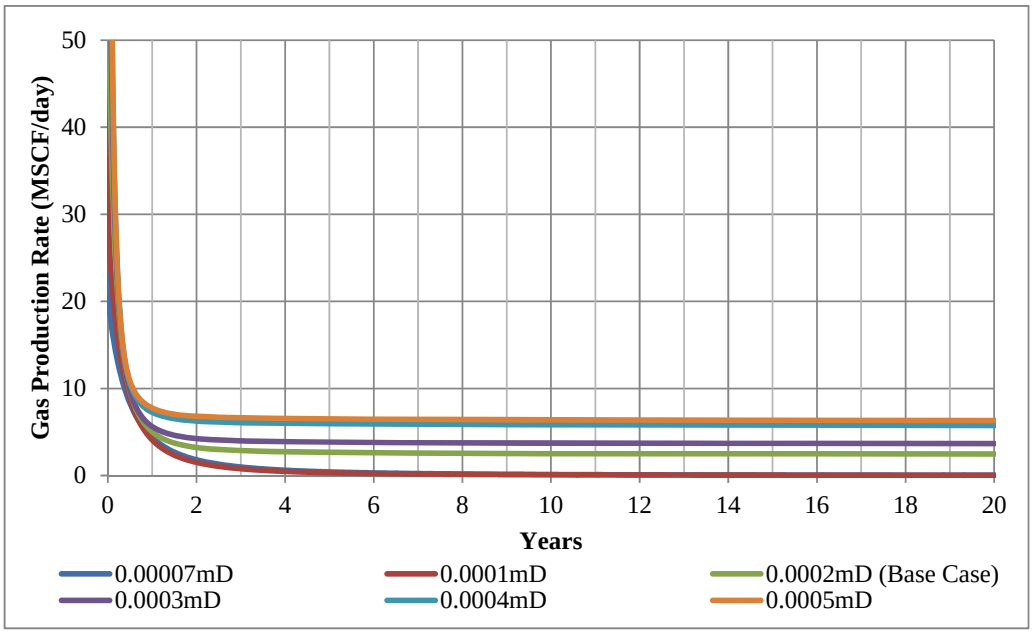

Figure 5.12 Gas production rate for different matrix permeabilities

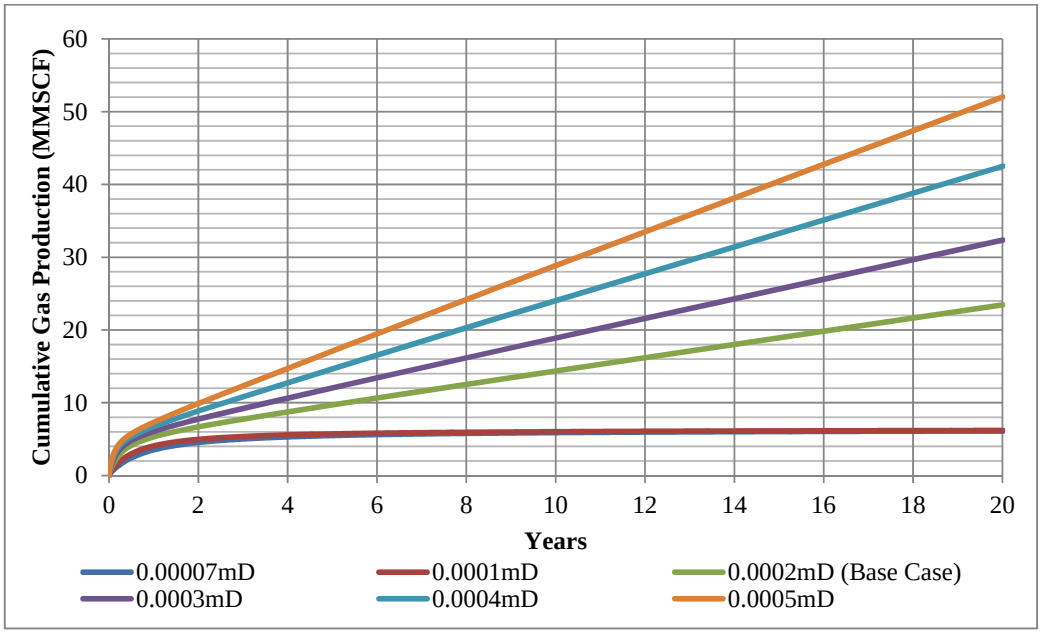

Figure 5.13 Cumulative gas productions for different matrix permeabilities

Figure 5.14 represents the reservoir pressure profile plot against production time for different permeabilities. The average pressure drops for the two least permeability cases are greater than other cases. This is due to the fact that reservoir

with ultra-low permeability; gas has limited capability to flow across the matrix therefore gas production mostly come from the fractures or around the fractures only. Since the gas flow from the formation to the fractures is slower in the low matrix permeability case, the pressure in the fractures decreases more quickly and the gas expansion does not fully occur. The higher pressure drop in the low matrix permeability cases can be a result. When the matrix permeabilities are increased to 0.0002mD through 0.0005mD, the ability of gas flow in the matrix becomes more pronounced. The produced gas zone in the fractures and the wellbore areas are then displaced with gas from the formation more rapidly as well as gas expansion occurs in the matrix itself. As a result, the pressure change across the reservoir for the 0.0002mD through 0.0005mD cases is not clearly seen.

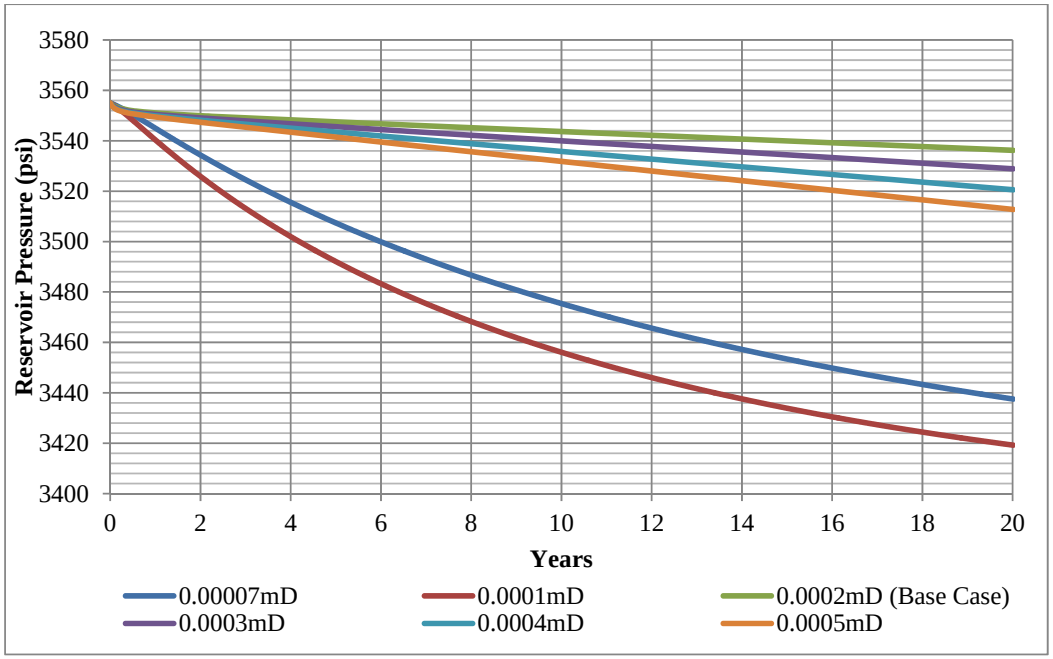

Figure 5.14 Reservoir pressure for different matrix permeabilities

Gas saturation profiles exhibit similarly to reservoir pressure. The two least permeability cases (Figures 5.15 and 5.16) show gas saturation profiles reduce rapidly around the fractures and the well bore but their production rates are less than other cases. This is because gas flow slower in the matrix compare to other cases. Figures

5.17 through 5.20 show the similar saturation profile; gas saturation reduction is not obviously seen when matrix permeabilities are increased.

Table 5.3 shows the summary of cumulative gas production and gas recovery factor for different matrix permeabilities. Figure 5.21 shows matrix permeability and gas recovery factor relationship. Gas recovery factors for 0.00007mD and 0.0001mD matrix permeability display similarly. Significant changes in gas productivity when increasing matrix permeability from 0.0002mD to 0.0005mD can be observed.

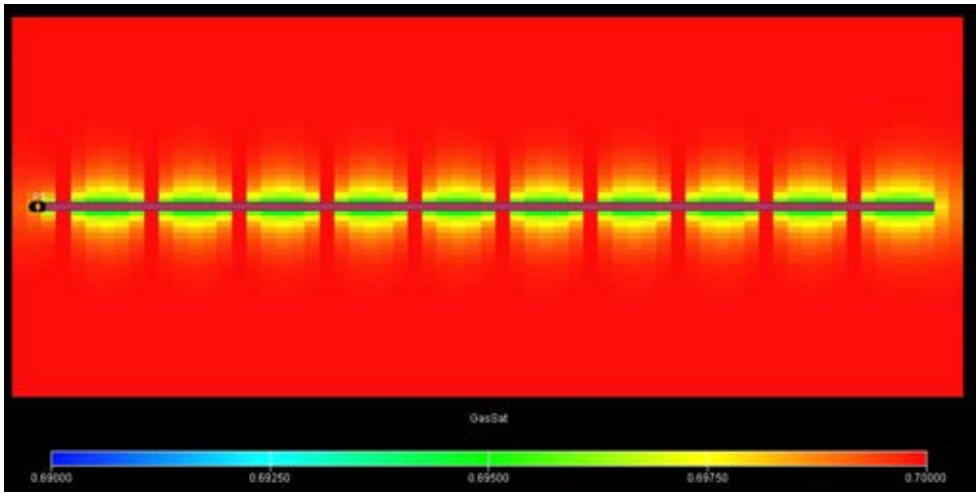

Figure 5.15 Gas Saturation Profile, 0.00007mD

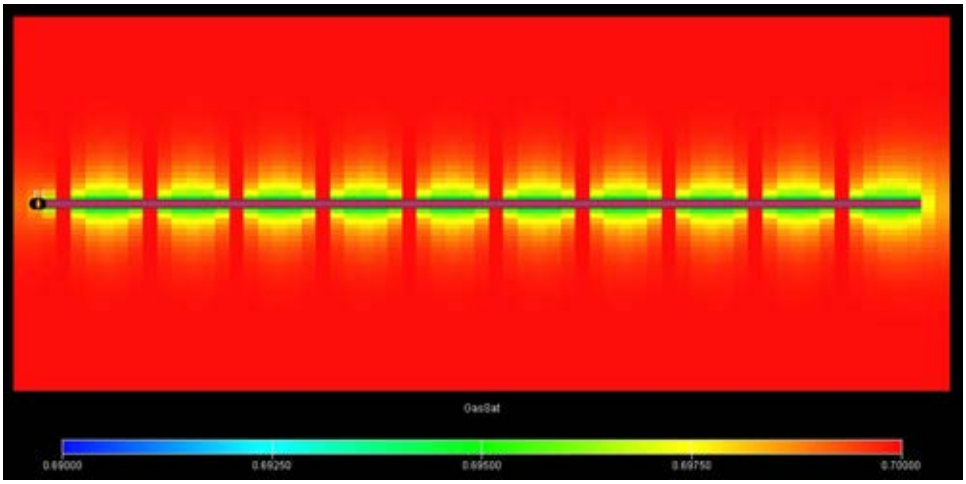

Figure 5.16 Gas Saturation Profile, 0.0001mD

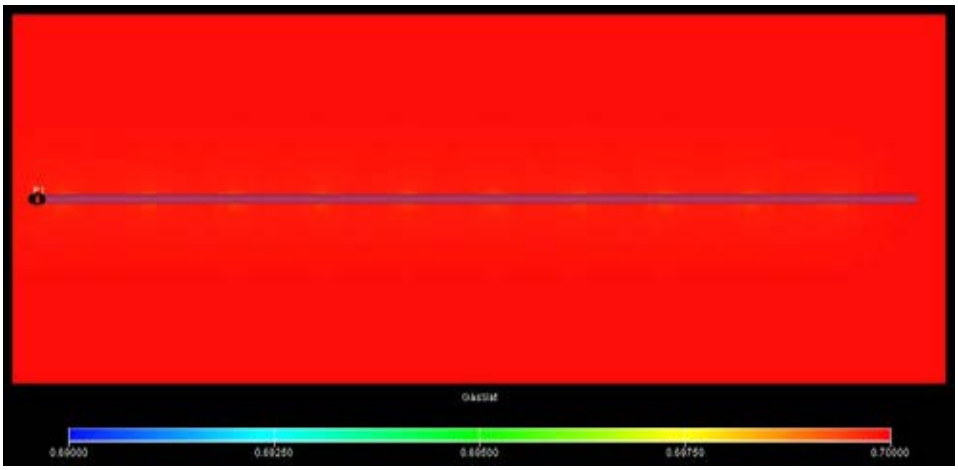

Figure 5.17 Gas Saturation Profile, 0.0002mD

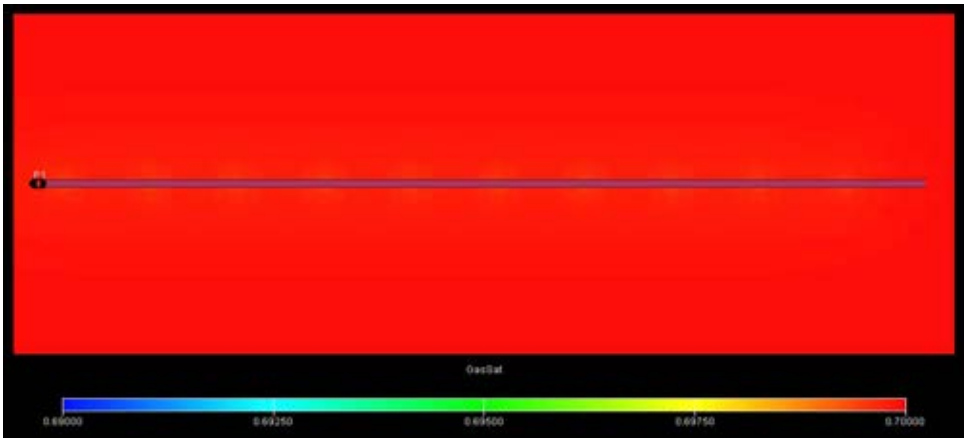

Figure 5.18 Gas Saturation Profile, 0.0003mD

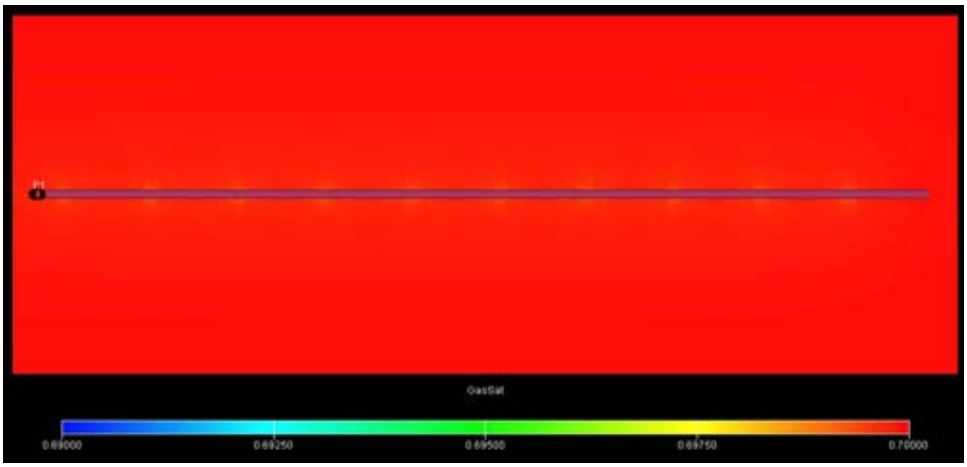

Figure 5.19 Gas Saturation Profile, 0.0004mD

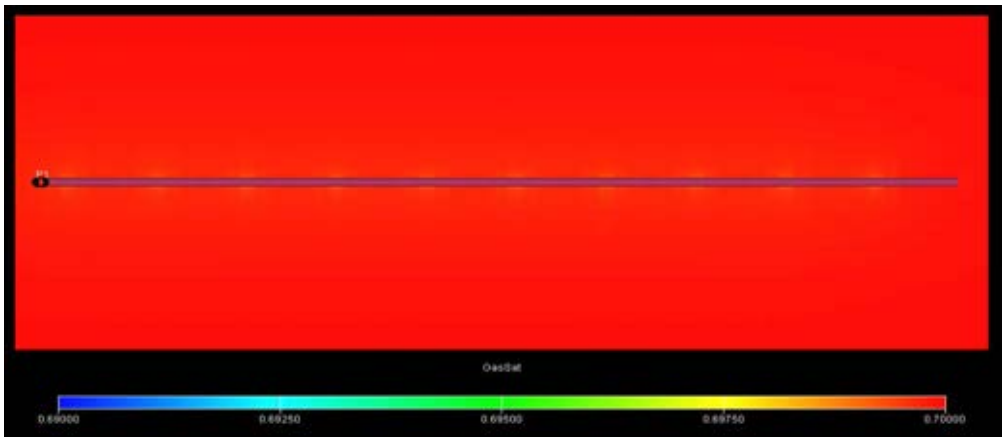

Figure 5.20 Gas Saturation Profile, 0.0005mD

Table 5.3 Summary of gas recovery factor for
different matrix permeabilities at the end of production

Matrix Permeability (mD)	OGIP (BSCF)	Cumulative Gas Production (BSCF)	Gas Recovery Factor (%)
0.00007	4.78	0.0061	0.13
0.0001	4.78	0.0062	0.13
0.0002	4.78	0.0235	0.49
0.0003	4.78	0.0324	0.68
0.0004	4.78	0.0425	0.89
0.0005	4.78	0.0520	1.09

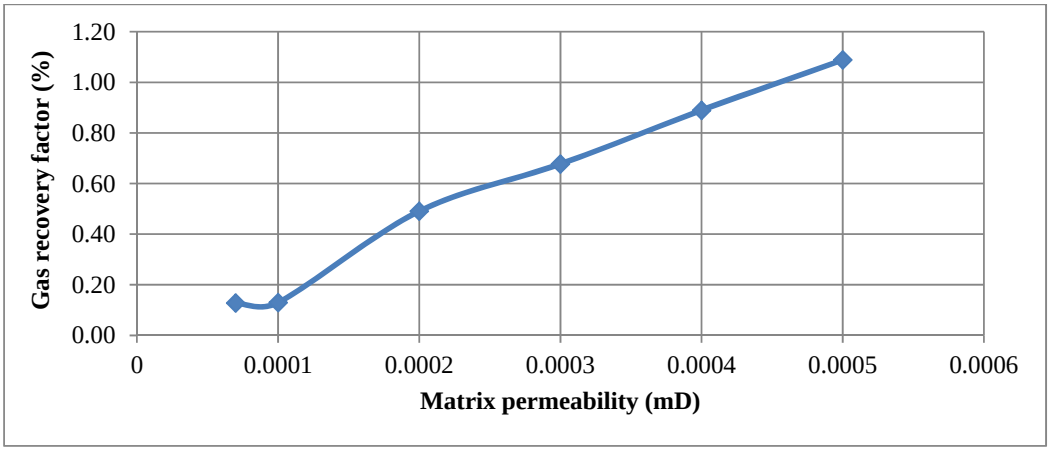

Figure 5.21 Matrix permeability and gas recovery factor relationship

5.3 Effect of Number of Fractures and Spacing

Various number of fractures are modeled include 10 (base case), 20, 30 and 60 fractures and symmetrical spacing are maintained of 300ft, 150ft, 100ft, and 50ft, respectively. Other reservoir properties are kept constant same as in the base case using 0.03mm fracture width, 8% porosity, and 0.0002mD matrix permeability. Figures 5.22 and 5.23 show the comparison of gas production rate and cumulative gas production for various number of fractures. Figure 5.24 represents pressure profile comparison. Gas saturation profile of 60 fractures case is shown on Figure 5.25. For other cases can be found in the appendix section from A-1 through A-3.

From the results show 60 fractures case provides the highest gas production rate and greatest cumulative gas production. The production rate drastically declines from 91 MSCF/day to 15 MSCF/day in 2.5 months then maintains stable at 13 MSCF/day throughout the end of production. The other cases, the initial gas production rate is greater than 100 MSCF/day but it rapidly decreases and maintain stable at less than 10 MSCF/day after 2 years production. The higher number of fractures cases exhibit less gas production rate at the initial production as a result of the gas in the formation near the well bore partially flows into the fractures instead of flows directly to the wellbore. At the end of production, gas recovery factor for 10 fractures through 60 fractures case are 0.49%, 0.80%, 1.18%, and 1.99%, respectively. Table 5.4 shows the summary of cumulative gas production and gas recovery at the end of production.

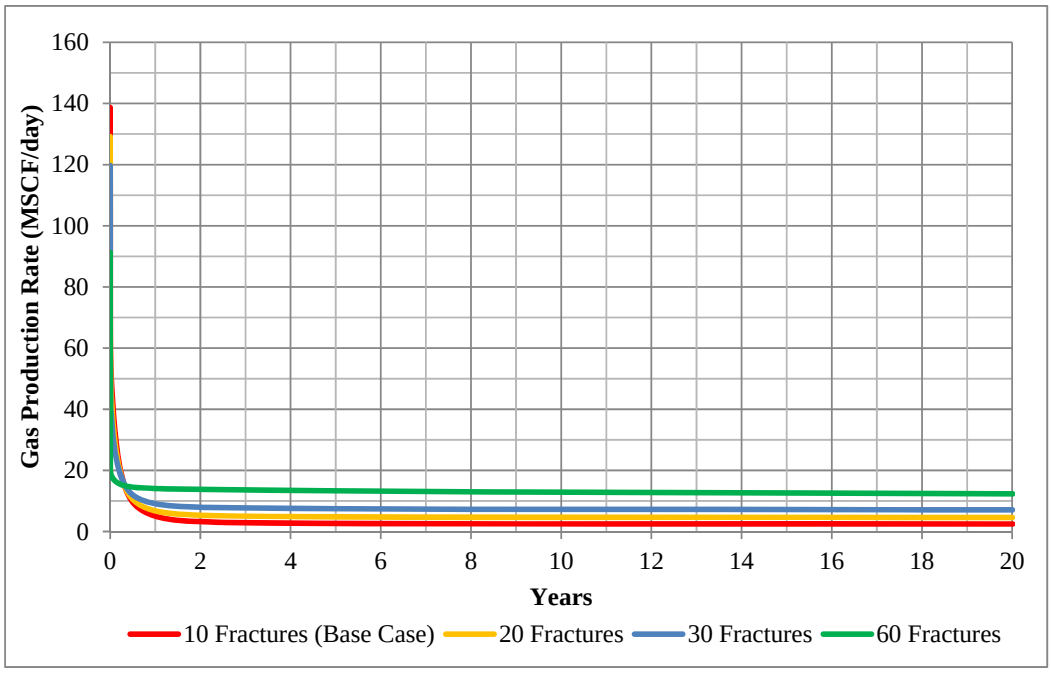

Figure 5.22 Gas production rate for different number of fractures

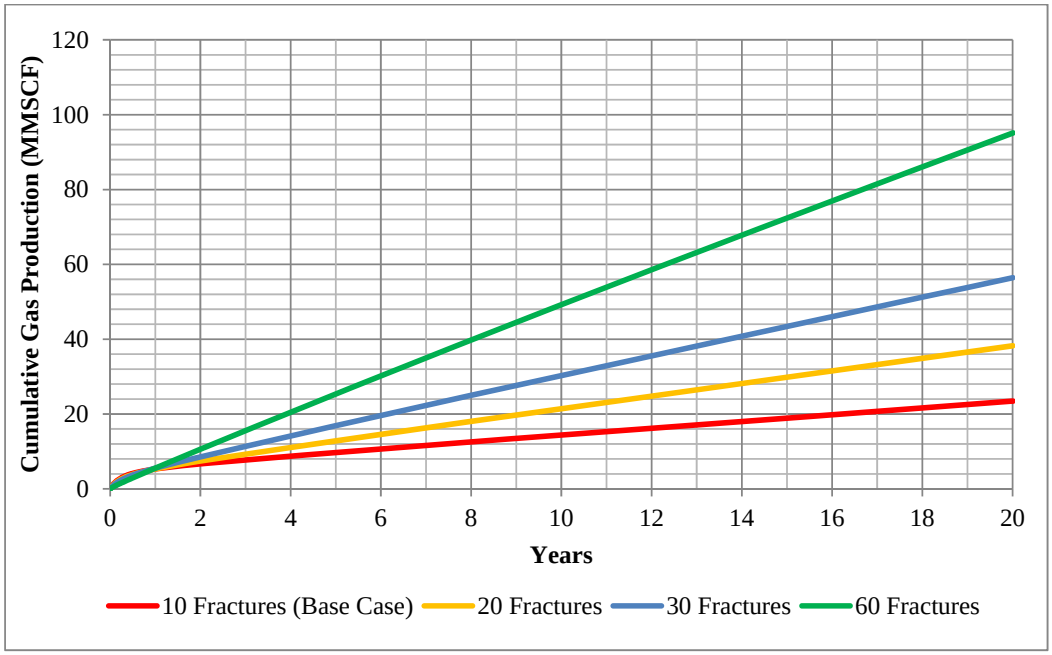

Figure 5.23 Cumulative gas productions for different number of fractures

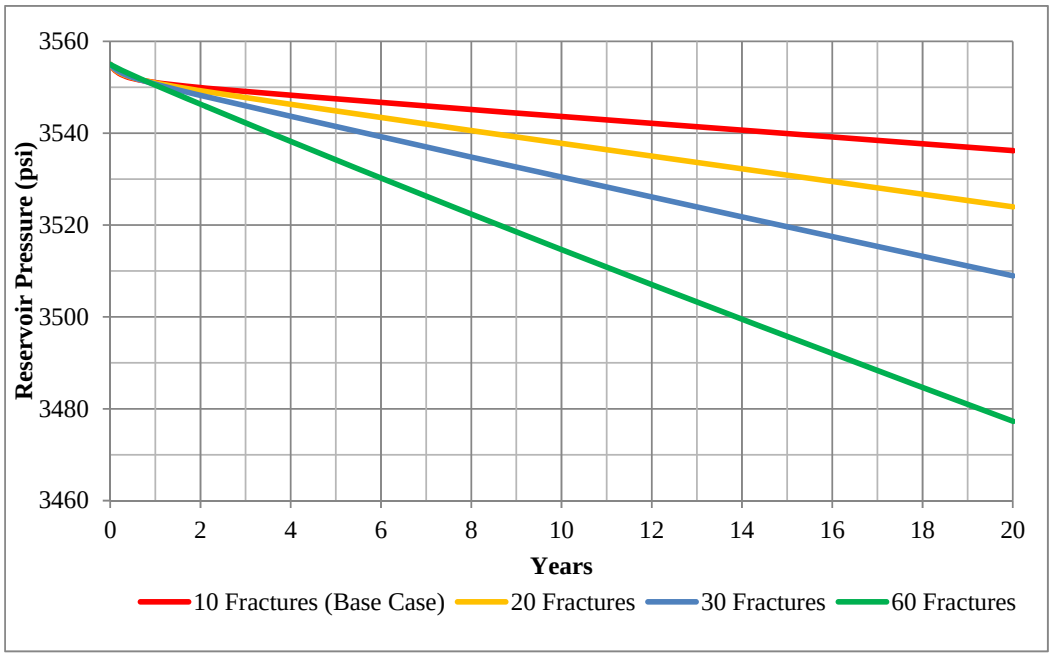

Figure 5.24 Reservoir pressure profile for different number of fractures

The change in gas saturation profile is greatest for 60 fractures case. It can be defined that the increase in number of fractures can bring more contact area of the reservoir into the fractures so the gas can be drained to the greater degree.

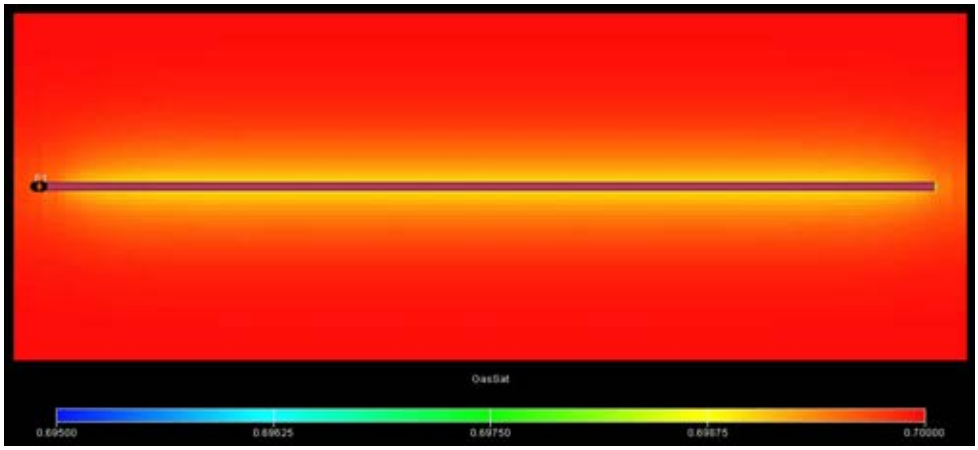

Figure 5.25 Gas saturation for 60 fractures
at the end of well production

Table 5.4 Summary of gas recovery factor for
different number of fractures at the end of production

Number of Fractures	OGIP (BSCF)	Cumulative Gas Production (BSCF)	Recovery (%)
10	4.78	0.0235	0.49
20	4.78	0.0382	0.80
30	4.78	0.0564	1.18
60	4.78	0.0951	1.99

Gas recovery factor is plotted against number of fractures as shown in Figure 5.26. It shows linear relationship between these two factors. The more number of fractures delivers the higher gas recovery factor given 8% matrix porosity, 0.03mm fracture width, and 0.0002mD matrix permeability. At the end of production, 60 fracture yields the greatest gas recovery factor of 1.99%.

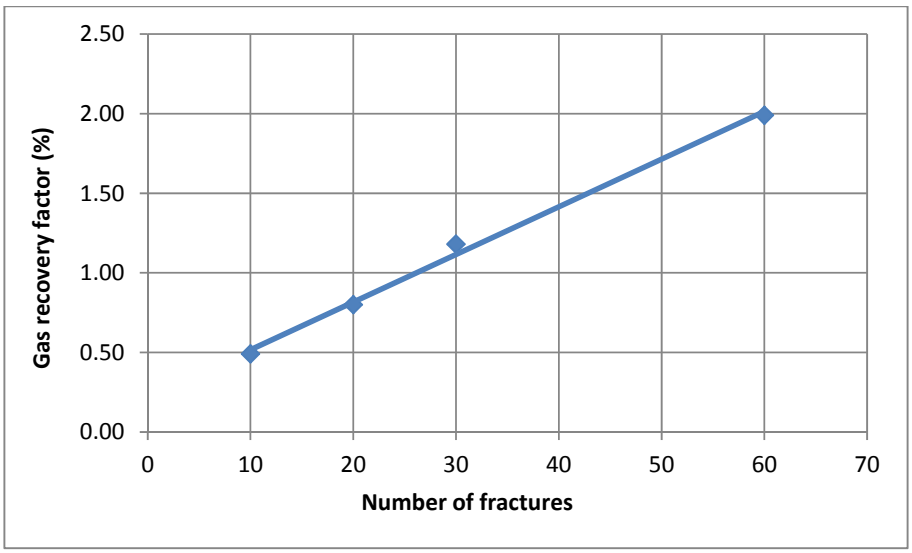

Figure 5.26 Number of fractures and gas recovery factor relationship

5.4 Effect of Number of Fractures for Minimum and Maximum Matrix Permeability

The objective of this section is to investigate the effect of matrix permeability to observe corresponded gas productivity on different number of fractures. Matrix

porosity is not taken into account in this section. As shown in the previous section, matrix porosity has small effect on the production performance and impacts only in early-time of the production.

Each number of fractures case as discussed in the previous section is modeled with minimum and maximum matrix permeability. Figures 5.27 through 5.32 show gas production rate, cumulative gas production, and reservoir pressure for 10, 20, 30 and 60 fractures for matrix permeability of 0.00007mD and 0.0005mD, respectively. Gas saturation profiles can be found in Appendix section from B-1 through B-8. Table 5.5 shows the summary of cumulative gas production and gas recovery factor. The results of minimum matrix permeability cases depict that increasing number of fractures does not aid in gas production improvement as the gas flows difficultly in the matrix itself. The maximum matrix permeability cases exhibit the greater improvement in gas recovery. However, this result has to be considered the fact that fracture width is large as natural fractures width of 0.03mm which may not bring sufficient conductivity to each fracture hence gas production rate cannot be enhanced.

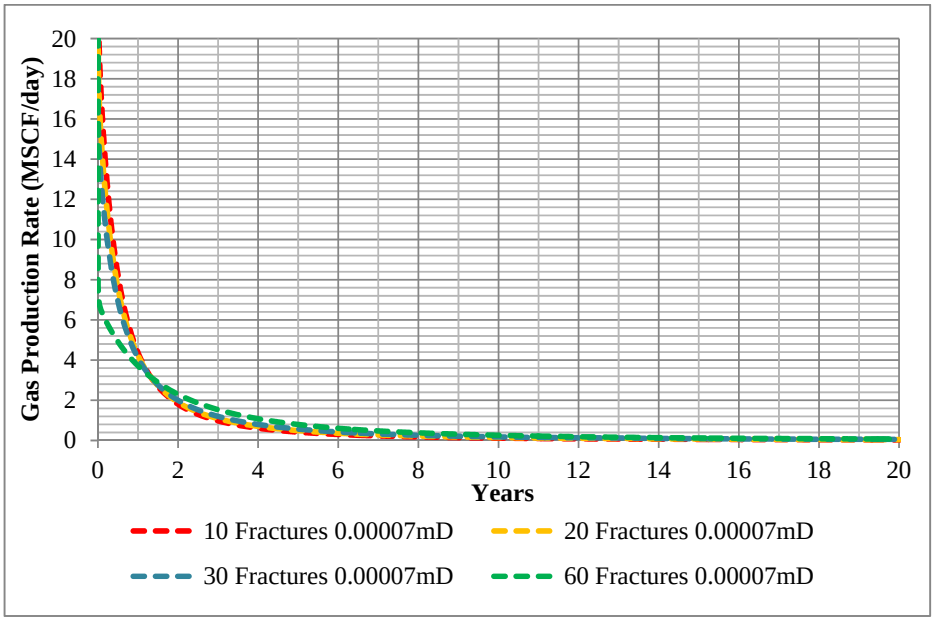

Figure 5.27 Gas production rate for minimum matrix permeability

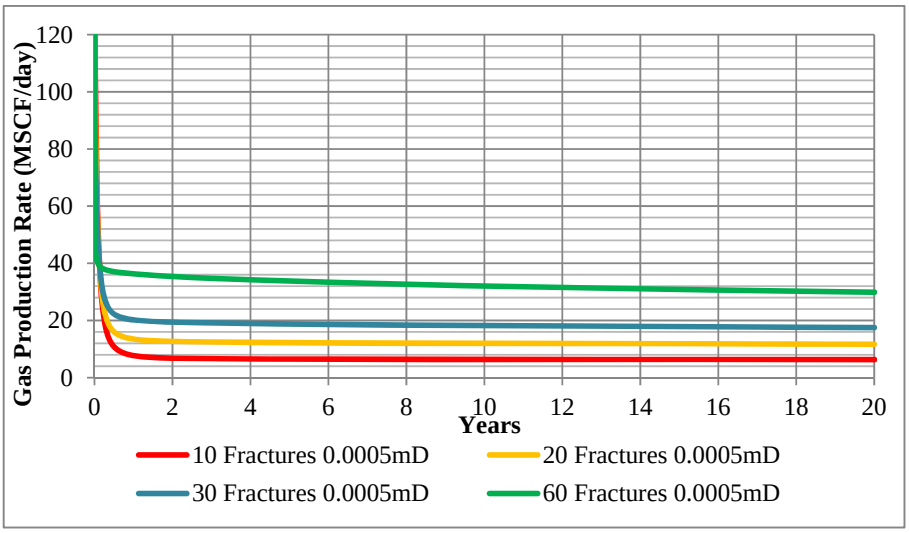

Figure 5.28 Gas production rate for maximum matrix permeability

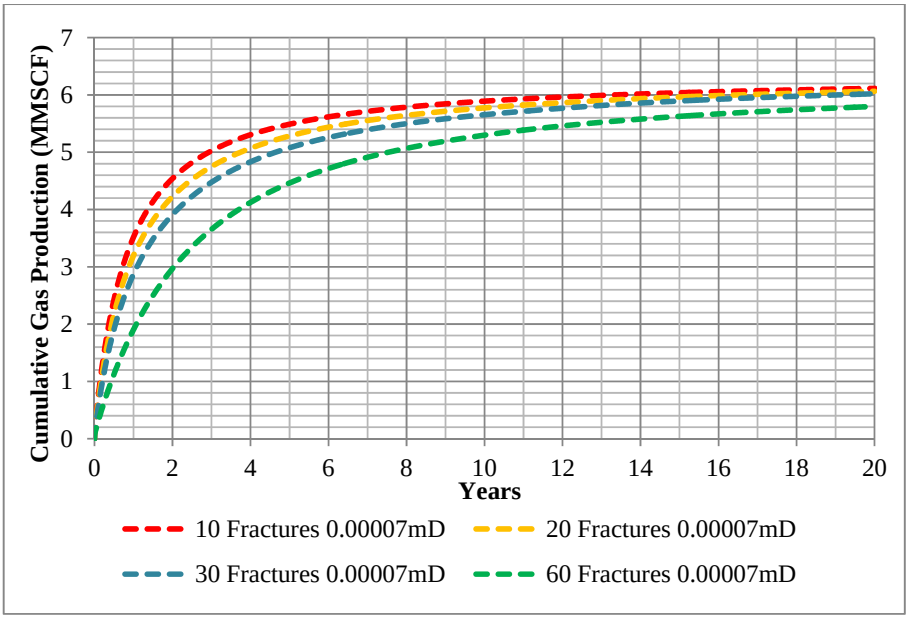

Figure 5.29 Cumulative gas production
for minimum matrix permeability

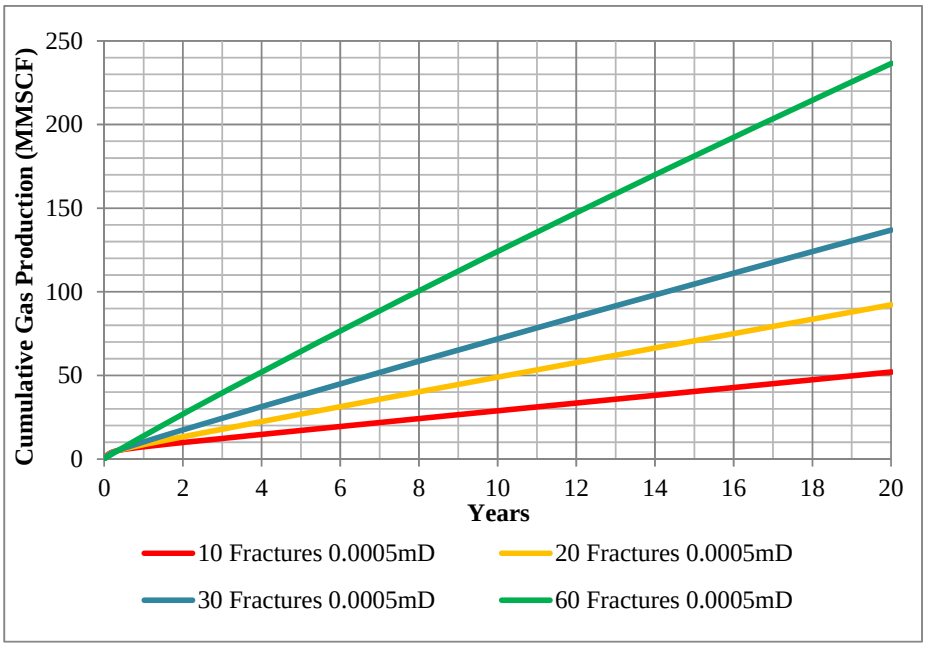

Figure 5.30 Cumulative gas production

for maximum matrix permeability

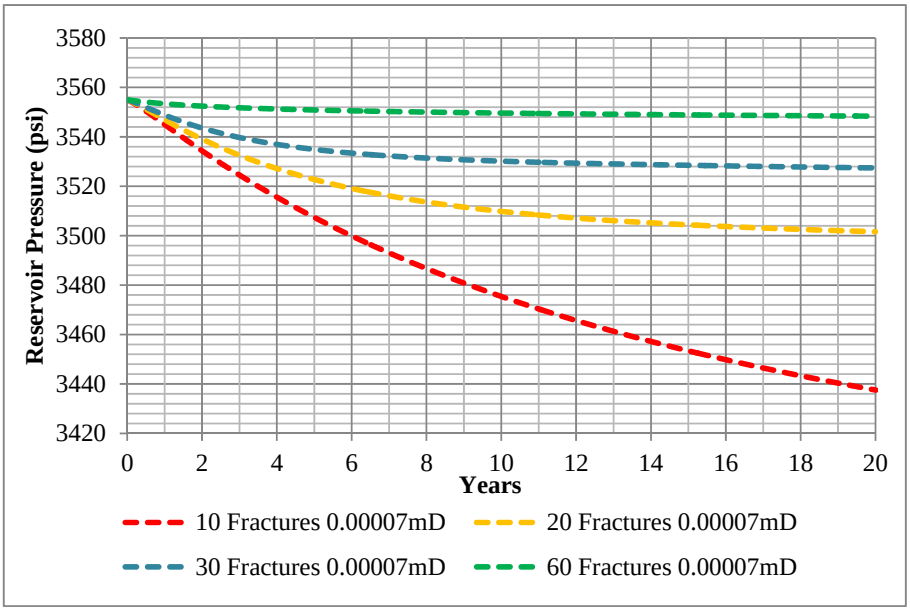

Figure 5.31 Reservoir pressure profile

for minimum matrix permeability

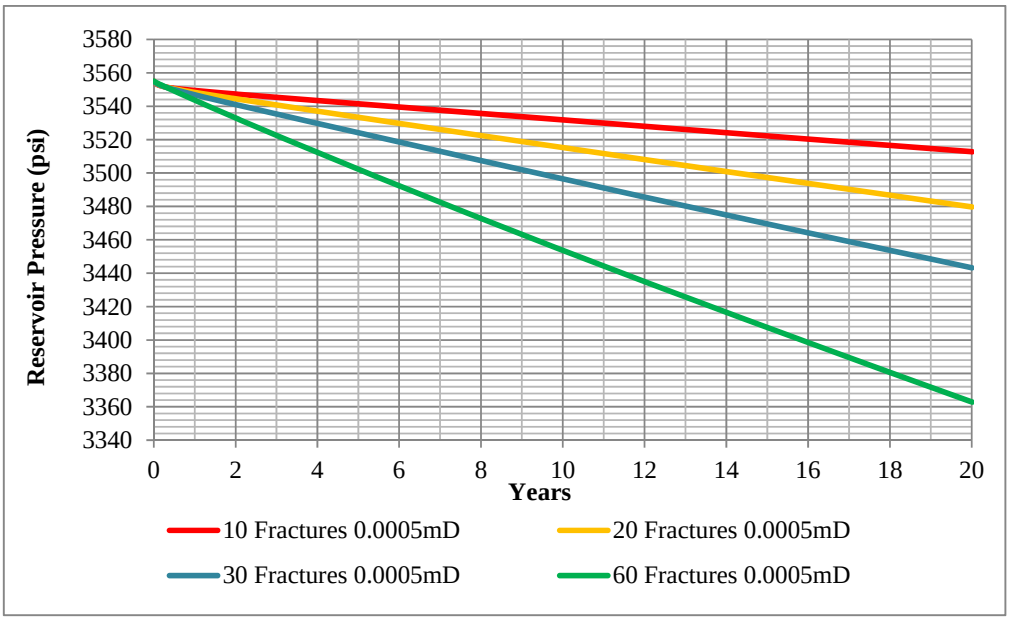

Figure 5.32 Reservoir pressure profile
for maximum matrix permeability

Table 5.5 Summary of gas recovery factor for different
number of fractures and matrix permeabilities at the end of production

Number of Fracture	Matrix Permeability (mD)	OGIP (BSCF)	Cumulative Gas Production (BSCF)	Recovery (%)
10	0.00007	4.78	0.0061	0.13
20	0.00007	4.78	0.0061	0.13
30	0.00007	4.78	0.0060	0.13
60	0.00007	4.78	0.0058	0.12
10	0.0005	4.78	0.0520	1.09
20	0.0005	4.78	0.0922	1.93
30	0.0005	4.78	0.1369	2.86
60	0.0005	4.78	0.2365	4.95

Figure 5.33 illustrates the relationship of number of fractures and gas recovery factor for minimum and maximum matrix permeability.

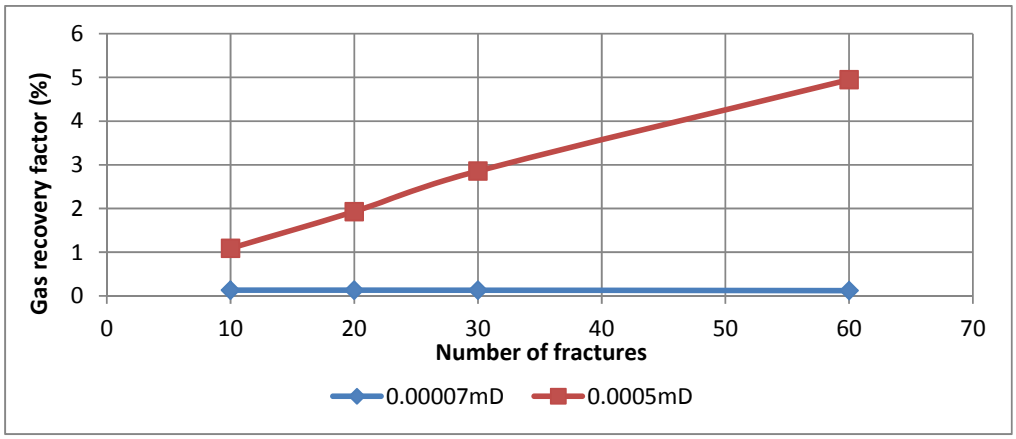

Figure 5.33 Number of fractures and gas recovery factor
for minimum and maximum matrix permeability

5.5 Effect of Fracture Width

Fracture width is another important factor which indicates fracture conductivity as the fracture permeability is corresponded to fracture width. The fracture width are varied from 0.015mm, 0.030mm, 0.15mm, 0.30mm, 0.60mm, 1.20mm, 2.40mm and 3.00mm. Fracture permeabilities are calculated as shown in Table 5.6. The objective of this analysis is to examine the effect of fracture width on the production performance. The other reservoir properties are the same as in the base case.

Table 5.6 Width and fracture permeability

Fracture Width (mm)	Fracture Permeability (mD)
0.015	0.04
0.030	0.30
0.15	37.36
0.30	298.88
0.60	2391.06
1.20	19128.48
2.40	153027.85
3.00	298882.51

Figures 5.34 through 5.36 represent gas production rate, cumulative gas production comparison, and reservoir pressure for different fracture widths. Figures 5.37 represent gas saturation profile for the fracture width of 3.00mm. For other cases, gas saturation profile can be found in Appendix section from C-1 through C-7.

Significant increasing in gas production is obviously seen when increasing fracture widths. Increasing fracture width to 3.00mm can improve gas production rate only slightly compare to 2.40mm case. Since the gas is effectively drained around the fractures provided the fact that the matrix permeability is still low, there will be a certain fracture width that could provide the maximum gas production enhancement. So it is worth to note that the most effective fracture width is 2.40mm which can deliver maximum gas recovery factor of 34%.

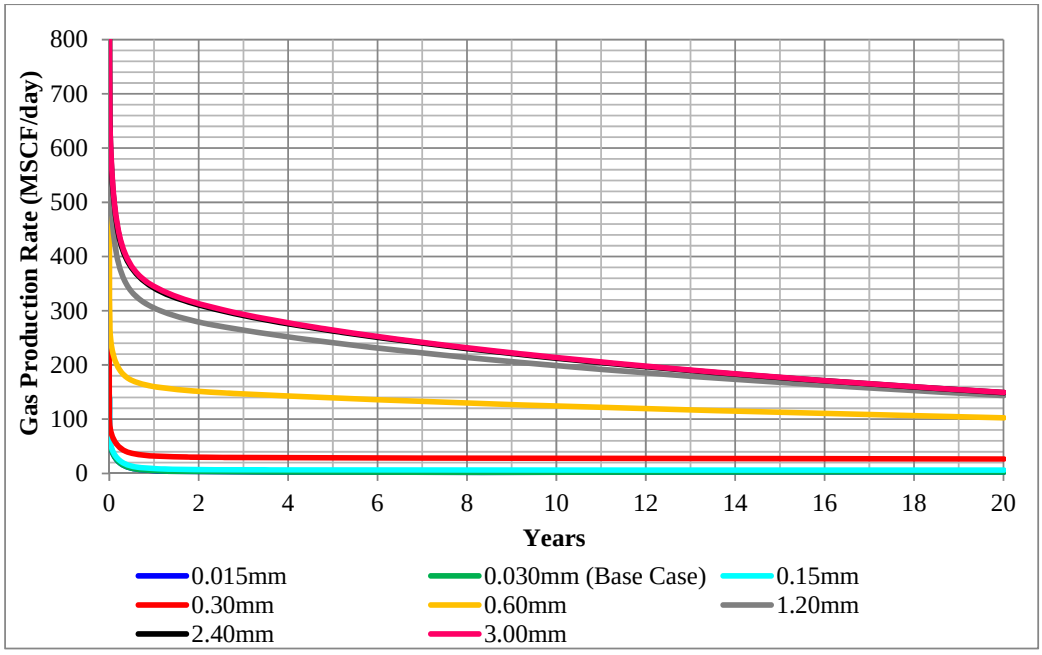

Figure 5.34 Gas production rate for different fracture widths

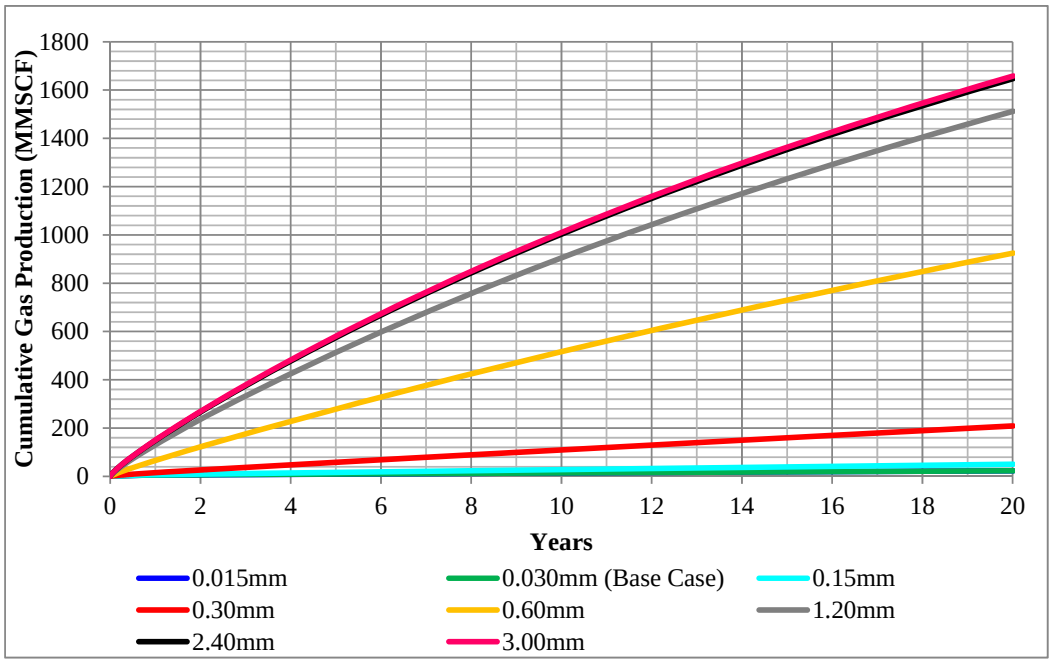

Figure 5.35 Cumulative gas production for different fracture widths

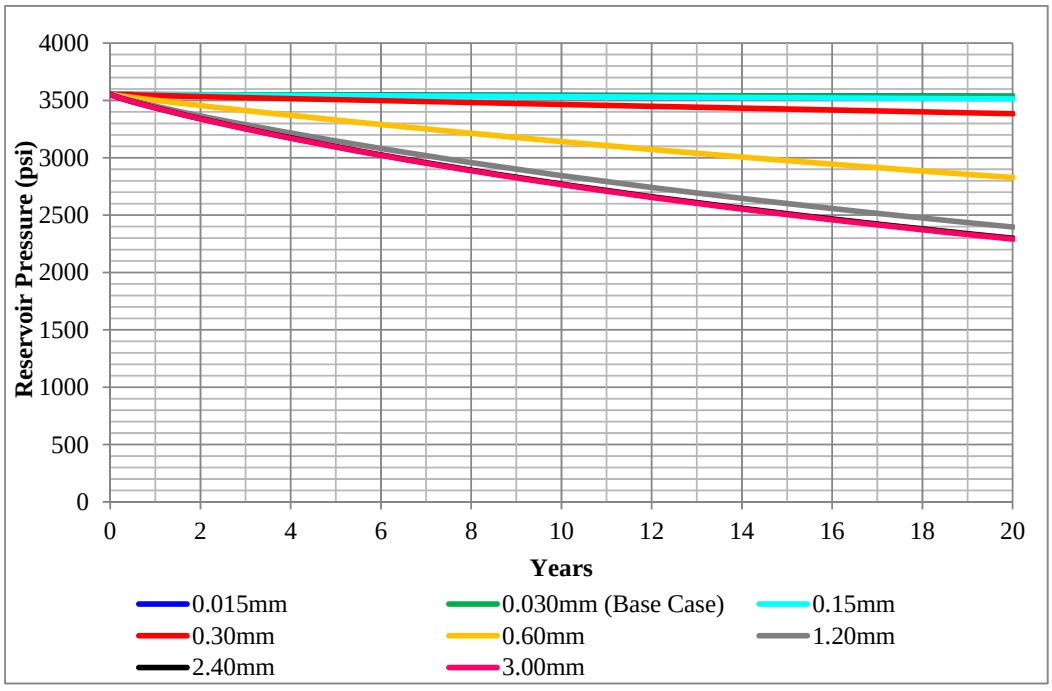

Figure 5.36 Pressure profile for different fracture widths

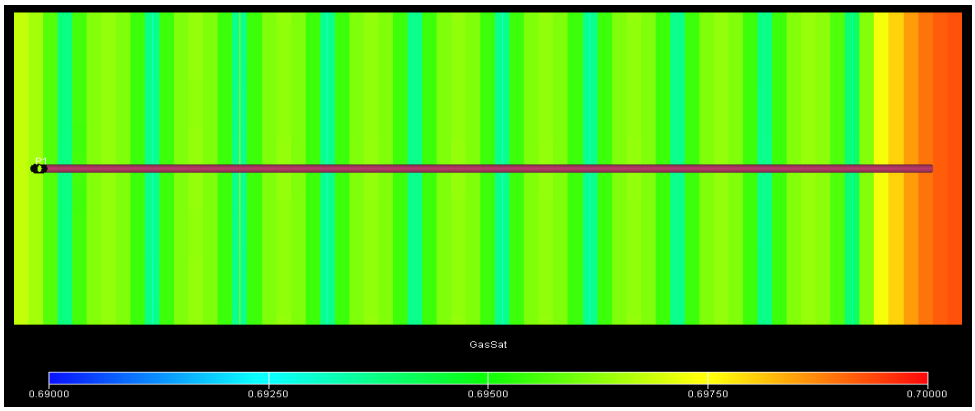

Figure 5.37 Gas saturation profile for 3.00mm fracture width
at the end of production

Changing in gas saturation profile can be clearly seen when increase fracture width especially along the fractures. The larger width cases express the higher fracture conductivity result in the gas flows from the formation last longer as the duration of linear flow from the formation depends on fracture conductivity [22]. Table 5.7 shows summary of cumulative gas production and gas recovery factor for various fracture widths.

Table 5.7 Summary of gas recovery factor for
different fracture widths at the end of production

Fracture Width (mm)	**OGIP (BSCF)**	**Cumulative Gas Production (BSCF)**	**Recovery (%)**
0.015	4.78	0.02	0.49
0.03	4.78	0.02	0.49
0.15	4.78	0.05	1.06
0.30	4.78	0.21	4.37
0.60	4.78	0.92	19.35
1.20	4.78	1.51	31.64
2.40	4.78	1.65	34.47
3.00	4.78	1.66	34.69

Figure 5.38 shows the relationship of fracture width and gas recovery factor. It can be seen that the maximum gas recovery factor can be achieved around 34% since the graph starts to exhibit steady from this point forward.

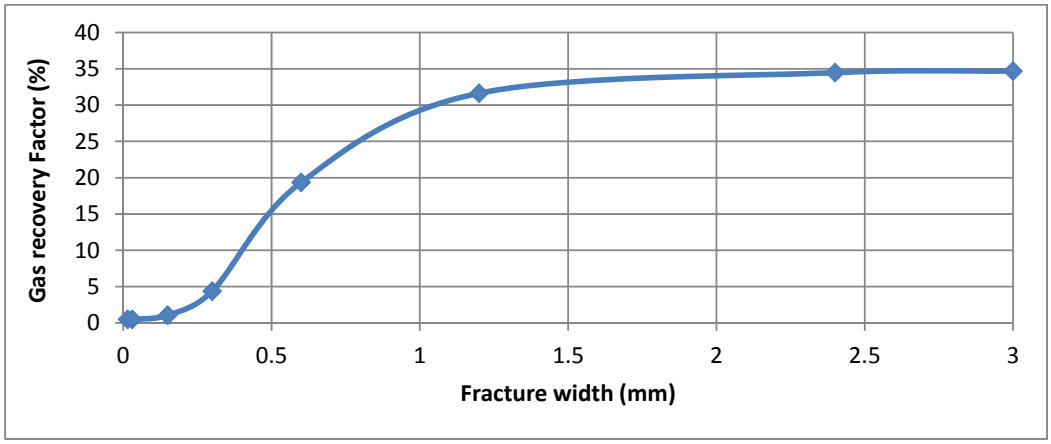

Figure 5.38 Fracture width and gas recovery factor relationship

5.6 Effect of Fracture Width for Minimum and Maximum Matrix Permeability

The objective of this section is to examine the effect of matrix permeability to observe corresponded production performance based on fracture widths. Each fracture width as discussed in the previous section is modeled with minimum and maximum matrix permeability. Figures 5.39 through 5.44 show gas production rate, cumulative gas production, and reservoir pressure throughout 20 years production for the fracture width of 0.015mm through 3.00mm with the minimum and maximum matrix permeability of 0.00007mD and 0.0005mD, respectively. Gas saturation profile for all cases can be found in Appendix section from D-1 through D-16. The results of this study found that fracture widths yield significant effects on gas production performance in a certain fracture width range for both minimum and maximum matrix permeability. From the result of minimum matrix permeability case discovered that the fracture width of 1.20mm, 2.40mm, and 3.00mm yield similar gas production rate. This result indicates that increasing fracture width above 1.20mm; it will not offer any gas production improvement. Therefore, 1.20mm width is considerably the most effective fracture width to provide maximum gas production rate based on this study.

Similarly to maximum matrix permeability case where 2.40mm fracture width is the most effective fracture width. At the end of production, the maximum gas recovery factors that are achievable by increasing fracture width are 9% and 57% for minimum and maximum matrix permeability cases, respectively. Table 5.8 shows summary of cumulative gas production and gas recovery of various fracture widths for minimum and maximum matrix permeability of 0.00007mD and 0.0005mD.

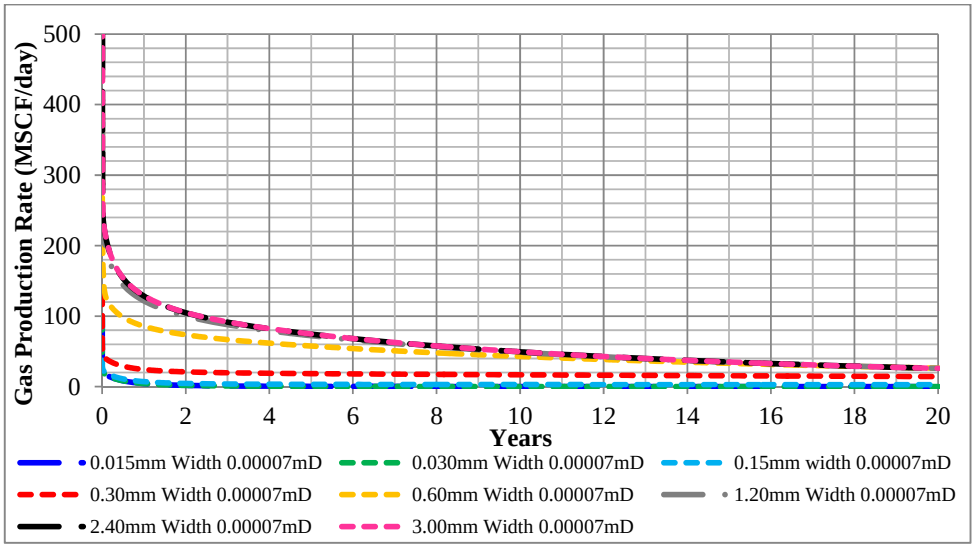

Figure 5.39 Gas production rate for different fracture widths and minimum permeability

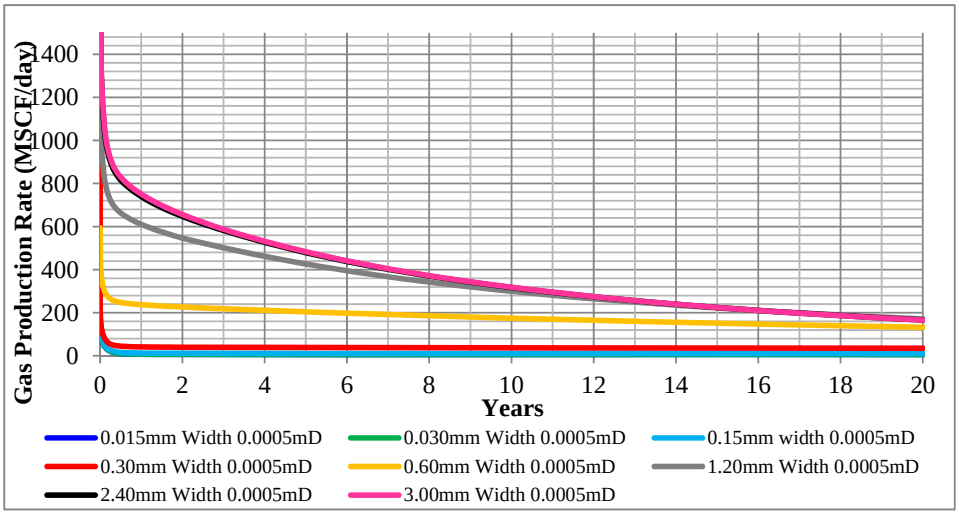

Figure 5.40 Gas production rate for different fracture widths and maximum permeability

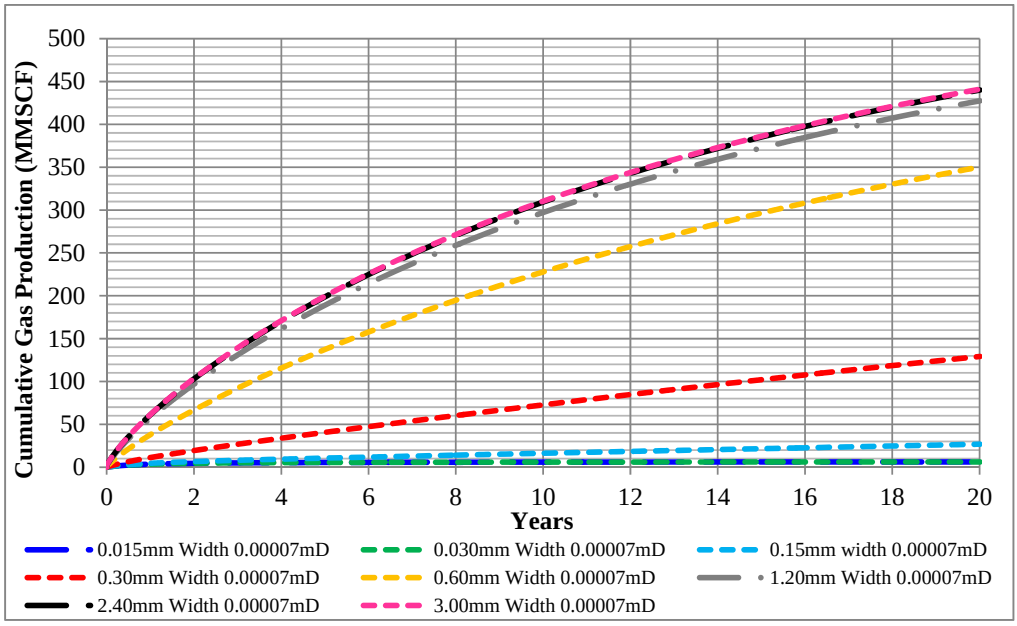

Figure 5.41 Cumulative gas production for different fracture widths and minimum permeability

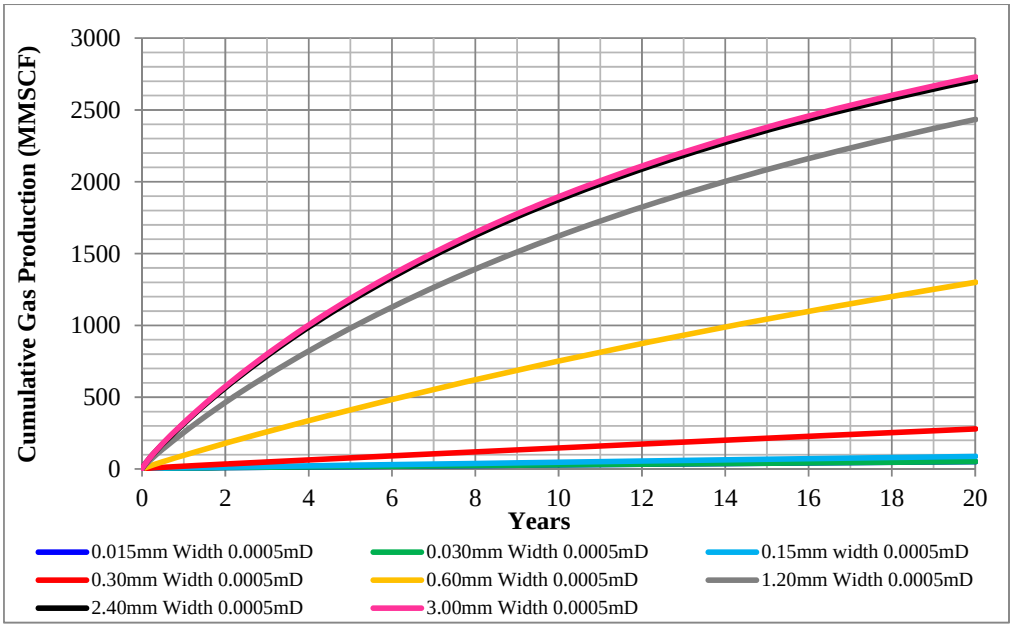

Figure 5.42 Cumulative gas production for different fracture widths and maximum permeability

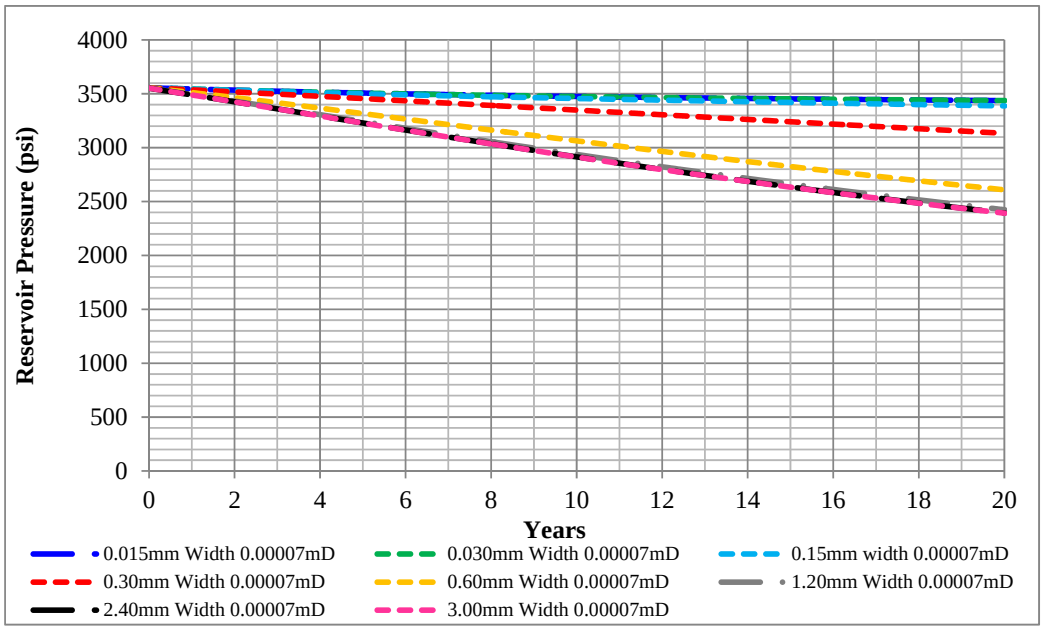

Figure 5.43 Reservoir pressure for different fracture widths and minimum permeability

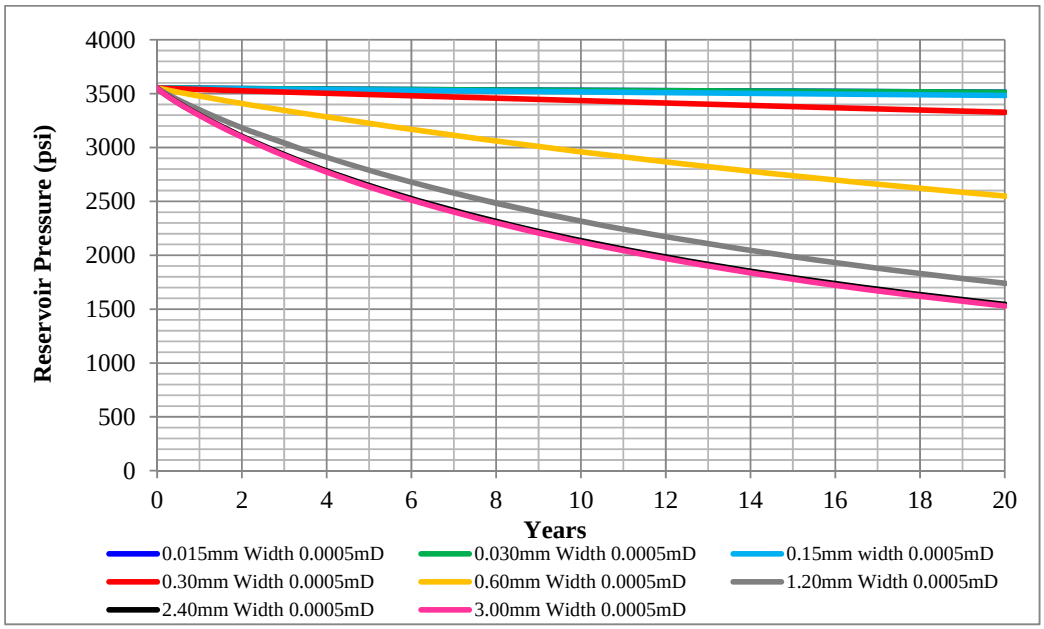

Figure 5.44 Reservoir pressure for different fracture widths and maximum permeability

Table 5.8 Summary of gas recovery factor for different fracture widths and different matrix permeabilities at the end of production

Fracture Width (mm)	Matrix Permeability (mD)	OGIP (BSCF)	Cumulative Gas Production (BSCF)	Recovery (%)
0.015	0.00007	4.78	0.01	0.13
0.03	0.00007	4.78	0.01	0.13
0.15	0.00007	4.78	0.03	0.56
0.30	0.00007	4.78	0.13	2.70
0.60	0.00007	4.78	0.35	7.33
1.20	0.00007	4.78	0.43	8.94
2.40	0.00007	4.78	0.44	9.21
3.00	0.00007	4.78	0.44	9.23
0.015	0.0005	4.78	0.05	1.09
0.03	0.0005	4.78	0.05	1.09
0.15	0.0005	4.78	0.09	1.85
0.30	0.0005	4.78	0.28	5.85
0.60	0.0005	4.78	1.30	27.21
1.20	0.0005	4.78	2.43	50.92
2.40	0.0005	4.78	2.71	56.65
3.00	0.0005	4.78	2.73	57.10

Figure 5.45 illustrates the relationship between fracture width and gas recovery factor for minimum and maximum matrix permeability. It can be seen that gas recovery factor remains almost unchanged when increasing fracture width above 1.20mm for minimum matrix permeability. Similarly to maximum matrix permeability case, the graph shows steady gas recovery factor when fracture width is greater than 2.40mm. These results can be defined that fracture width can improve gas drainage area mostly along the fractures. In the matrix area where the permeability is

still low, gas cannot flow easily from the formation to the fractures as a result gas recovery factor cannot be further enhanced after a certain fracture width.

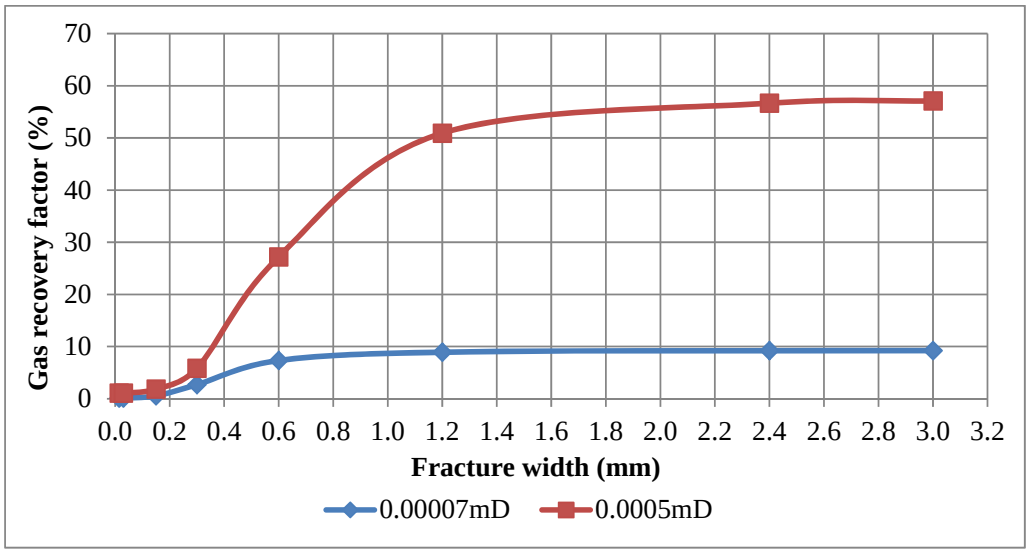

Figure 5.45 Fracture widths and gas recovery factor relationship

5.7 Hydraulic Fracturing Design Strategies

This section discusses two main hydraulic fracturing strategies which include conducting hydraulic fracturing on pre-exisitng natural fractures and conducting hydraulic fracturing to create new fractures as well as enhancement on the natural fractures.

5.7.1 Hydraulic Fracturing on Pre-Existing Natural Fractures

This strategy aims to enlarge the pre-existing natural fractures only. Fracture width of 0.30mm, 1.20mm, and 2.40mm are selected to simulate the production performance. These selections based on Figure 5.38 where the points are representative to the significant changes in gas recovery factor. Table 5.9 illustrates various hydraulic fracturing designs for hydraulic fracturing on pre-existing natural fractures. The reservoir properties other than shown in Table 5.9 are kept constant as in the base case.

Table 5.9 Hydraulic fracturing designs for
hydraulic fracturing on pre-existing natural fractures

No.	Design	Number of Fractures	Width (mm)
1	A-1	10	0.30
2	A-2	10	1.20
3	A-3	10	2.40

Production performance for the above designs can be found on Figures 5.46 through 5.48. Gas saturation profile for all cases are shown in Appendix section from E-1 through E-3.

In order to define the optimum strategy, the gas production efficiency is calculated based on the change in gas recovery factor relative to the change in Stimulated Reservoir Volume (SRV) reference to the base case. Stimulated Reservoir Volume (SRV) can be used as a representative to conductivity through the reservoir and the effort input by means of the amount of the injected fluids and proppants. The production efficiency is defined by observing the change of output relative to input.

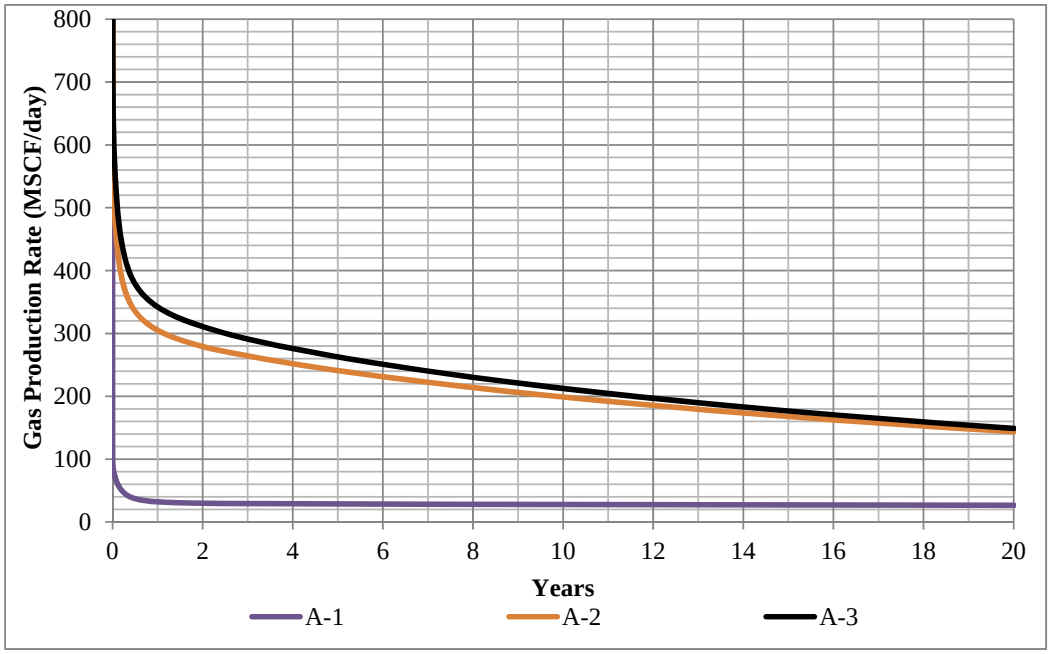

Figure 5.46 Gas production rate for different designs

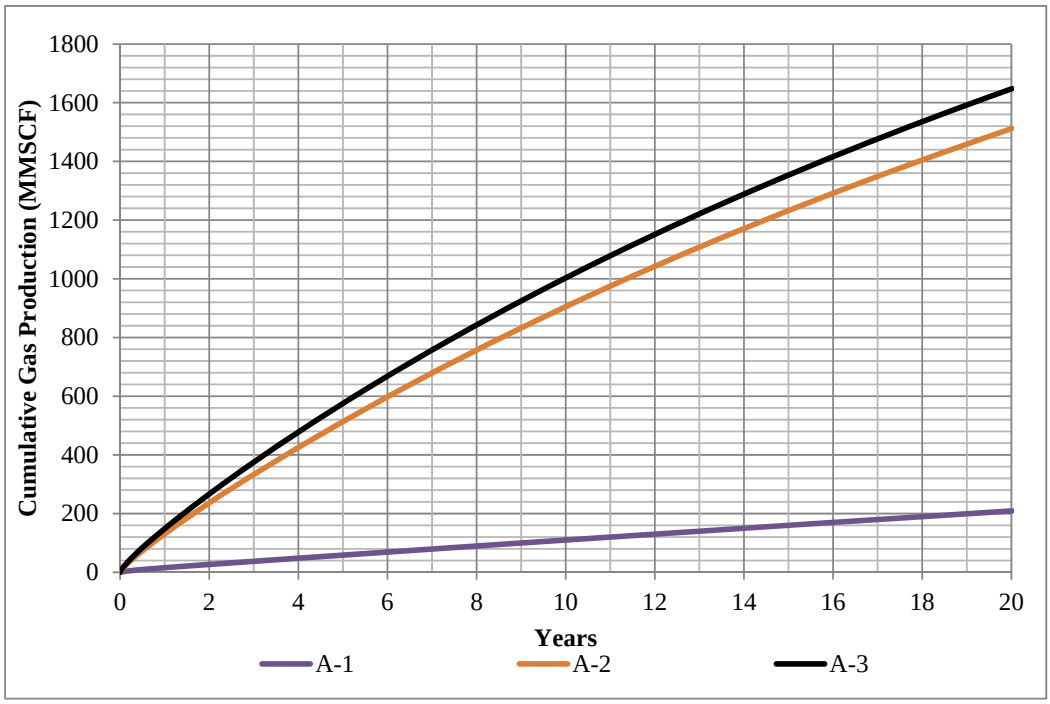

Figure 5.47 Cumulative gas production for different designs

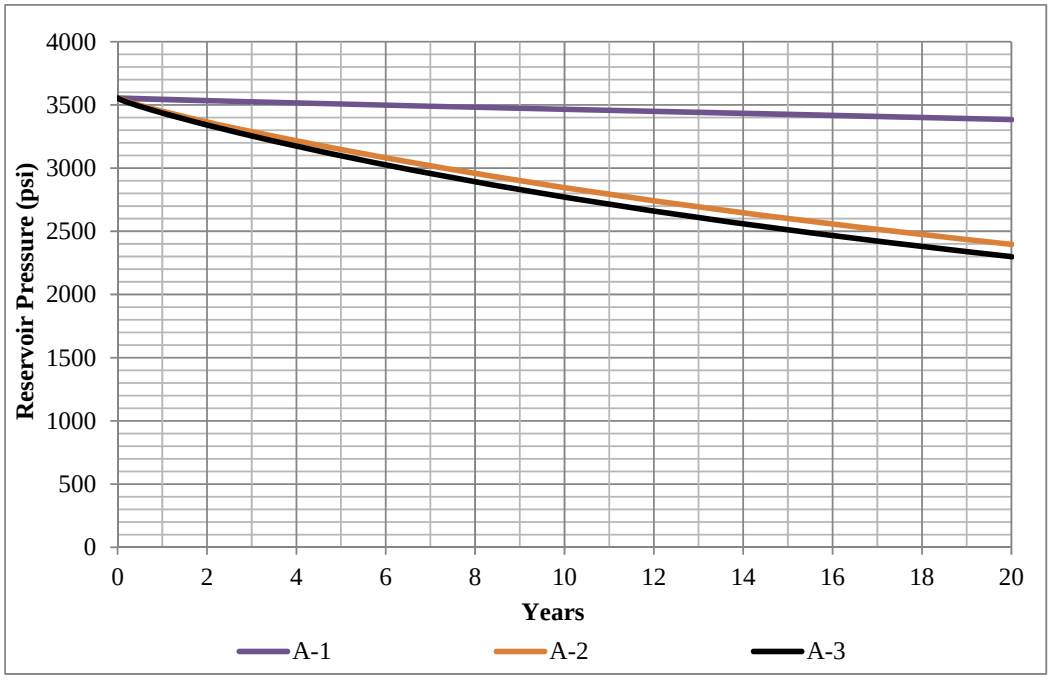

Figure 5.48 Pressure profile for different designs

Table 5.10 Production efficiency for
hydraulic fracturing on pre-existing natural fractures

Design	Number of fractures	Fracture width (mm)	Cumulative Gas Production (BSCF)	Gas recovery factor (%)	SRV (ft^3)	Production efficiency (% per 1000 unit volume)
A-1	10	0.30	0.21	4.37	1430	3.01
A-2	10	1.20	1.51	31.64	5720	5.59
A-3	10	2.40	1.65	34.47	11440	3.01

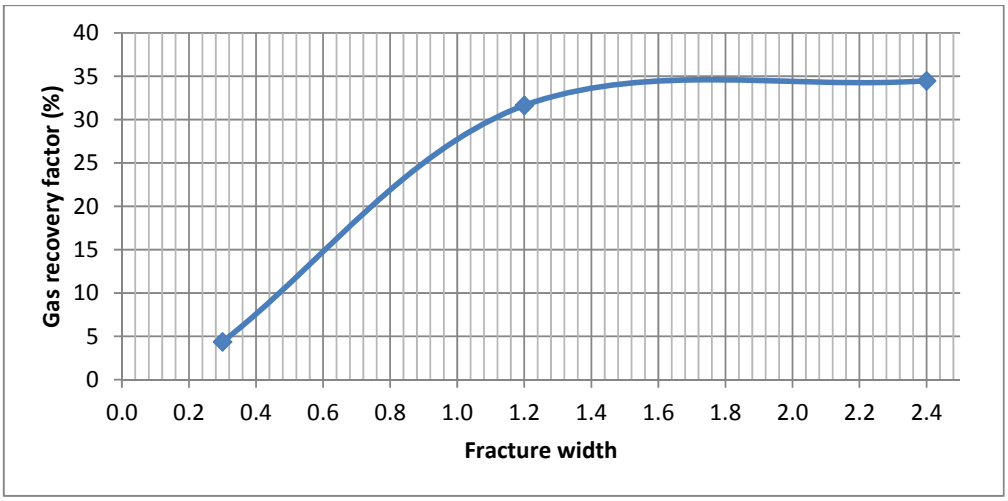

Figure 5.49 Fracture width and gas recovery factor relationship

Table 5.10 above shows gas production efficiency. Figure 5.49 represents the relationship of gas recovery factor and various hydraulic fracturing designs. The fracture width of 2.40mm exhibits slightly improvement from the 1.20mm fracture width case. Table 5.10 can be defined that Design A-2 yields the highest gas production efficiency. At the end of production, gas recovery factor of 31.64% can be achieved. Figure 5.50 shows production efficiency comparison plot for all designs.

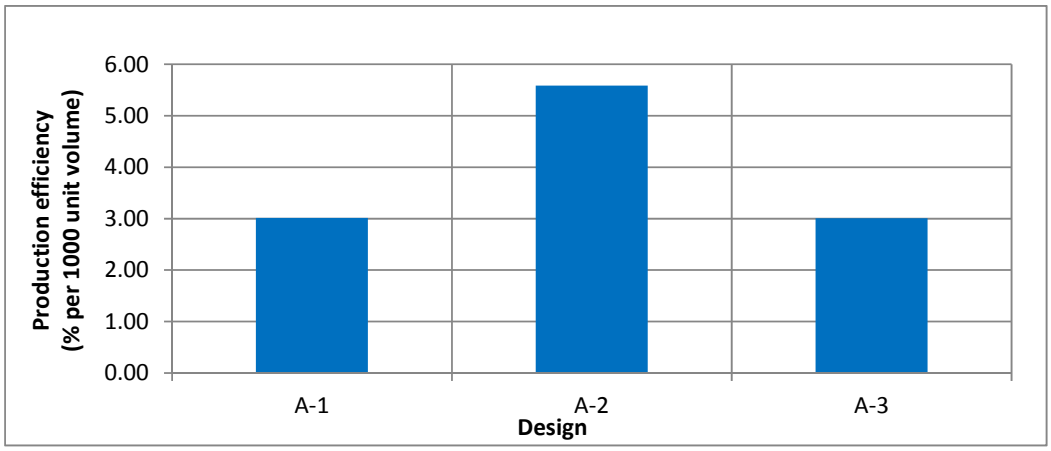

Figure 5.50 Production efficiency for
hydraulic fracturing on pre-existing natural fractures

5.7.2 Hydraulic Fracturing Designs

After investigated the parameters in the previous sections, various hydraulic fracturing designs are simulated based on fracture width and number of fractures. The following cases in Table 5.11 are modeled in order to define the optimum hydraulic fracturing design. The other reservoir properties beyond those shown in Table 5.11 are maintained constant same as in the base case.

Table 5.11 Hydraulic fracturing designs

No.	Design	Number of Fractures	Width (mm)
1	B-1	20	0.30
2	B-2	20	1.20
3	B-3	20	2.40
4	C-1	30	0.30
5	C-2	30	1.20
6	C-3	30	2.40
7	D-1	60	0.30
8	D-2	60	1.20
9	D-3	60	2.40

The ranges of fracture widths are selected to design hydraulic fracturing include 0.30mm, 1.20mm and 2.40mm. These selections based on Figure 5.38 where the points are representative to the significant changes in gas recovery factor.

Figures 5.51 through 5.53 represent gas production rate, cumulative gas production, and reservoir pressure for different hydraulic fracturing designs. Gas saturation profile for all design are shown in Appendix section from E-4 through E-12. These results can define that Design D-3, 60 fractures and 2.4mm fracture width case yields the greatest gas production rate and achieves the highest cumulative gas production. Table 5.12 shows the summary of gas recovery factor and production efficiency for all studied designs reference to the base case at given 0.03mm fracture width and 10 natural fractures. Production efficiency is calculated based on the change in gas recovery factor relative to the change in SRV.

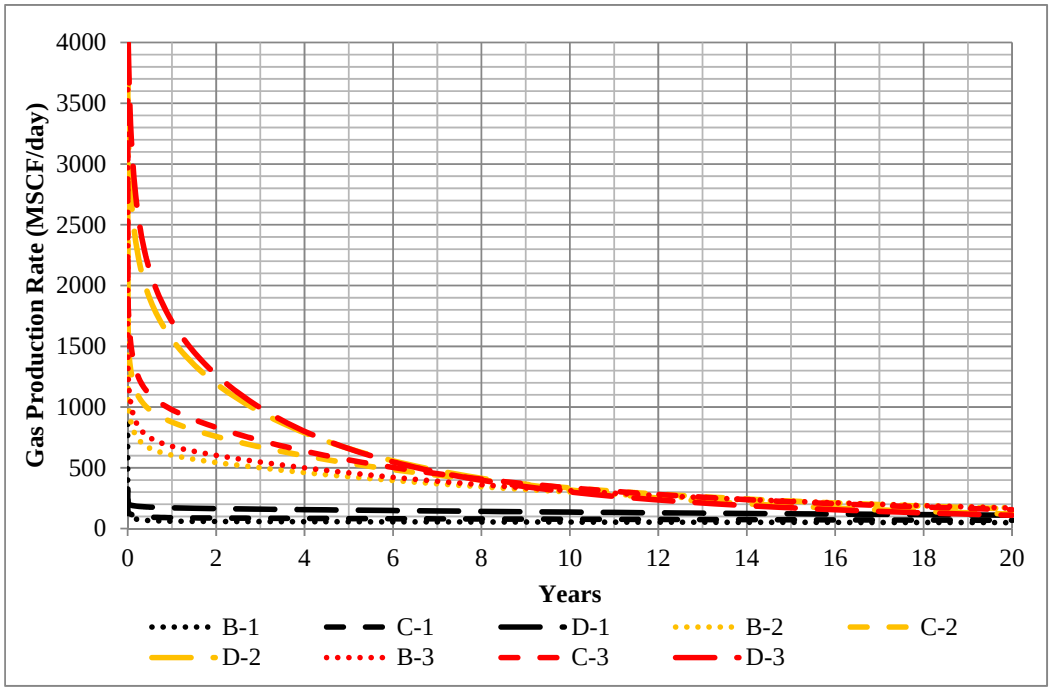

Figure 5.51 Gas production rate for different designs

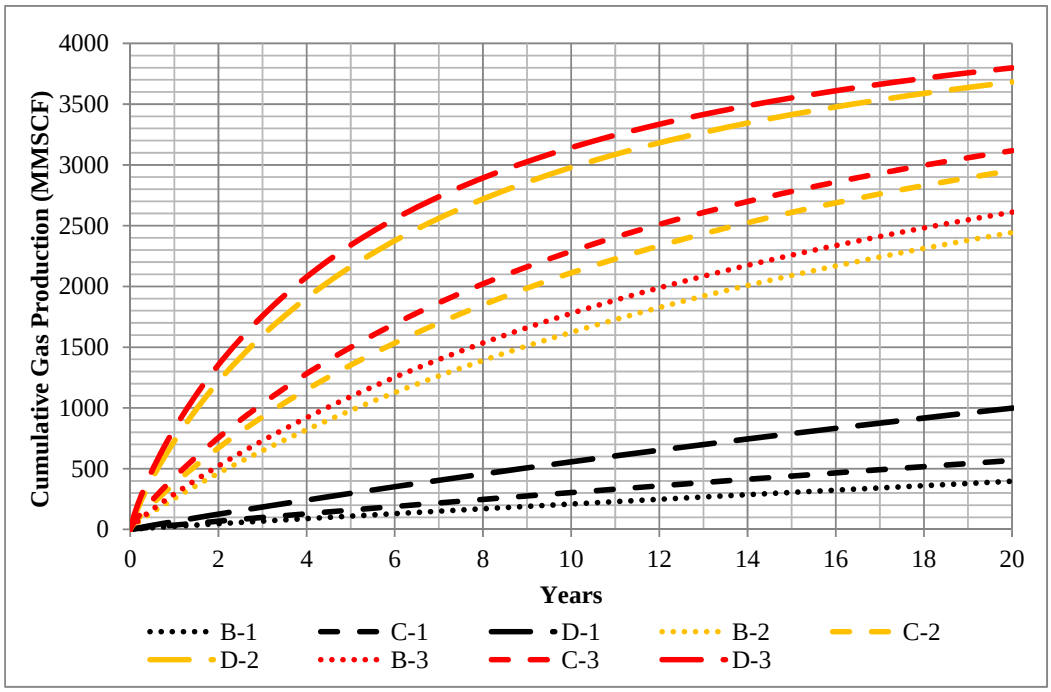

Figure 5.52 Cumulative gas production for different designs

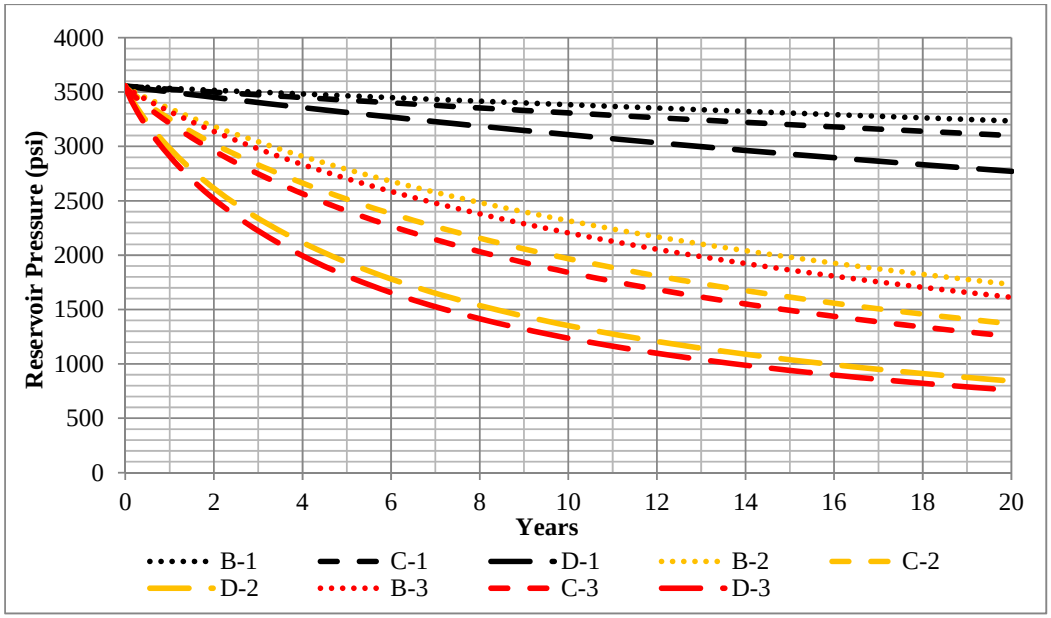

Figure 5.53 Reservoir pressure profile for different designs

Figure 5.54 shows the relationship between number of fractures and gas recovery factor for all fracture widths. It can be observed that the graph does not

exhibit linear relationship for 1.20mm and 2.40mm fracture width cases whereas it shows linear relationship for 0.30mm fracture width case.

Even though the results show that the higher number of fracture and larger fracture width would give the greatest gas productivity. However, it is not still a usual way for oil operators to maximize an effort to gain maximum gas recovery factor. As shown in Table 5.12 the fracture width of 2.40mm does not show much in gas recovery factor improvement compare to 1.20mm fracture width given the fact that the fracture width has to be double. This means that the double proppant amounts have to be injected to gain only 3% higher gas recovery factor. This may not be an optimum solution in term of economic. This study aims to identity the optimum hydraulic fracturing design in term of production efficiency.

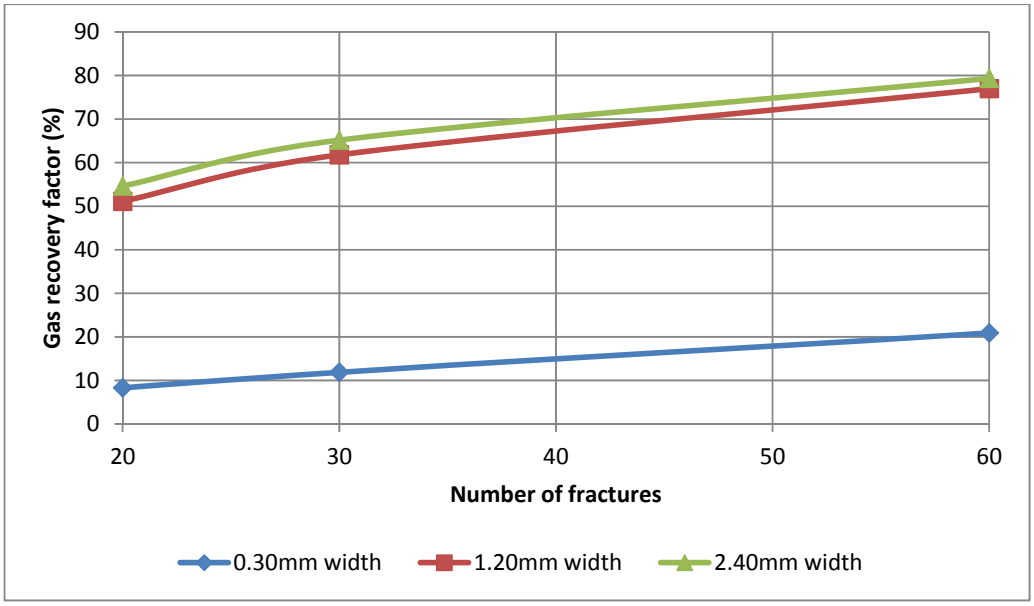

Figure 5.54 Number of fracture and gas recovery factor relationship

Table 5.12 Gas production efficiency for different hydraulic fracturing designs

Design	Number of fractures	Fracture width (mm)	Cumulative Gas Production (BSCF)	Gas recovery factor (%)	SRV (ft^3)	Production efficiency (% per 1000 unit volume)
B-1	20	0.30	0.40	8.30	2860	2.87
B-2	20	1.20	2.44	51.12	11440	4.48
B-3	20	2.40	2.61	54.63	22880	2.38
C-1	30	0.30	0.57	11.89	4290	2.75
C-2	30	1.20	2.95	61.79	17160	3.60
C-3	30	2.40	3.12	65.17	34320	1.89
D-1	60	0.30	1.00	20.90	8580	2.42
D-2	60	1.20	3.68	76.99	34320	2.24
D-3	60	2.40	3.80	79.47	68640	1.15

Figure 5.55 shows production efficiency for all strategies. It is evident that Design B-2; 20 fractures and 1.20mm fracture width yields the greatest production efficiency. This hydraulic fracturing design can achieve 51.11% gas recovery factor.

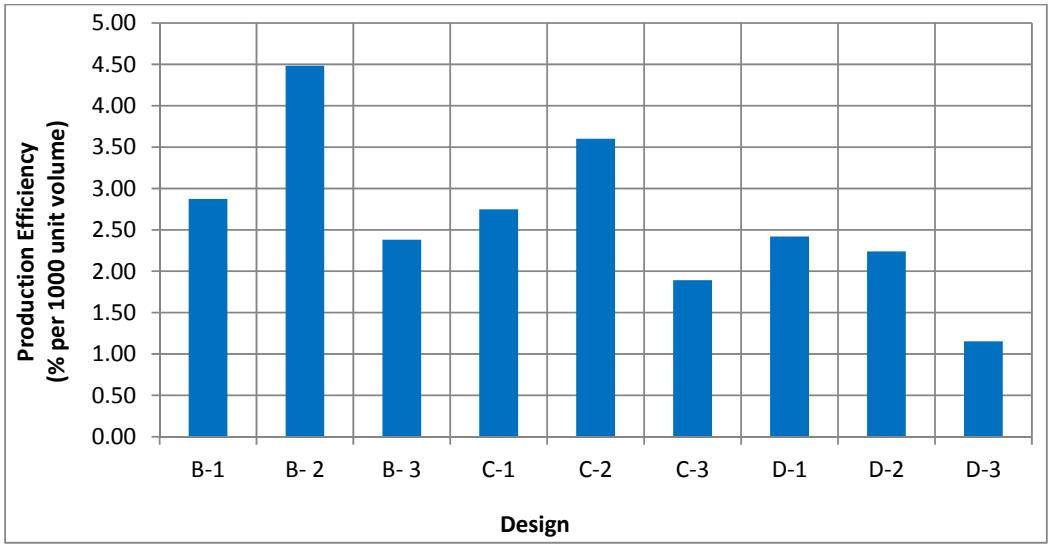

Figure 5.55 Production Efficiency for all designs

Sensitivity analysis is simulated for Design B-2. Three parameters are taken into account in sensitivity analysis to understand their effects on gas productivity. These parameters include matrix permeability, hydraulic fracturing pattern, and adsorbed gas concentration.

5.7.2.1 Matrix Permeability

Matrix permeabilities of 0.00007mD through 0.0005mD are used in the reservoir simulation models. Figures 5.56 through 5.58 show gas production rate, cumulative gas production, and reservoir pressure of Design B-2 for different matrix permeabilities.

As previously discussed on Figure 5.27 and Figure 5.39 that number of fractures would not improve gas recovery factor for the matrix permeability of 0.00007mD case but the recovery factor can be increased when increasing fracture width and gas recovery of 8.94% can be obtained. From the result of studying matrix permeability in sensitivity analysis illustrates that increasing number of fractures can improve gas recovery factor of 18.37% for 0.00007mD matrix permeability since the more conductivity is brought into the reservoir with the higher number of flow channels, therefore gas productivity can certainly be improved.

Figures 5.59 through 5.64 show gas saturation profile for different matrix permeabilities at the end of production.

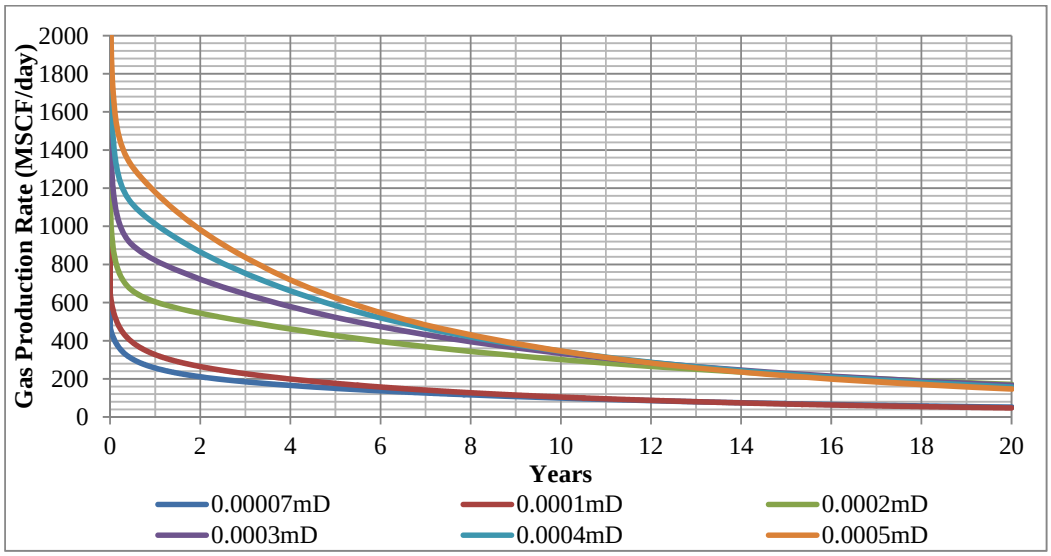

Figure 5.56 Gas production rate of Design B-2 for different matrix permeabilities

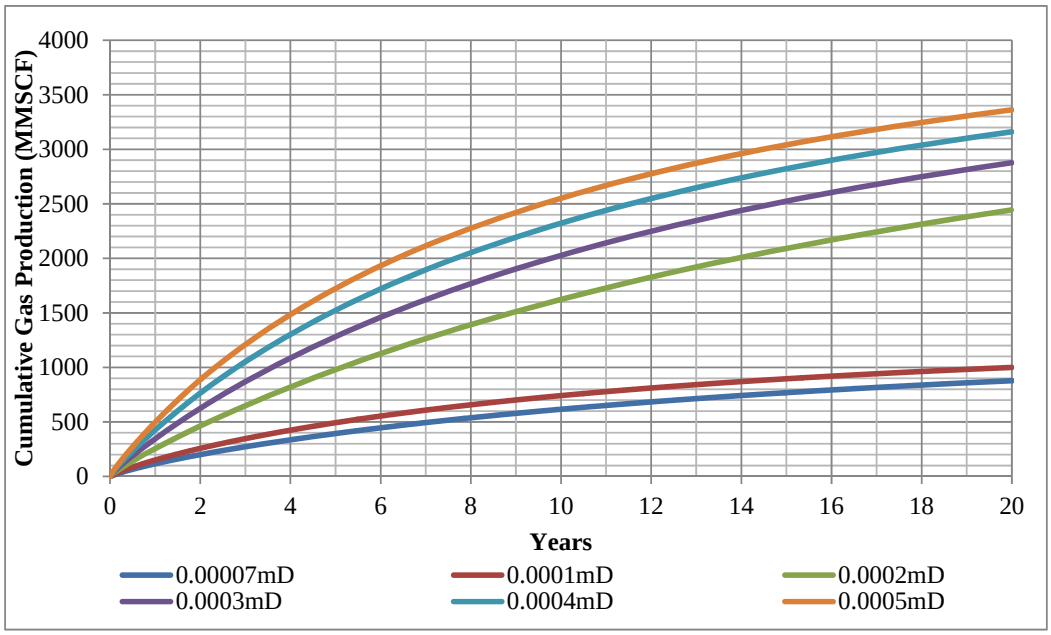

Figure 5.57 Cumulative gas production of Design B-2 for different matrix permeabilities

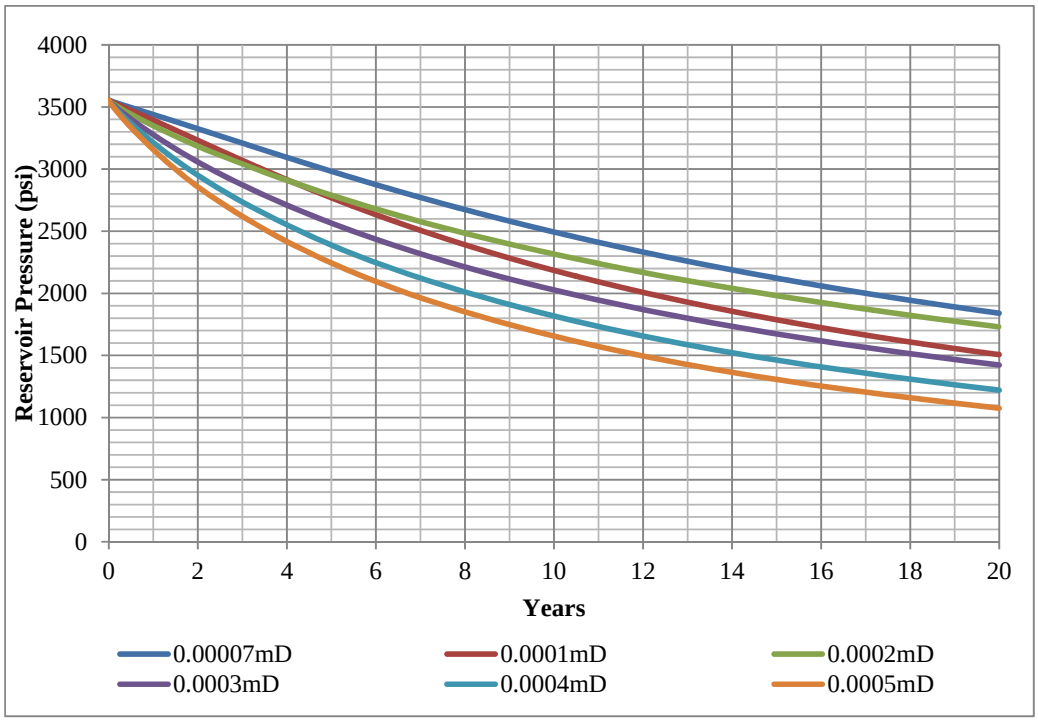

Figure 5.58 Reservoir pressure of Design B-2 for different matrix permeabilities

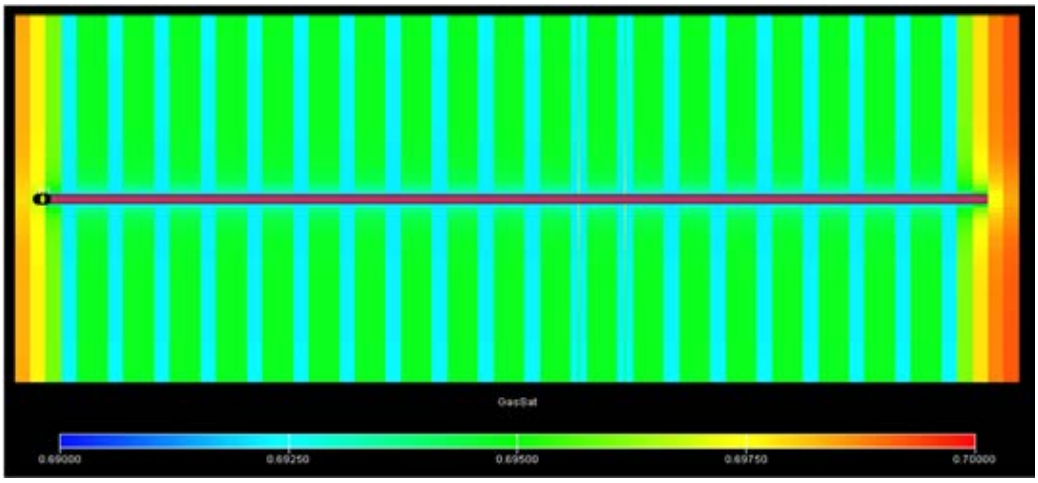

Figure 5.59 Gas saturation profile of Design B-2 for 0.00007mD matrix permeability

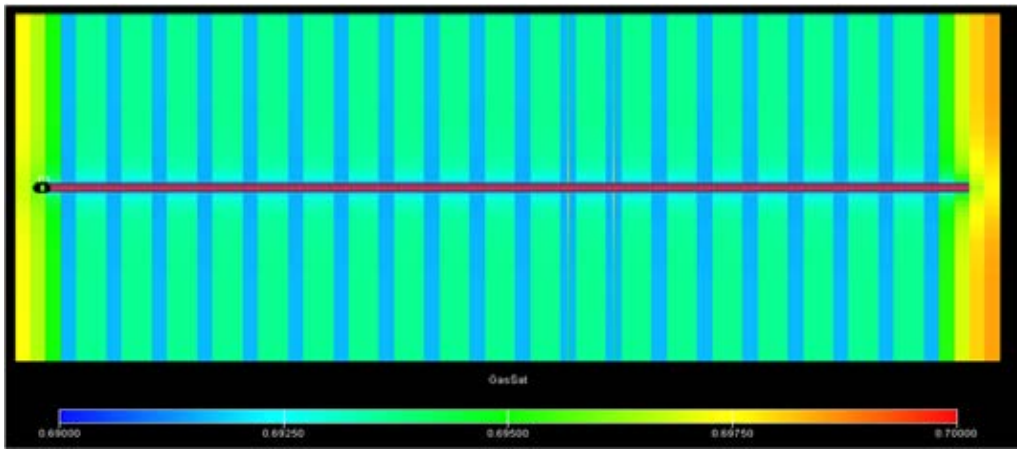

Figure 5.60 Gas saturation profile of Design B-2 for 0.0001mD matrix permeability

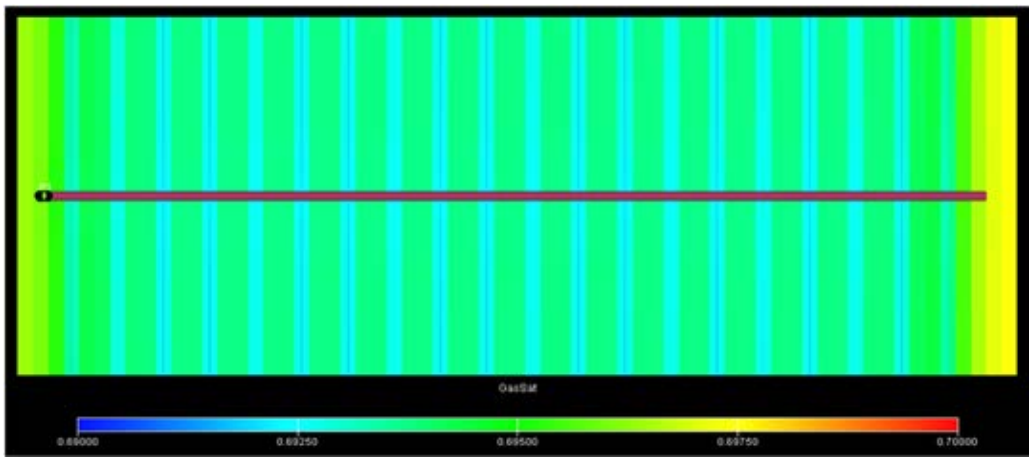

Figure 5.61 Gas saturation profile of Design B-2 for 0.0002mD matrix permeability

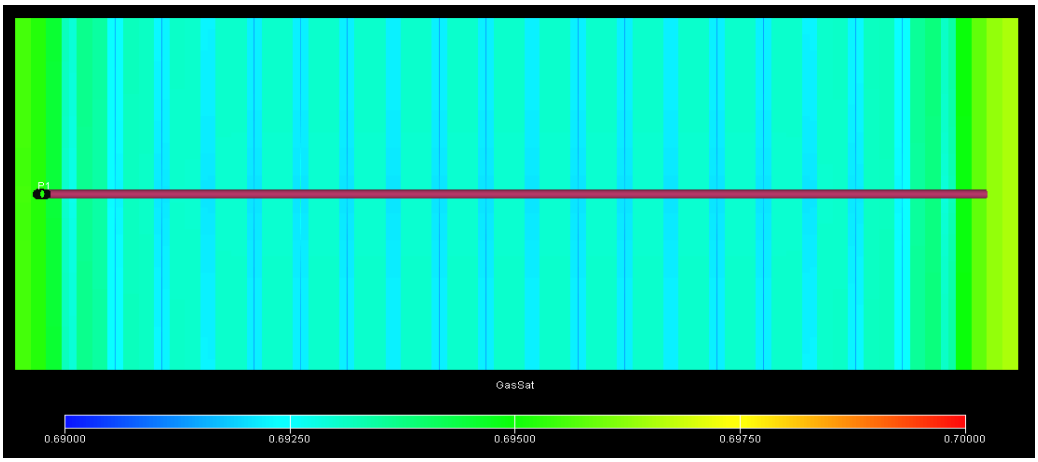

Figure 5.62 Gas saturation profile of Design B-2 for 0.0003mD matrix permeability

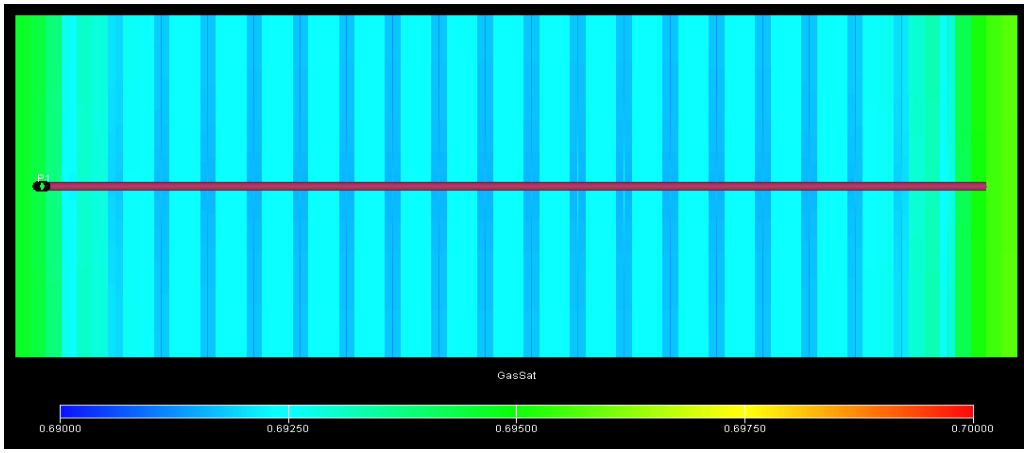

Figure 5.63 Gas saturation profile of Design B-2 for 0.0004mD matrix permeability

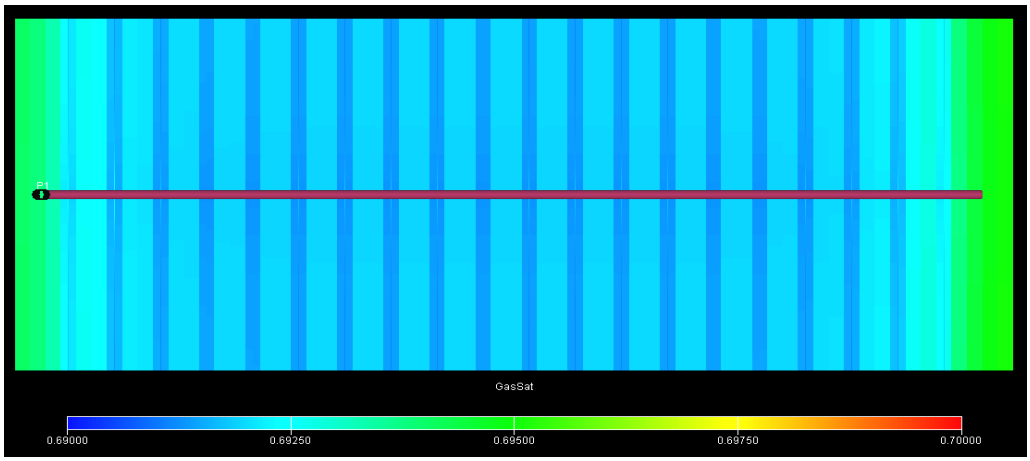

Figure 5.64 Gas saturation profile of Design B-2 for 0.0005mD matrix permeability

From gas saturation profiles from Figures 5.59 through 5.64, it is obviously seen the reduction in gas saturation along the fractures. The gas saturation colors become less contrast between the matrix and the fractures when matrix permeability increases. Table 5.13 shows the summary of gas recovery factor for different matrix permeabilities. The great effect of matrix permeability on gas productivity can be observed. The change in gas recovery can be distinguished between high matrix permeability and low matrix permeability where the low matrix permeability achieves 20% gas recovery and more than 50% gas recovery for high matrix permeability. The variation of recovery factor for changing in matrix permeabilities can be fluctuated from 2% up to 30%.

Table 5.13 Summary of gas recovery factor for Design B-2 and different matrix permeabilities at the end of production

Matrix Permeability (mD)	**OGIP (BSCF)**	**Cumulative Gas Production (BSCF)**	**Recovery (%)**
0.00007	4.78	0.88	18.37
0.0001	4.78	1.00	20.91
0.0002	4.78	2.44	51.11
0.0003	4.78	2.88	60.18
0.0004	4.78	3.16	66.11
0.0005	4.78	3.36	70.32

5.7.2.2 Hydraulic Fracturing Pattern

Different hydraulic fracturing patterns are investigated in this section. The objective is to understand the effect of pressure along the wellbore on the gas productivity since the pressure drop across the horizontal wellbore section may not be the same for the entire string. The patterns could be divided to four groups; fracture clusters at heel, centre, toe, and clustering equally spacing. Figures 5.65 through 5.67 represent gas production rate, cumulative gas production, and reservoir pressure for different clustering patterns. Figures 5.68 through 5.72 illustrates gas saturation profile for different patterns. It could be explained that more distribution of the

fractures in the reservoir can bring more reservoir matrix into contact with the fracture results in improving gas drainage area. Table 5.14 shows the summary of gas recovery factor for different hydraulic fracturing patterns. The variation of gas recovery factor is only 2-5%. However, from the results found that the more evenly distributed spacing would yield the highest gas productivity.

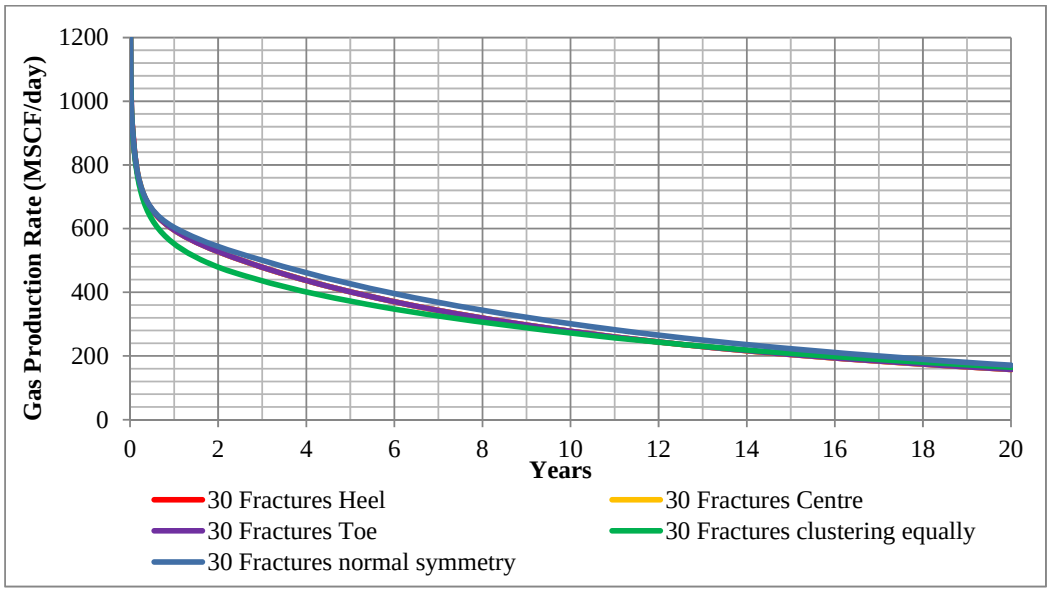

Figure 5.65 Gas production rate of Design B-2 for different hydraulic fracturing patterns

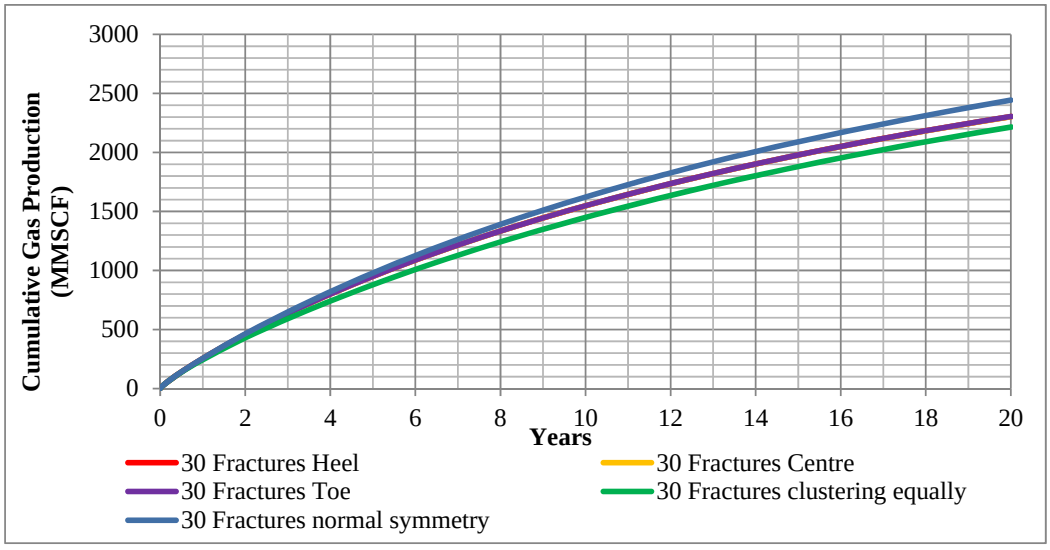

Figure 5.66 Cumulative gas production of Design B-2 for different hydraulic fracturing patterns

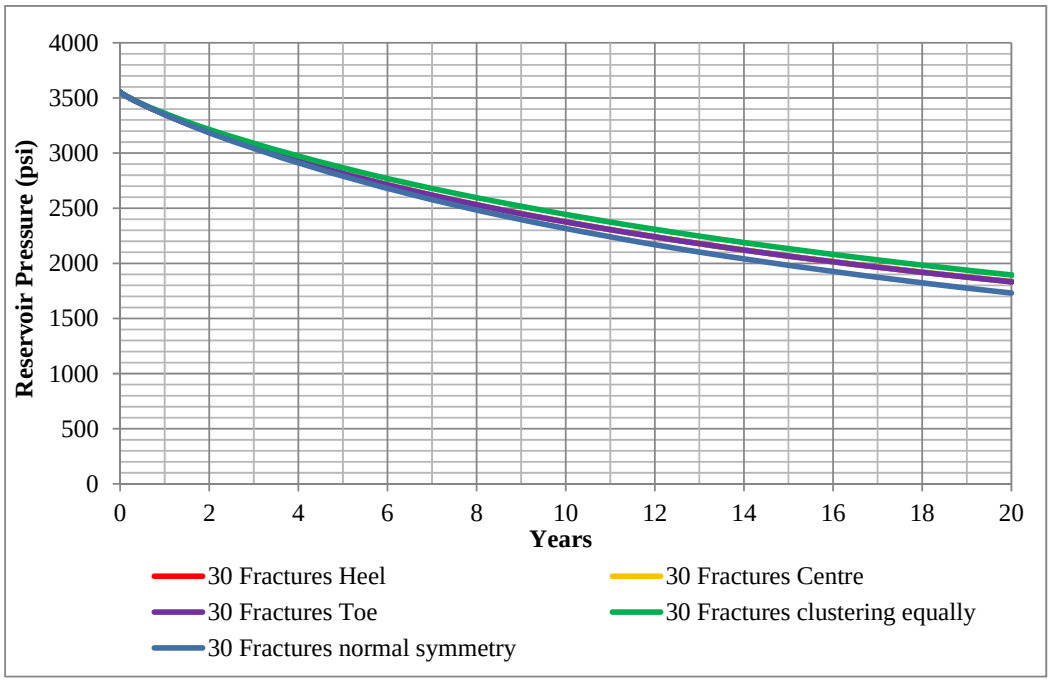

Figure 5.67 Reservoir pressure of Design B-2 for different hydraulic fracturing patterns

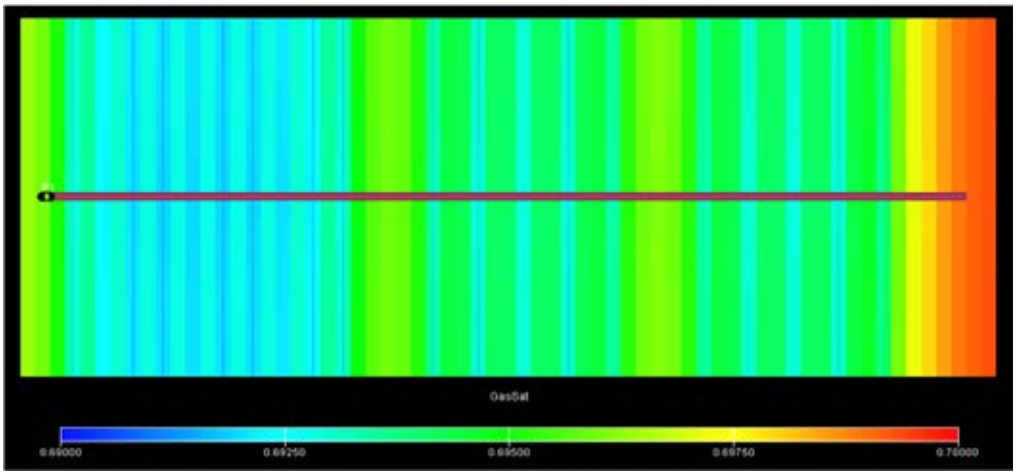

Figure 5.68 Gas saturation profile of Design B-2 for Heel patterns

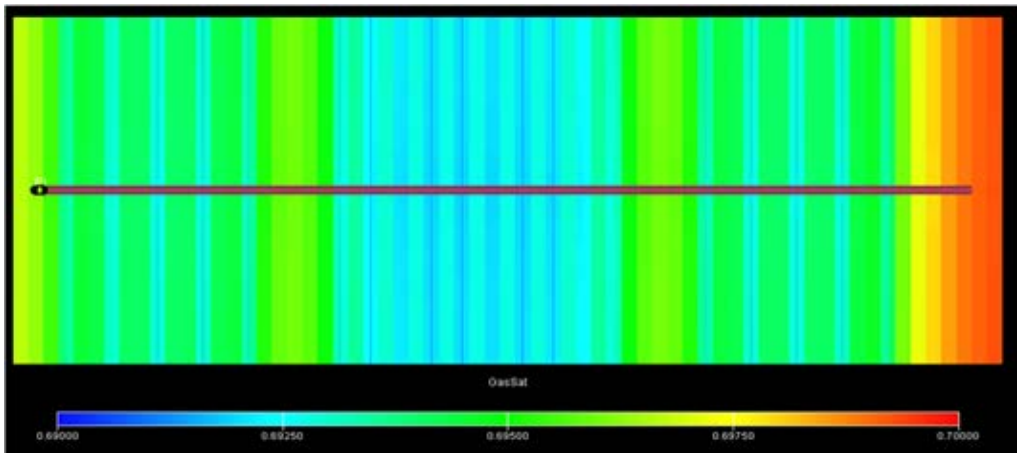

Figure 5.69 Gas saturation profile of Design B-2 for Centre patterns

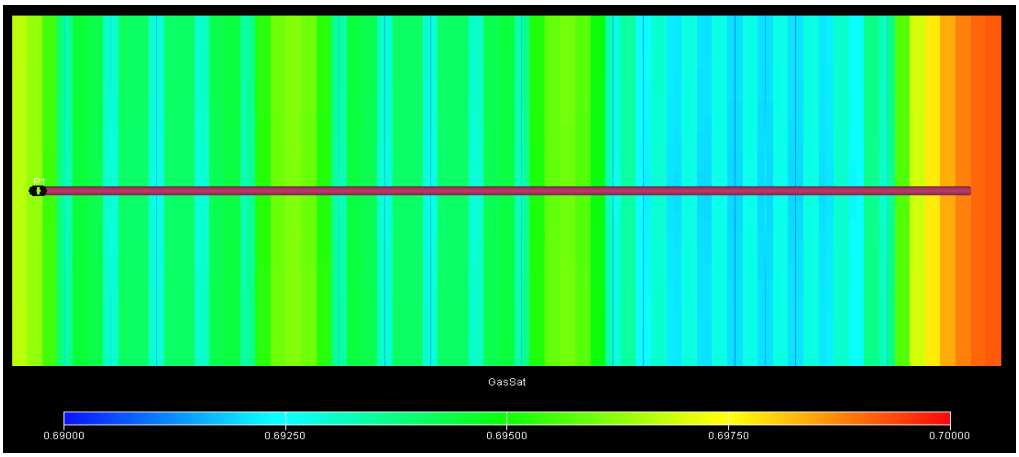

Figure 5.70 Gas saturation profile of Design B-2 for Toe patterns

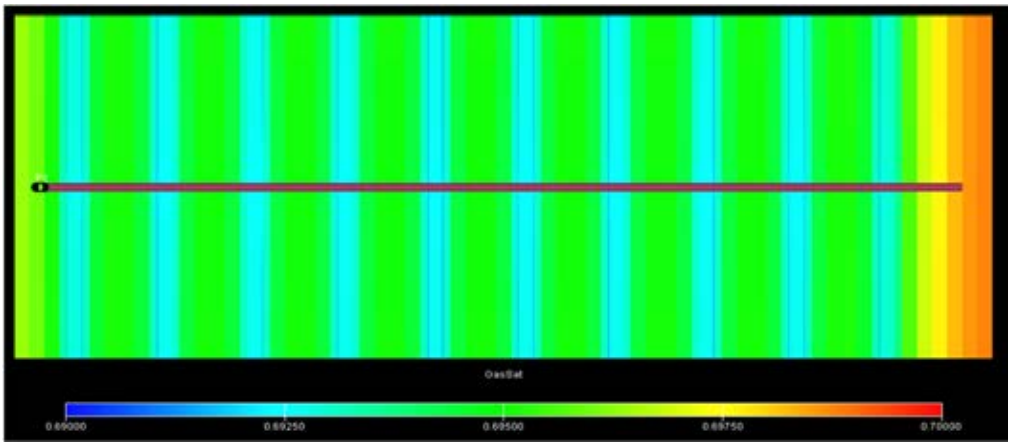

Figure 5.71 Gas saturation profile of Design B-2 for
Clustering Equally Spacing patterns

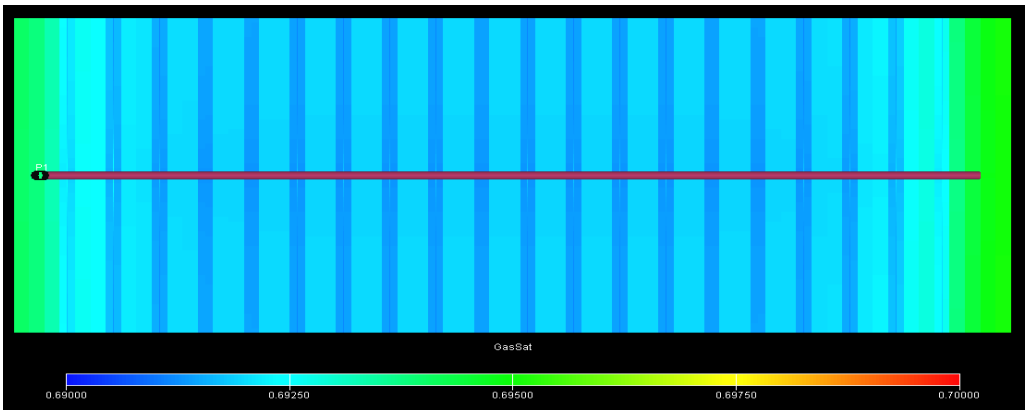

Figure 5.72 Gas saturation profile of Design B-2 for
Normal Symmetry patterns

Table 5.14 Summary of gas recovery factor for Design B-2
and different hydraulic fracturing patterns at the end of production

Hydraulic Fracturing Pattern	**OGIP (BSCF)**	**Cumulative Gas Production (BSCF)**	**Gas Recovery (%)**
Heel	4.78	2.30	48.21
Centre	4.78	2.30	48.19
Toe	4.78	2.31	48.22
Clustering Equally Spacing	4.78	2.22	46.35
Normal Symmetry Spacing	4.78	2.44	51.11

5.7.2.3 Gas Adsorption

Shale gas reservoirs have special characteristic where some of the gas might be adsorbed on the surface of the shale and some exists as a free gas in the matrix pore structure. The adsorbed gas on the surface of the shale is assumed to be a function of pressure, described by Langmuir Isotherm. Once reservoir pressure declines, gas on the shale surface can be gradually released. It will act as a free gas which flows to the fractures and eventually towards the wellbore. This section describes the adsorbed gas concentration effects on gas productivity. Figure 5.73 through 5.75 illustrate gas production rate, cumulative gas production, and reservoir pressure for different adsorbed gas concentrations, respectively.

From the graphs, the higher adsorbed gas concentration provides the greater productivity. Figure 5.73 shows that the higher gas concentration starts to divert in the later-time production compare to non-adsorbed gas concentration case. This result depicts that the more pressure decline can bring the more adsorbed gas to be released from the shale surface. Figures 5.121 through 5.123 show gas saturation profile for different gas concentrations. It can be observed in the higher gas concentration case, the matrix color appear more green expressing the higher gas saturation as a result of the more gas is released. Table 5.16 shows the summary of gas recovery factor for different adsorbed gas concentrations. Apparently, it can improve gas recovery factor of only 1-6%.

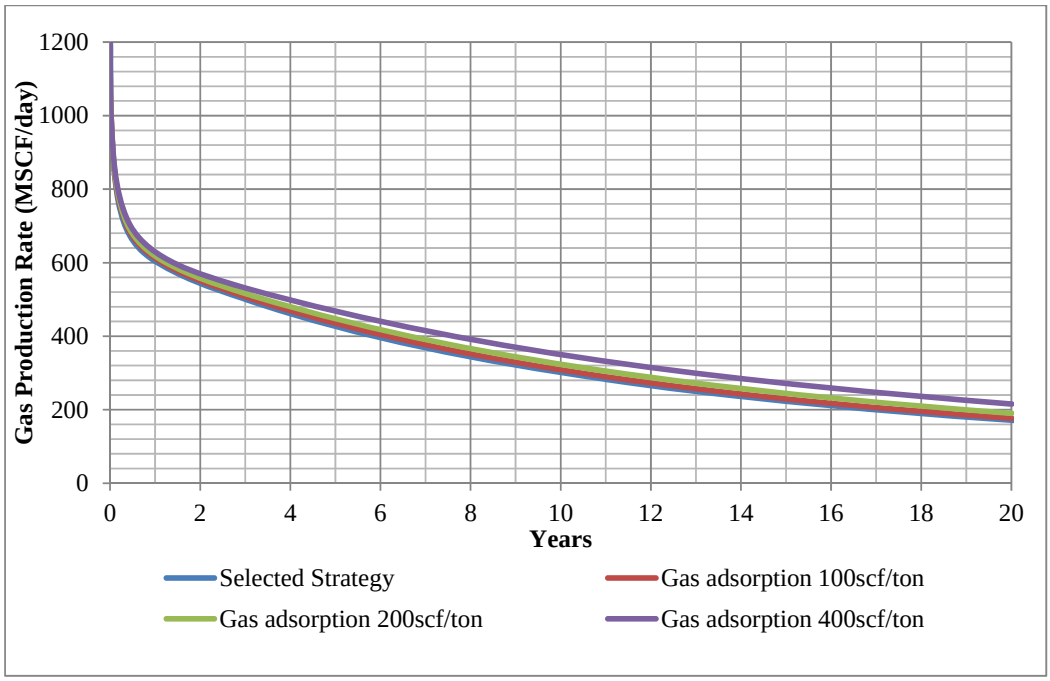

Figure 5.73 Gas production rate of Design B-2 for different gas concentrations

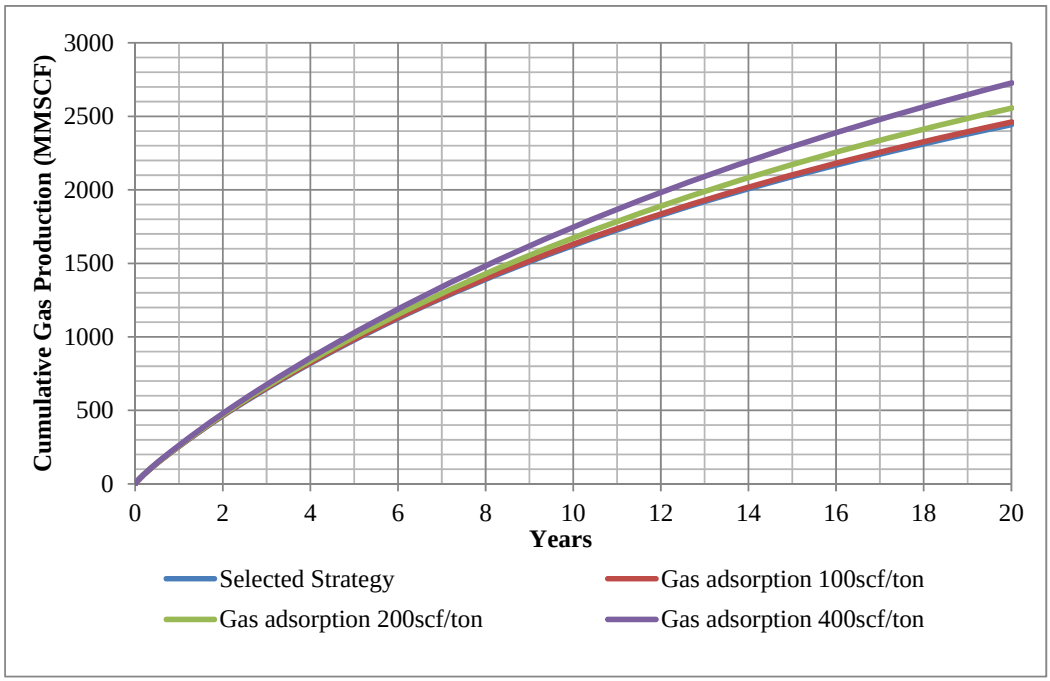

Figure 5.74 Cumulative gas production of Design B-2 for different gas concentrations

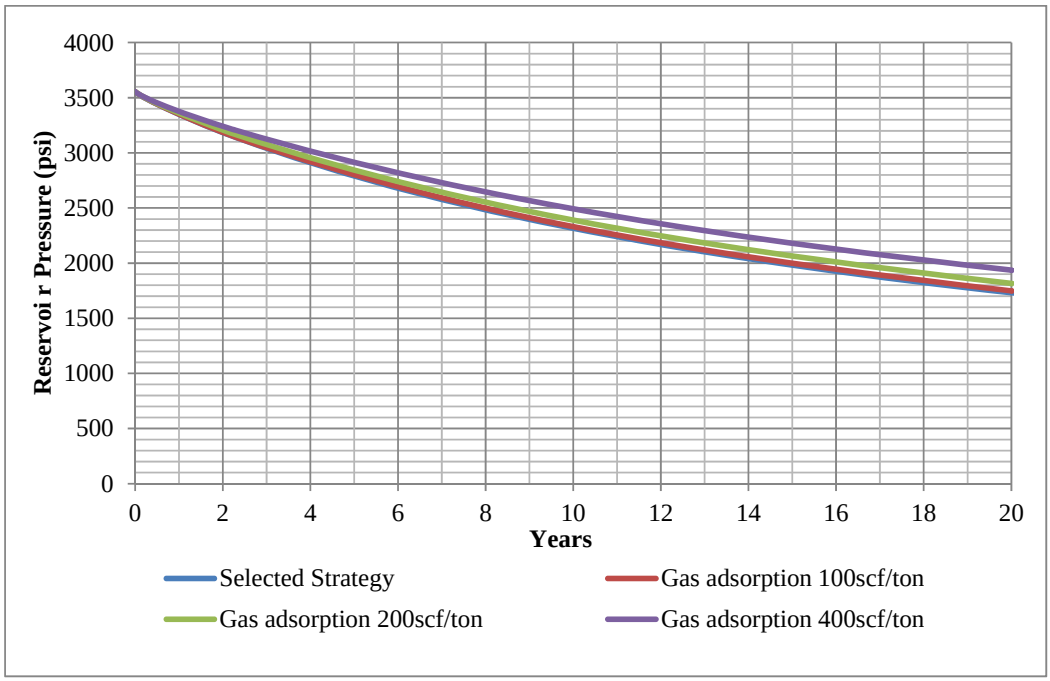

Figure 5.75 Reservoir pressure of Design B-2 for different gas concentrations

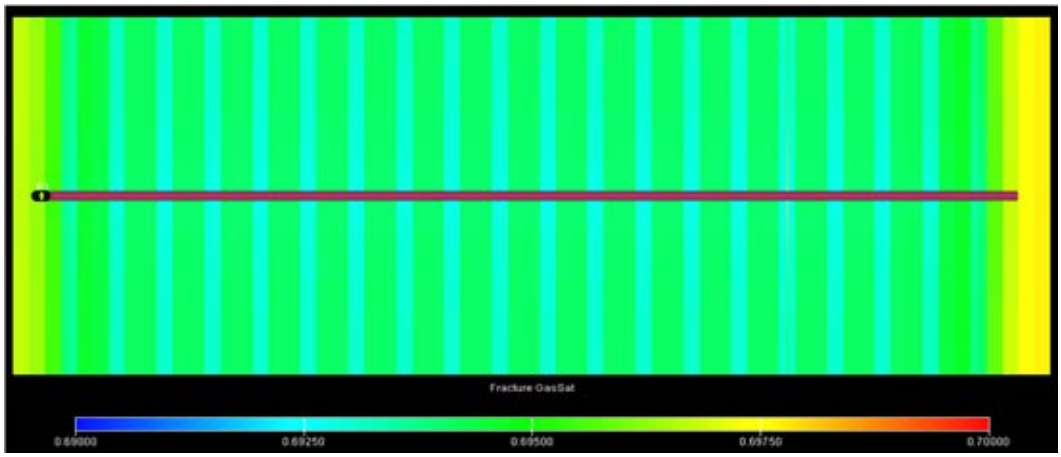

Figure 5.76 Gas saturation profile of Design B-2 for 100scf/ton gas concentration

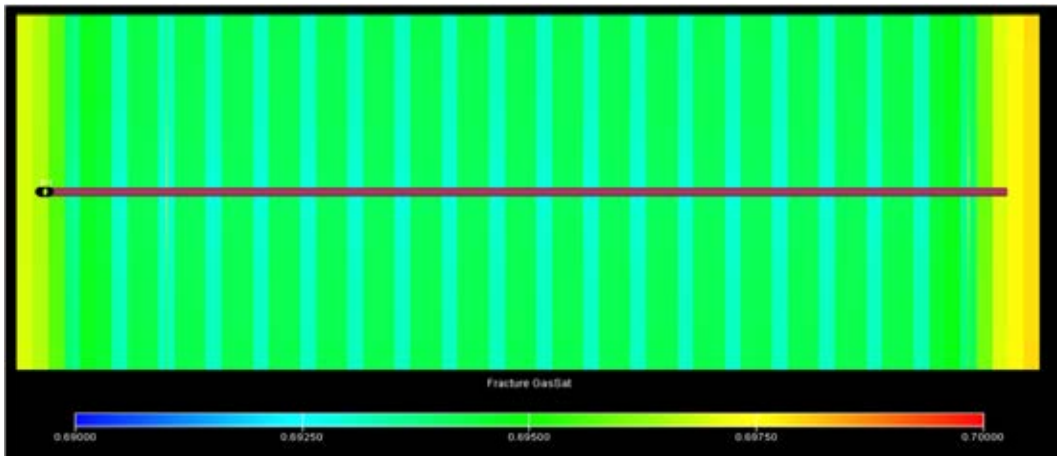

Figure 5.77 Gas saturation profile of Design B-2 for 200scf/ton gas concentration

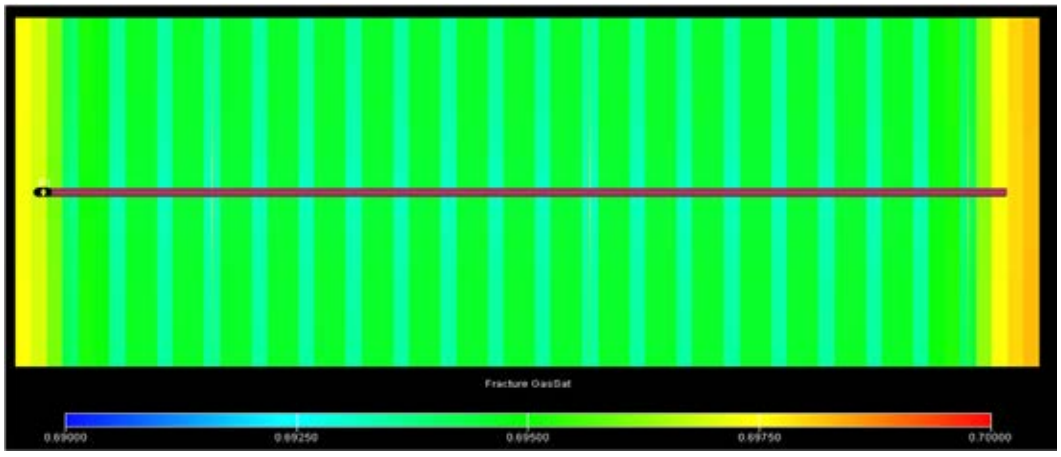

Figure 5.78 Gas saturation profile of Design B-2 for 400scf/ton gas concentration

Table 5.15 Summary of gas recovery factor for Design B-2
and different adsorbed gas concentrations at the end of production

Adsorbed Gas Concentration (scf/ton)	**OGIP (BSCF)**	**Cumulative Gas Production (BSCF)**	**Recovery (%)**
0	4.78	2.44	51.11
100	4.78	2.46	51.48
200	4.78	2.56	53.48
400	4.78	2.73	57.05

CHAPTER VI
CONCLUSIONS AND RECOMMENDATION

Producing gas purely from naturally fractured shale gas reservoir would not yield any benefit to oil operators since the gas recovery factor that can be obtained is only 0.49%. Therefore, hydraulic fracturing is applied on this type of reservoir to gain more gas recovery. This chapter concludes all results obtained from this study which includes reservoir performance based on reservoir parameters and hydraulic fracturing strategy selection. Recommendation is provided for future study.

6.1 Conclusions

1. Reservoir performance

- Matrix porosity does not have significant effect on gas production performance. The higher matrix porosity delivers slightly higher gas productivity in the early-time production.
- Matrix permeability can define gas flow ability significantly. Increasing of gas recovery factor can be achieved when matrix permeability increases.
- Increasing number of fractures offers higher gas productivity expressed in linear relationship. In the very low matrix permeability, number of fractures does not have much effect when producing gas from the natural fractures whereas it shows greater production improvement in high matrix permeability case.
- It is obviously seen an improvement in gas productivity when increasing fracture width for all matrix permeabilities. The larger fracture widths yield higher gas productivity. Nevertheless, there are certain points where the fracture widths cannot provide further production enhancement. For the minimum matrix permeability shale defines that 1.20mm is the most effective fracture width that can provide the maximum gas recovery factor of 9% whereas 2.40mm can

be defined as the most effective fracture width for the maximum matrix permeability. It delivers maximum gas recover factor of 57%.

2. Hydraulic strategy selection

- Gas production efficiency is defined as the ratio of gas recovery improvement relative to stimulated reservoir volume enhancement. The production efficiency is used to determine the optimum hydraulic fracturing design. The optimum design for hydraulic fracturing on pre-existing natural fracture is to enlarge fracture width to 1.20mm. This design can provide gas recovery factor of 31%.
- The optimum design for hydraulic fracturing is to conduct 20 fractures and 1.20mm fracture width. This strategy can obtain 51% gas recovery factor.
- Significant effect of matrix permeability on gas productivity for the optimum hydraulic fracturing design can be observed. The higher matrix permeability yields greater gas recovery factor.
- With the same number of fractures, different hydraulic fracturing patterns or different fracture spacing has only slight effect on production performance. The result showed that the more evenly distributed of fractures in the reservoir would yield the greatest gas productivity.
- The results showed some gas improvement from gas desorption as the pressure declines. The higher adsorbed gas concentrations can provide more gas productivity but it has insignificant effect.

6.2 Recommendation

Economic analysis is an important factor to finalize the hydraulic fracturing design strategy for the decision maker. It is strongly recommended for future study to further evaluate these technical hydraulic fracturing designs with economic terms.

References

[1] H.D. Murphy and M.C. Fehler, Hydraulic Fracturing of Jointed Formations, Paper SPE 14088, presented at SPE 1966 International Meeting on Petroleum Engineering held in Benjing, China, 17-20 March, 1966.

[2] Neal Nagel, Itasca Houston, Branko Damjanac and Xavier Garcia, Discrete Element Hydraulic Fracture Modeling-Evaluating Changes in Natural Fracture Aperture and Transmisivity, Paper CSUG/SPE 14957, presented at the Canadian Unconventional Resources Conference held in Calgary, Alberta, Canada, 15-17 November, 2011.

[3] Daniel Moos, Improving Shale Gas Production Using Geomechanics, Exploration & Production – Oil & Gas Review – Volume 9 Issue 2.

[4] N. Potluri, D. Zhu, and A.D. Hill, Effect of Natural Fractures on Hydraulic Fracture Propagation, Paper SPE 94568, presented at the SPE European Formation Damage Conference held in Scheveningen, Netherland, 25-27 May, 2005.

[5] Warpinski, N.R.,Teufel, L.W., Influence of Geologic Discontinuities on Hydraulic Fracture Propagation, Paper SPE 13224, Journal of Petroleum Technology Volume 39, Number 2, 1987.

[6] Jian Zhou, Chengjin Zue, Experimental Investigation of Fracture Interaction between Natural Fractures and Hydraulic Fracture in Naturally Fractured Reservoirs, Paper SPE 142890, Presented at the SPE EUROPEC/EAGE Annual Conference and Exhibition held in Vienna, Austria, 23-26, 2011.

[7] Changan M. Du, Xu Zhang, Lang Zhan, Hongren Gu, Brad Hay, Keith Tushingham, Y. Zee Ma, Modeling Hydraulic Fracturing Induced Fracture Networks in Shale Gas Reservoirs as a Dual Porosity System, Paper SPE 132180, Presented the CPS/SPE International Oil & Gas Conference and Exhibition in China held in Benjing, China, 8-10 June, 2010.

[8] Les B., W.S Birk, Julian D., Leo E., Jim G., Richard C.K., Kazuhiko T., The Source for Hydraulic Fracture Characterization, Oilfield review, Winter 2005/2006.

[9] Herschel McDivitt, Hydraulic Fracturing and Other Trends in Oiland Gas Production, Well Completion Reports Division 2005-2012.

[10] C.L. Cipolla, E.P. Lolon, J.C. Erdle and B. Rubin, Reservoir Modeling in Shale Gas Reservoirs, Paper SPE 125530, Presented at the SPE Eastern Regional Meeting held in Charleston, West Virginia, USA, 23-25 September, 2009.

[11] C.M. Freeman, G. Moridis, Lawrence Berkeley, D. Ilk, T.A. Blasingama, A numerical Study of Performance for Tight Gas and Shale Gas Reservoir Systems, Paper SPE 124961, Presented at the SPE Annual Technical Conference and Exhibition held in New Orleans, Louisiana, USA, 4-7 October, 2009.

[12] M. Mirzaei, C.L. Cipolla, A Workflow for Modeling and Simulation of Hydraulic Fractures in Unconventional Gas Reservoir, Paper SPE 153022, Presented at the SPE Middle East Unconventional Gas Conference and Exhibition held in Abu Dhabi, UAE, 23-25 January, 2012.

[13] Bin Gong, Guan Qin, Brain F., Hongyan Wang, Discrete Modeling of Natural and Hydraulic Fractures in Shale-Gas Reservoirs, Paper SPE 146842, Presented at the SPE Annual Technical Conference and Exhibition held in Denver, Colorado, USA, 30 October – 2 November, 2011.

[14] K. Uleberge, J. Kleppe, Dual Porosity, Dual Permeability Formulation for Fractured Reservoir Simulation, Paper TPG4150 Reservoir Recovery Techniques 2011.

[15] A. Aboaba, Y. Cheng, Estimation of Fracture Properties for a Horizontal Well with Multiple Hydraulic Fractures in Gas Shale, Paper SPE 138524, Presented at the SPE Eastern Regional Meeting held in Morgantown, West Virginia, USA, 12-14 October, 2010.

[16] A. Sakhaee-Pour, Steven L. Bryant, Gas Permeability of Shale, Paper SPE 146944, Presented at the SPE Annual Technical Conference and Exhibition held in Denver, Colorado, USA, 30 October – 2 November, 2011.

[17] Yueming Cheng, Pressure Transient Characteristics of Hydraulically Fractured Horizontal Shale Gas Wells, Paper SPE 149311, Presented at the SPE Eastern Regional Meeting held in Columbus, Ohio, USA, 17-19 August, 2011.

[18] Friedel Torsten, Numerical Simulation of Production from Tight-Gas Reservoir by Advanced Stimulation Technologies, Master's thesis, Department of Geoscience, Geoengineering and Mining, Faculty of Engineering, Freiberg University of Mining and Technology, 2004.

[19] Michael J. Economides, Tony Martin, Modern Fracturing Enhancing Natural Gas Production book, 1st Edition, Energy Triune Publication, 2007.

[20] Terzaghi K., Theoretical Soil Mechanics book, John Wiley and Sons, New York, 1943.

[21] Expert Panel Report Bainbridge Township Subsurface Gas Invasion, Chapter 2 Hydraulic Fracturing.

[22] Heber Cinco-Ley, Fernando Samaniego-V, Transient Pressure Analysis, Paper SPE 7490, SPE, Inst, Mexicano Del Petroleo, 1981.

[23] M. King Hubbert, Darcy's Lay and the Field Equations of the Flow of Underground Fluids, Paper T.P. 4352, Journal Petroleum, Houston, Taxas, 1956.

[24] J. Geertsma, Estimating the Coefficient of Intertial Resistance in Fluid Flow Through Porous Media, Paper SPE 4706, Copyright American Institute of Mining, Metallurgical, and Petroleum Engineers, Inc, October, 1974.

[25] T.M. Herge, Hydraulically Fractured Horizontal Well Simulation, Paper SPE 35506, Presented at the European 3D Reservoir Modeling Conference held in Stavanger, Norway, 16-17 April, 1996.

[26] Petroleum Experts, PROSPER Single Well Systems Analysis user guide version 9.1.

[27] Schlumberger Information Solution, ECLIPSE Reference Manual 2007.1 and ECLIPSE Technical Description 2007.1.

[28] Fredd, C.N., McConnell, S.B., Boney, C.L., and England, K.W., Experimental Study of Fracture Conductivity for Water-Fracturing and Conventional Fracturing Applications, Paper SPE 74138, Presented at the 2000 SPE Rocky Mountain Regional/Low Permeability Reservoirs Symposium and Exhibition, Devnver, Colorado, 12–15 March, 2000.

[29] Kuntol Chinrungkhakul, Hydraulic Fracturing Strategy in Gas Condensate Reservoirs, Master's Thesis, Department of Petroleum Engineering, Faculty of Engineering, Chulalongkorn University, 2010.

[30] Qinghui Li, Mian Chen, Yan Jin, and Yu Zhou, Rock Mechanical Properties of Shale Gas Reservoir and Their Influences on Hydraulic Fracture, Paper IPTC 16580, Presented at the International Petroleum Technology Conference held in Beijing, China, 26–28 March, 2013.

[31] A.A. Ketter, J.L. Daniels, J.R. Heinze and G. Water, A Field Study Optimizing Completion Strategies for Fracture Initiation in Barnett Shale Horizontal Wells, Paper SPE 103232, Presented at the 2006 SPE Annual Technical Conference and Exhibition held in San Antonio, Texas, U.S.A., 24–27 September, 2008.

[32] M.J. Mayerhofer, E.P. Lolon, N.R. Warpinski, C.L. Cipolla, D. Walser and C.M. Rightmire, What Is Stimulated Reservoir Volume, Paper SPE 119890, Presented at SPE Shale Gas Production Conference, Fort Worth, Taxas, 16–18 September, 2008.

APPENDIX

Appendix

A) Gas saturation profile for different number of factures

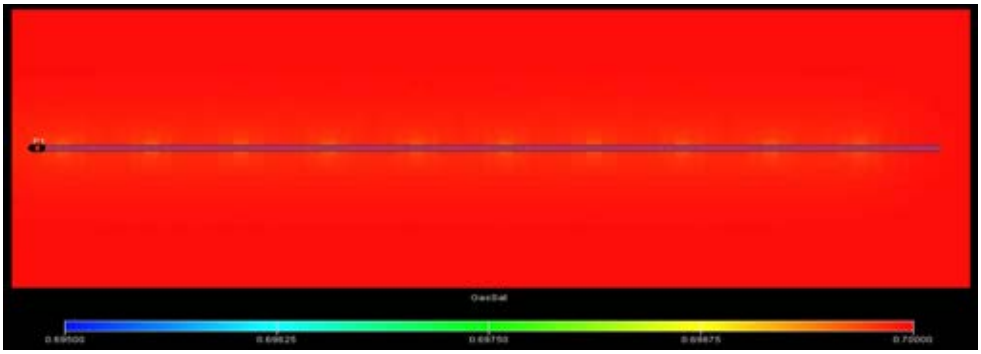

A-1 Gas saturation for 10 fractures
at the end of production (Base Case)

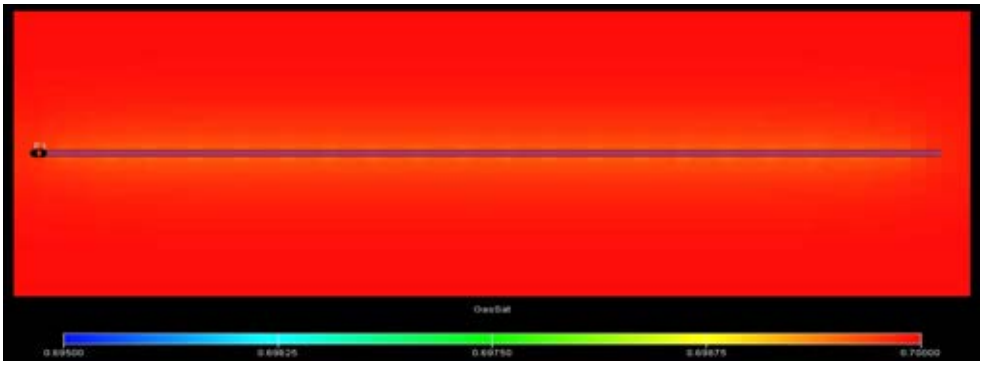

A-2 Gas saturation for 20 fractures
at the end of production

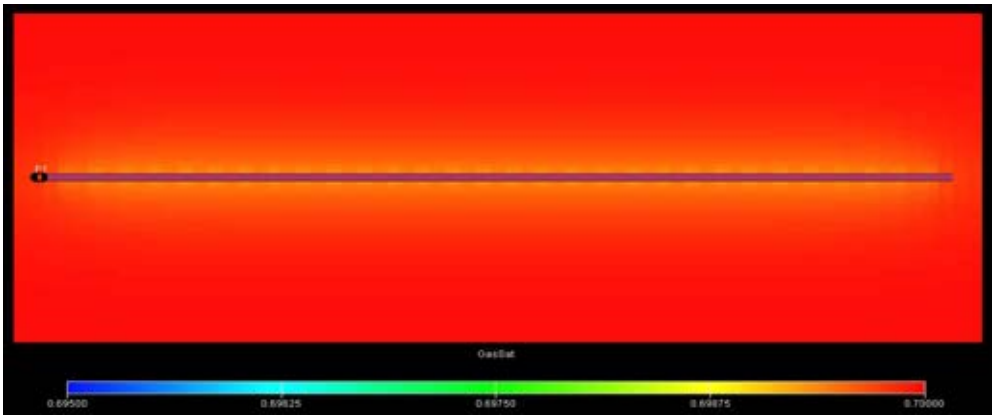

A-3 Gas saturation for 30 fractures
at the end of production

B) Gas saturation profile for different number of fractures at minimum and maximum matrix permeability

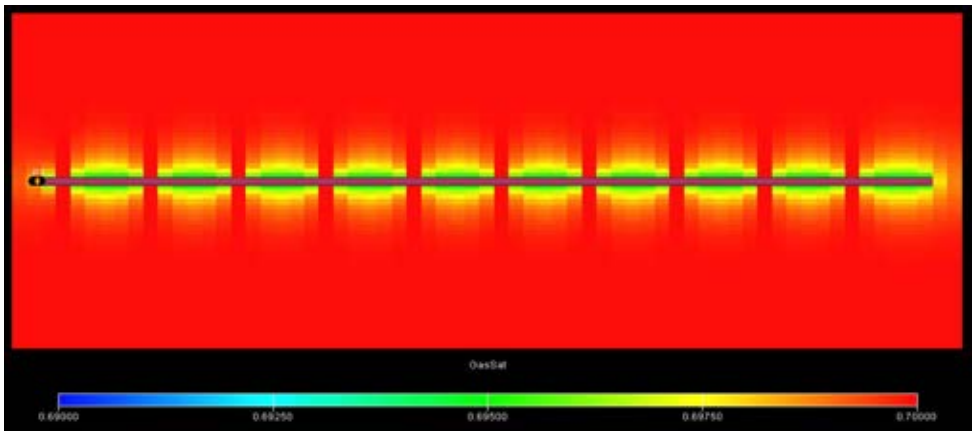

B-1 Gas saturation profile for 10 fractures and 0.00007mD

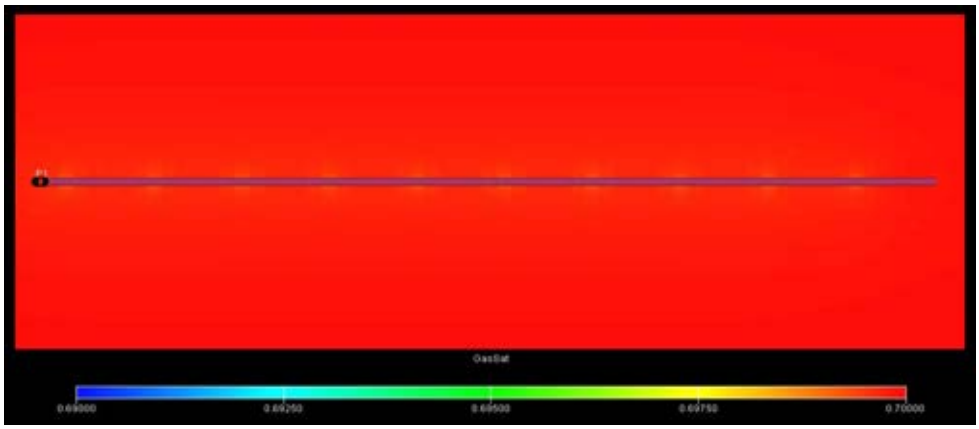

B-2 Gas saturation profile for 10 fractures and 0.0005mD

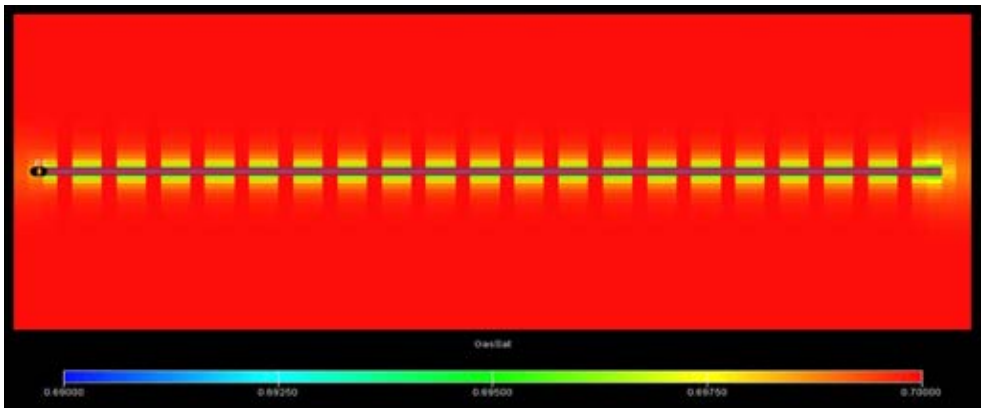

B-3 Gas saturation profile for 20 fractures and 0.00007mD

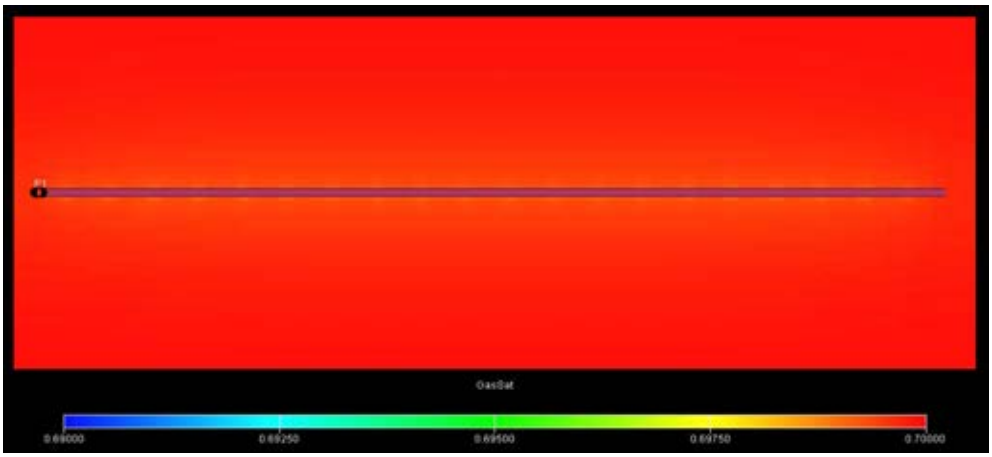

B-4 Gas saturation profile for 20 fractures and 0.0005mD

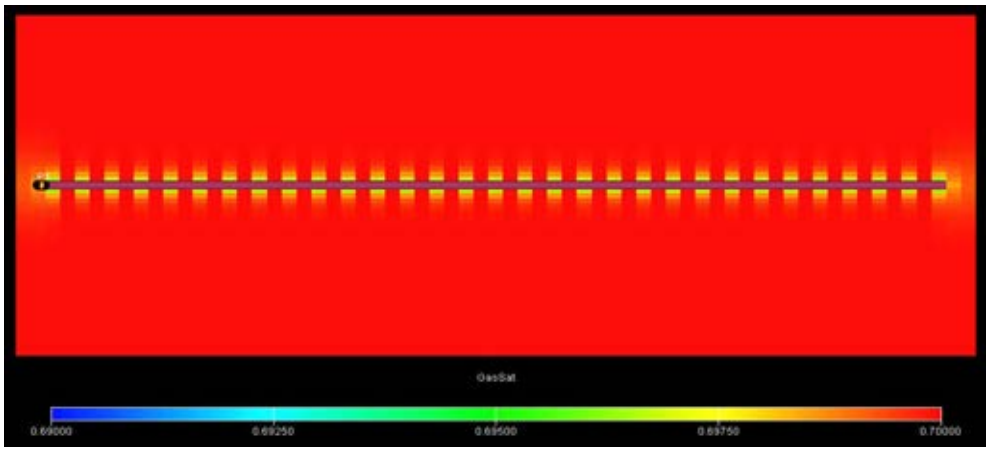

B-5 Gas saturation profile for 30 fractures and 0.00007mD

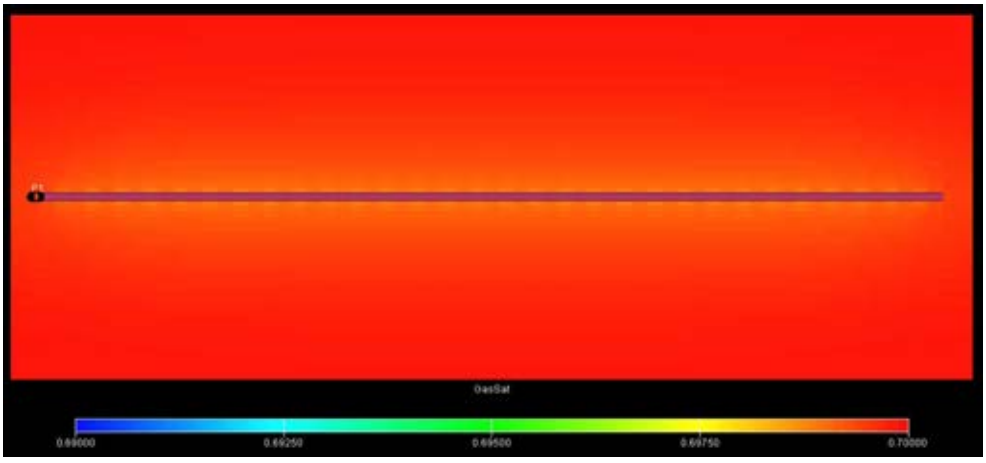

B-6 Gas saturation profile for 30 fractures and 0.0005mD

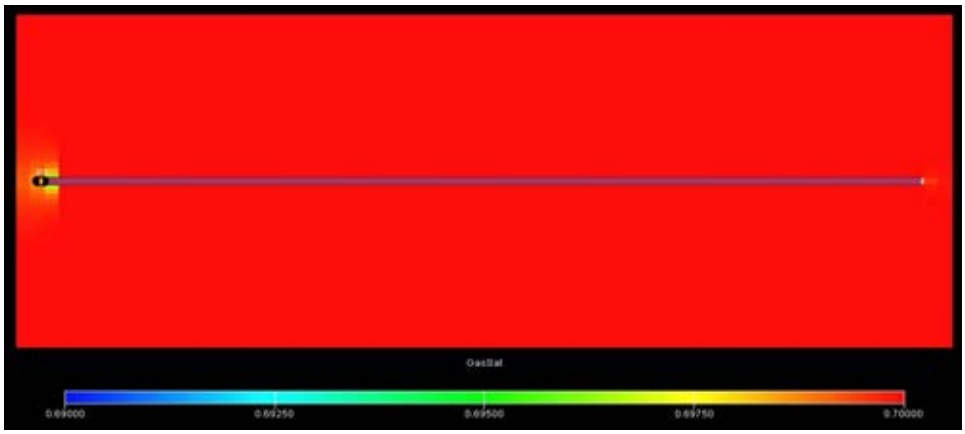

B-7 Gas saturation profile for 60 fractures and 0.00007mD

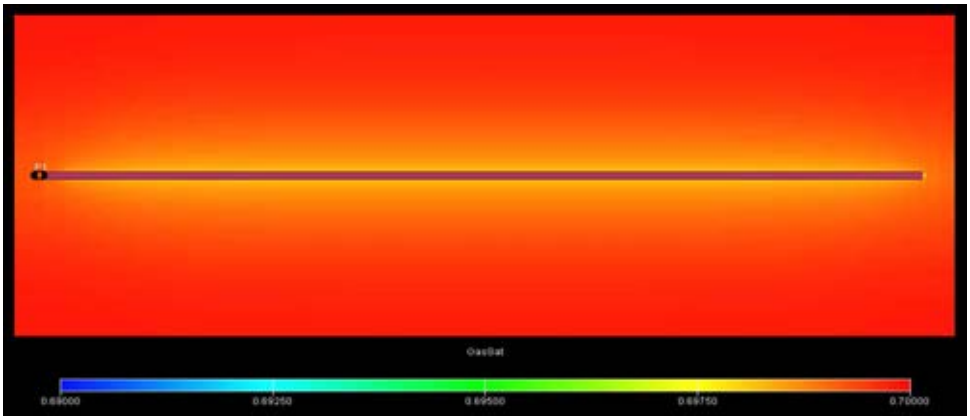

B-8 Gas saturation profile for 60 fractures and 0.0005mD

C) Gas saturation profile for different fracture widths

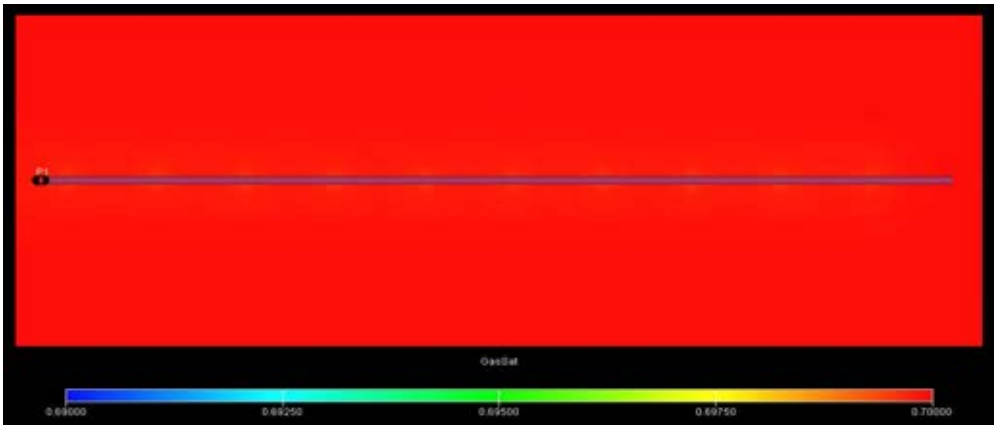

C-1 Gas saturation profile for 0.015mm fracture width
at the end of production

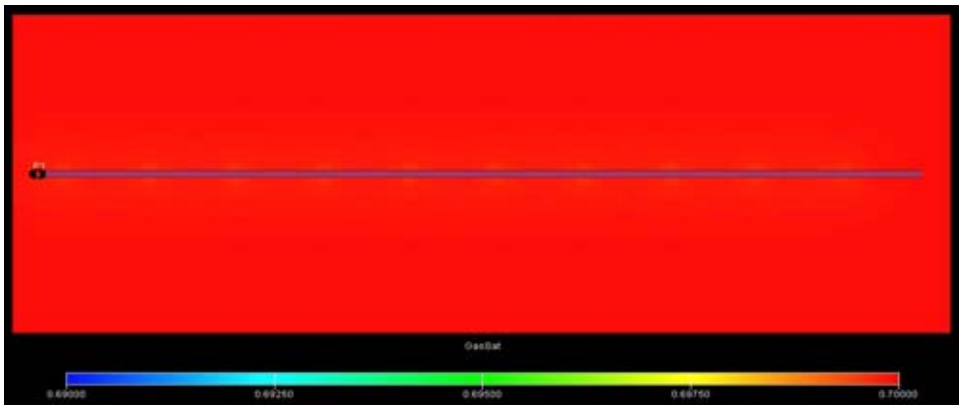

C-2 Gas saturation profile for 0.030mm fracture width
at the end of production (Base Case)

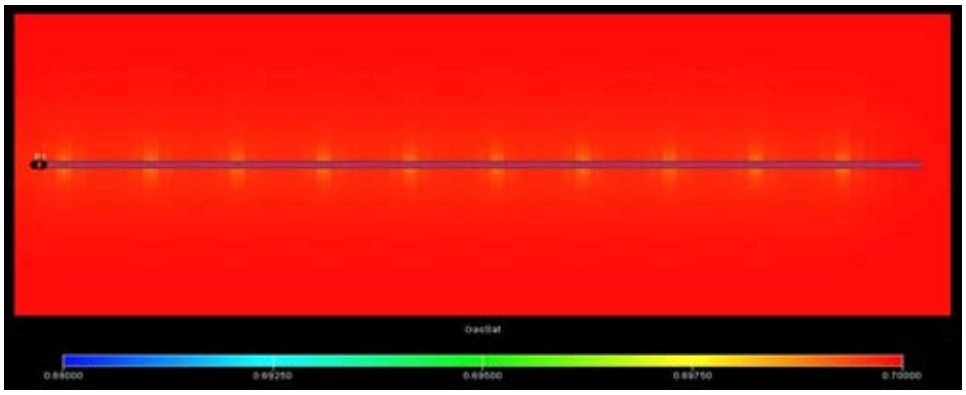

C-3 Gas saturation profile for 0.15mm fracture width
at the end of production

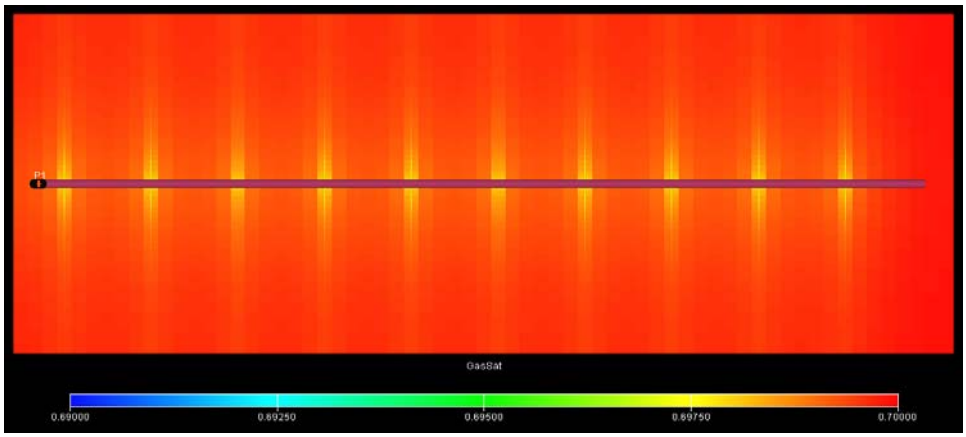

C-4 Gas saturation profile for 0.30mm fracture width
at the end of production

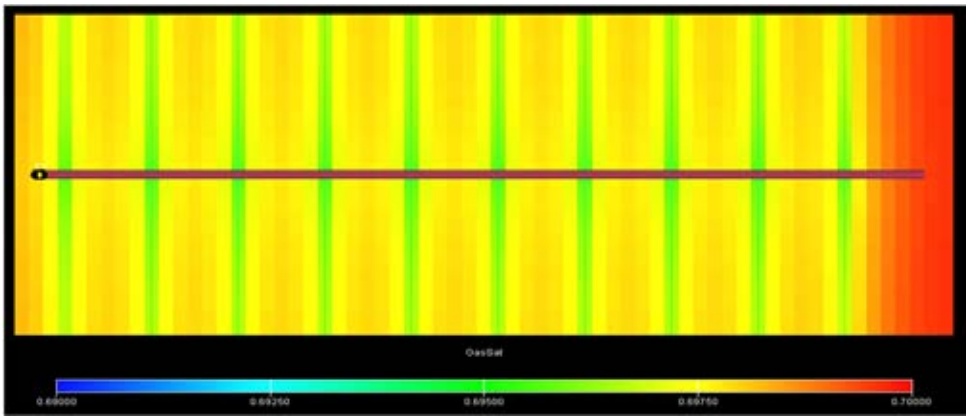

C-5 Gas saturation profile for 0.60mm fracture width
at the end of production

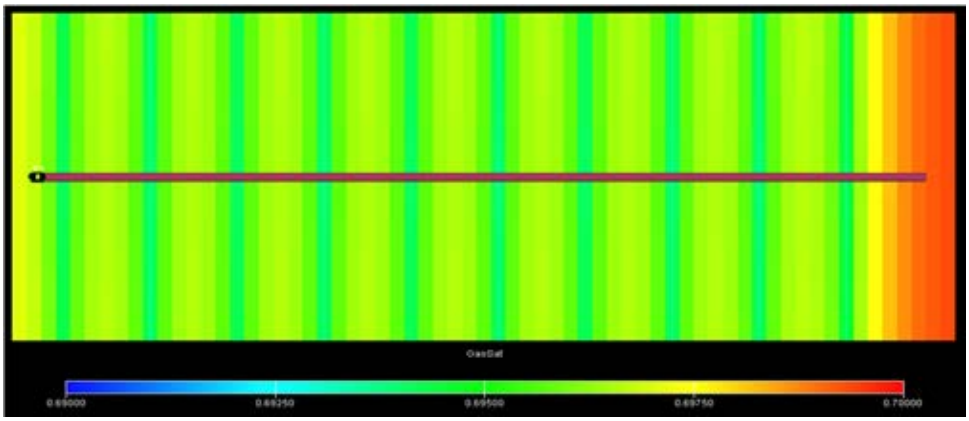

C-6 Gas saturation profile for 1.20mm fracture width
at the end of production

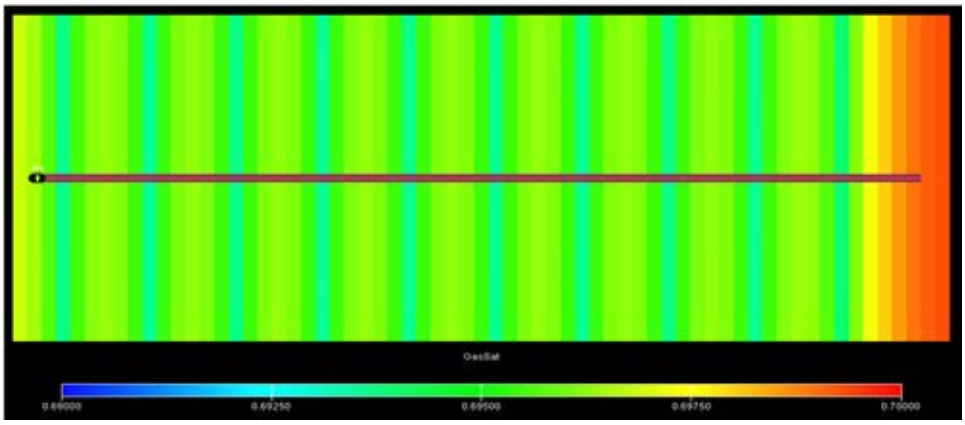

C-7 Gas saturation profile for 2.40mm fracture width
at the end of production

D) Gas saturation profile for different fracture widths at minimum and maximum matrix permeability

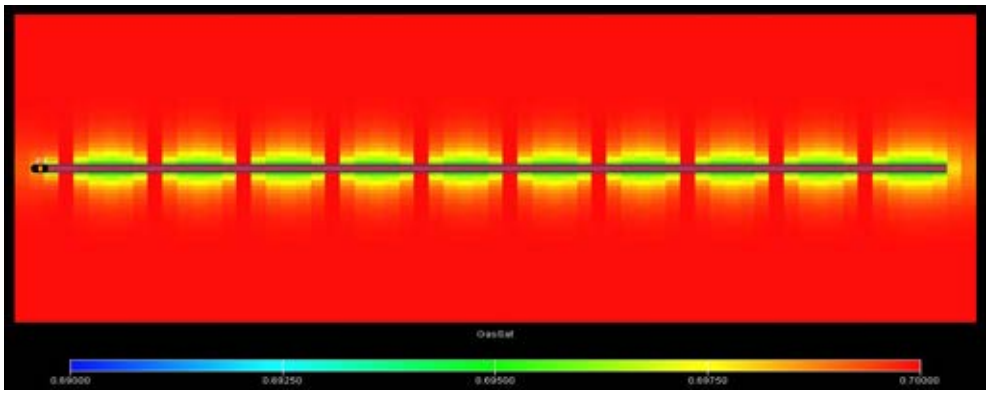

D-1 Gas saturation profile for fracture width of 0.015mm and matrix permeability of 0.00007mD

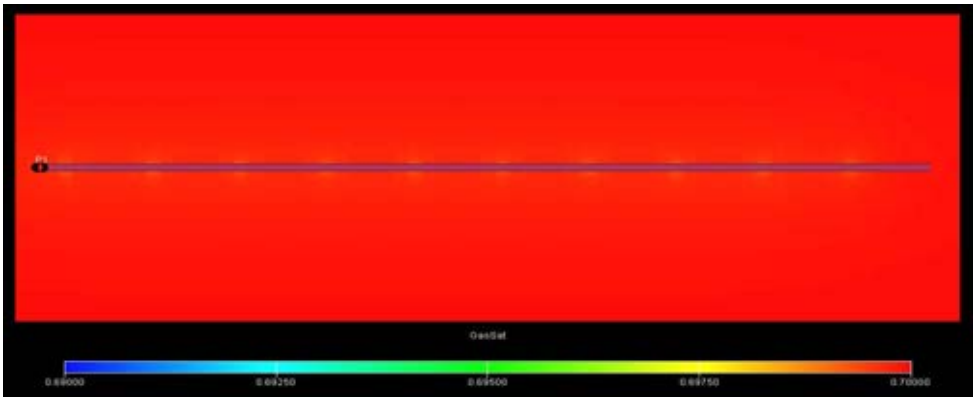

D-2 Gas saturation profile for fracture width of 0.015mm and matrix permeability of 0.0005mD

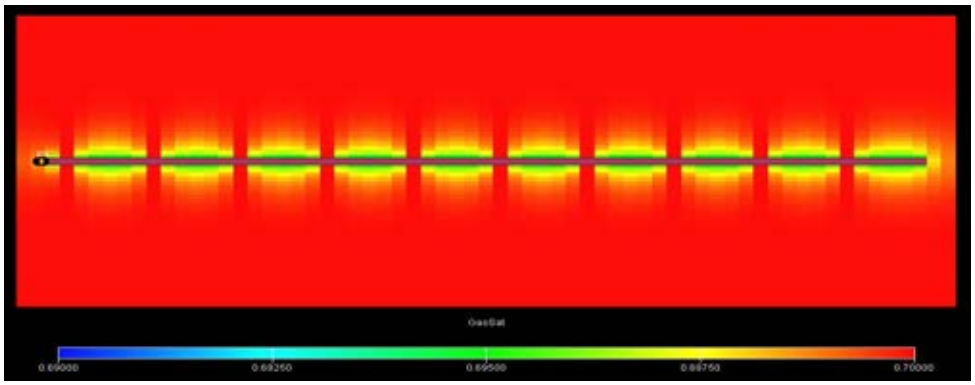

D-3 Gas saturation profile for fracture width of 0.03mm and matrix permeability of 0.00007mD

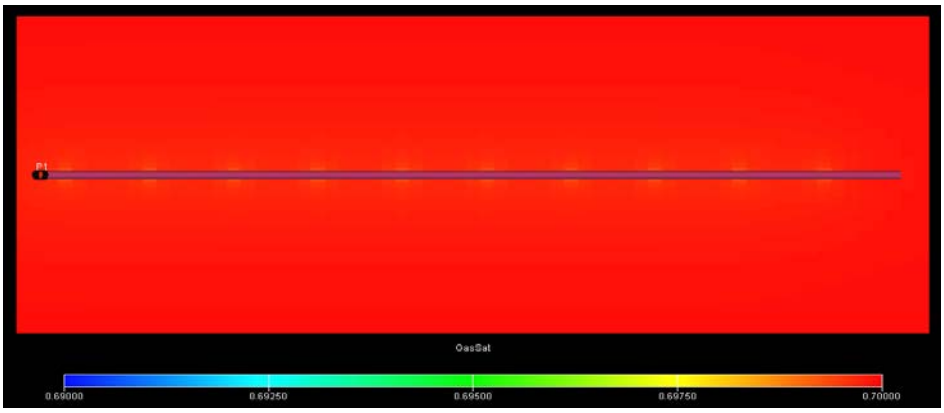

D-4 Gas saturation profile for fracture width of 0.03mm
and matrix permeability of 0.0005mD

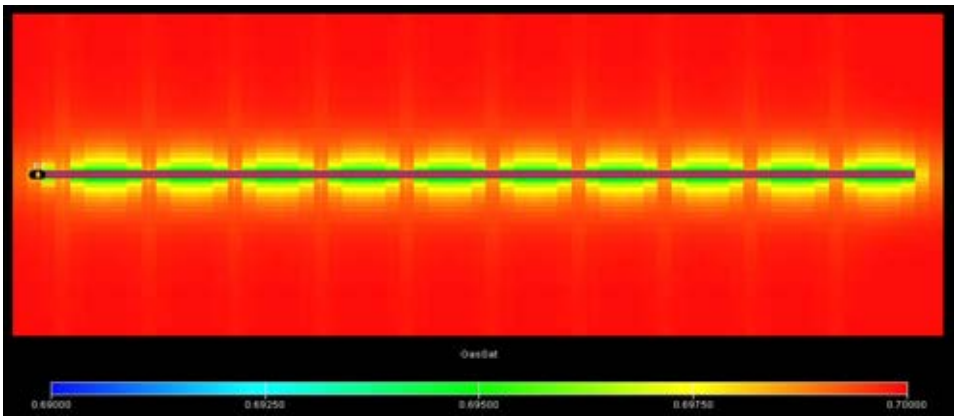

D-5 Gas saturation profile for fracture width of 0.15mm
and matrix permeability of 0.00007mD

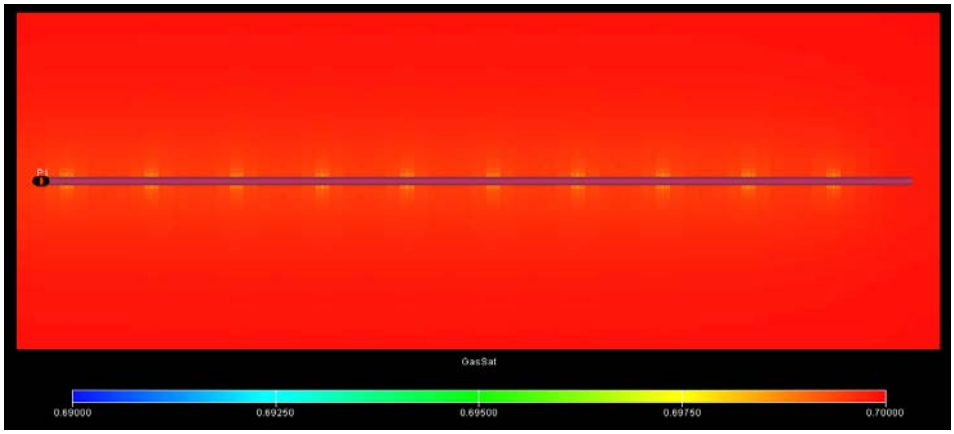

D-6 Gas saturation profile for fracture width of 0.15mm
and matrix permeability of 0.0005mD

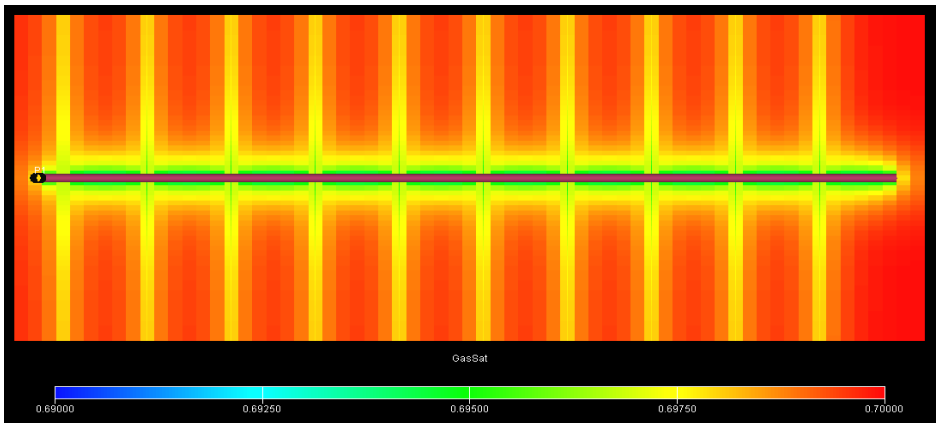

D-7 Gas saturation profile for fracture width of 0.30mm
and matrix permeability of 0.00007mD

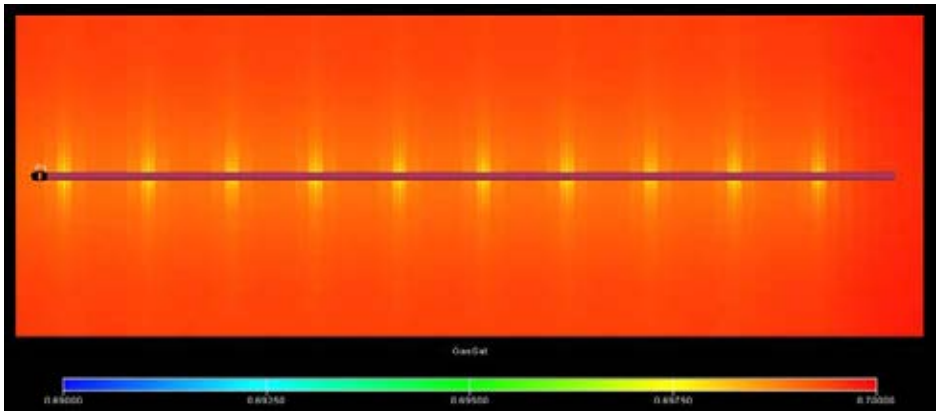

D-8 Gas saturation profile for fracture width of 0.30mm
and matrix permeability of 0.0005mD

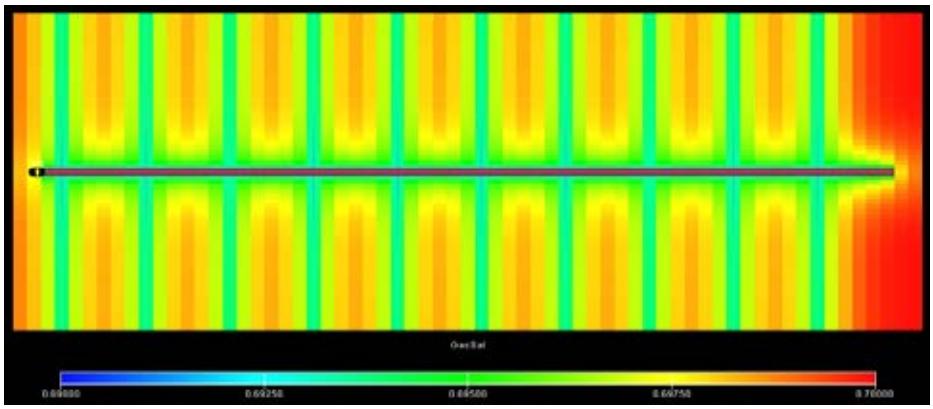

D-9 Gas saturation profile for fracture width of 0.60mm
and matrix permeability of 0.00007mD

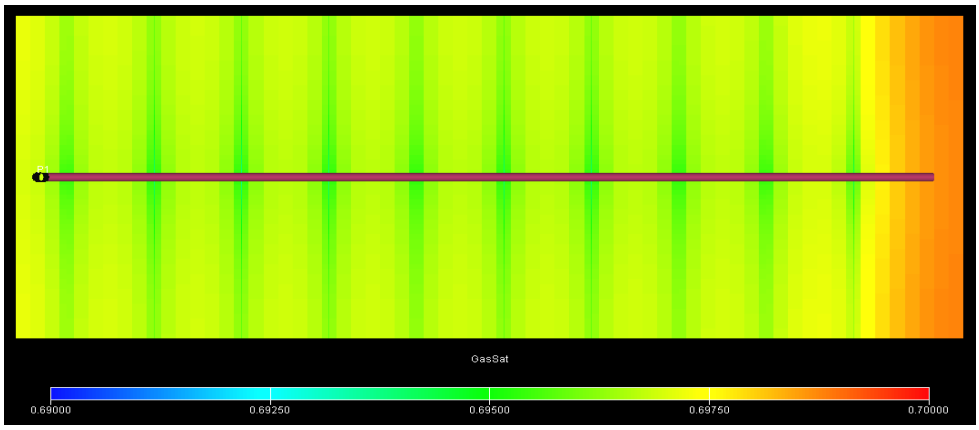

D-10 Gas saturation profile for fracture width of 0.60mm
and matrix permeability of 0.0005mD

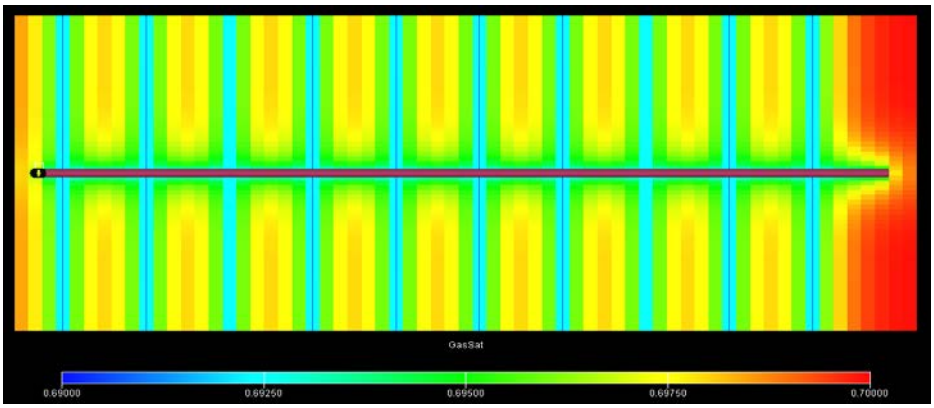

D-11 Gas saturation profile for fracture width of 1.20mm
and matrix permeability of 0.00007mD

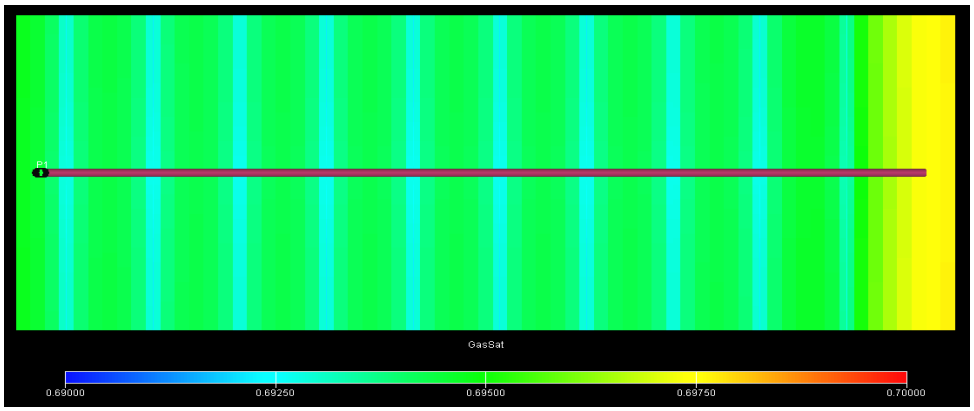

D-12 Gas saturation profile for fracture width of 1.20mm
and matrix permeability of 0.0005mD

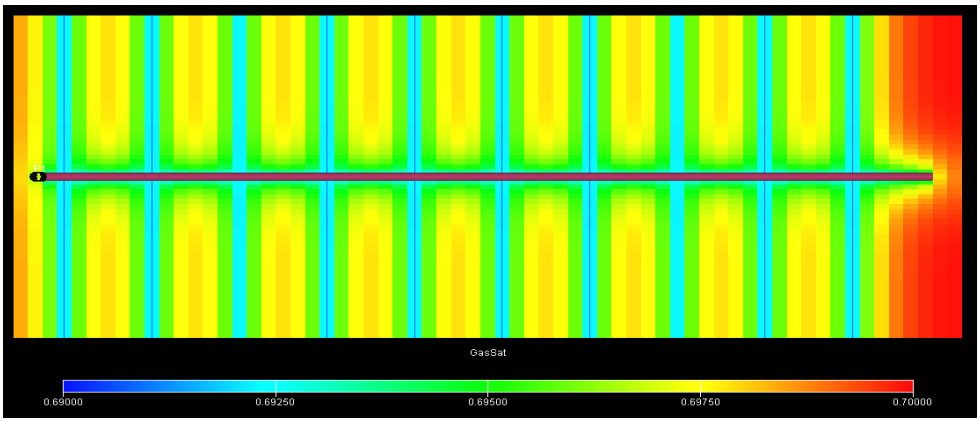

D-13 Gas saturation profile for fracture width of 2.40mm
and matrix permeability of 0.00007mD

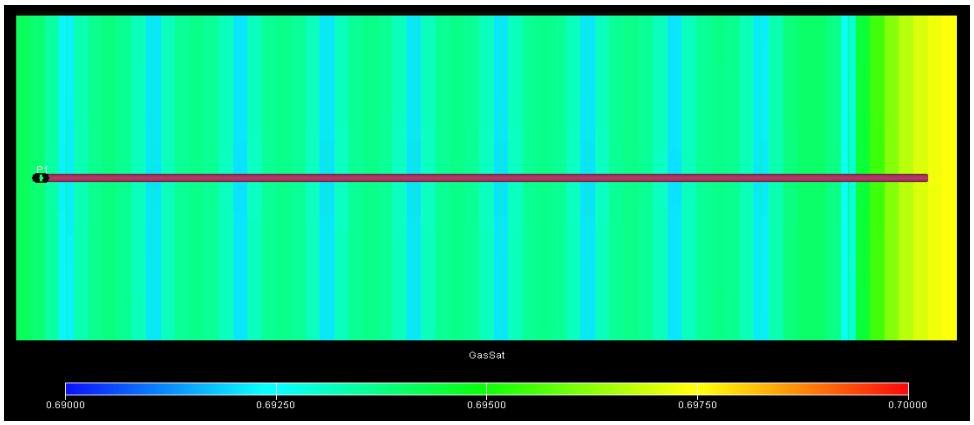

D-14 Gas saturation profile for fracture width of 2.40mm
and matrix permeability of 0.0005mD

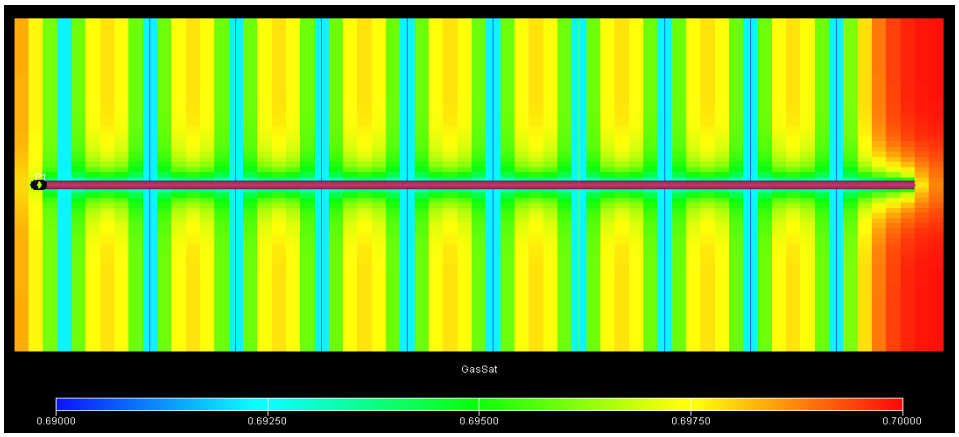

D-15 Gas saturation profile for fracture width of 3.00mm
and matrix permeability of 0.00007mD

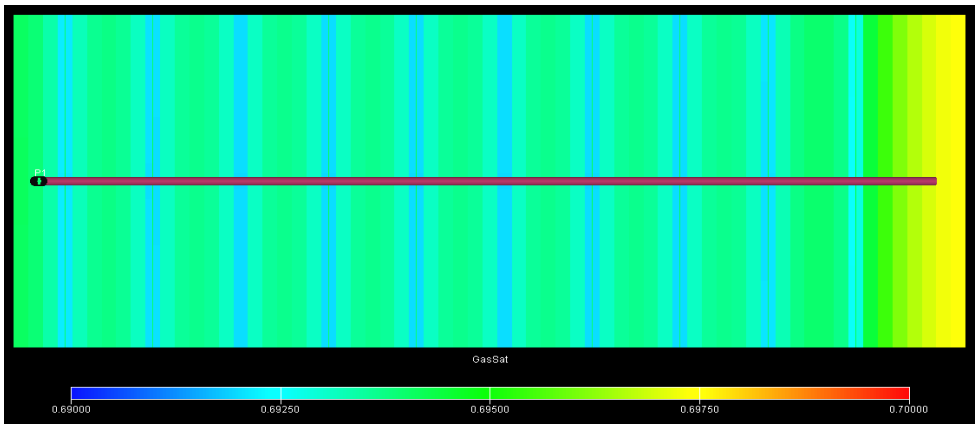

D-16 Gas saturation profile for fracture width of 3.00mm
and matrix permeability of 0.0005mD

E) Gas saturation profile for different hydraulic fracturing designs

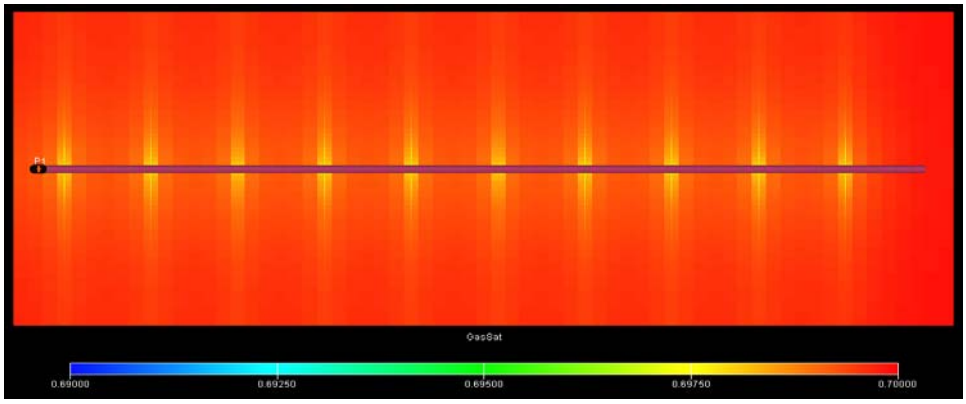

E-1 Gas saturation profile for Design A-1
at the end of production

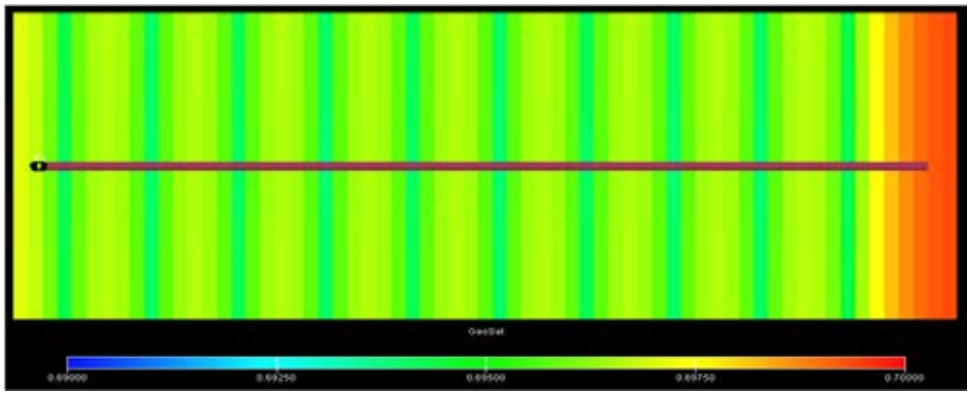

E-2 Gas saturation profile for Design A-2
at the end of production

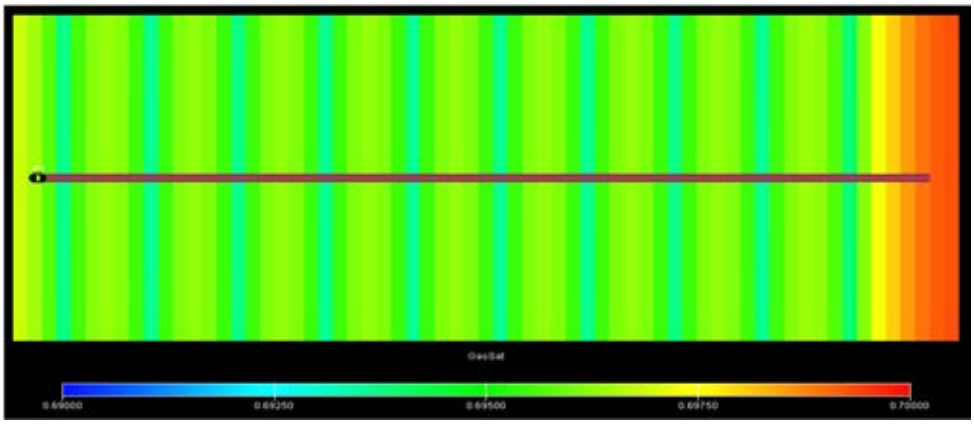

E-3 Gas saturation profile for Design A-3
at the end of production

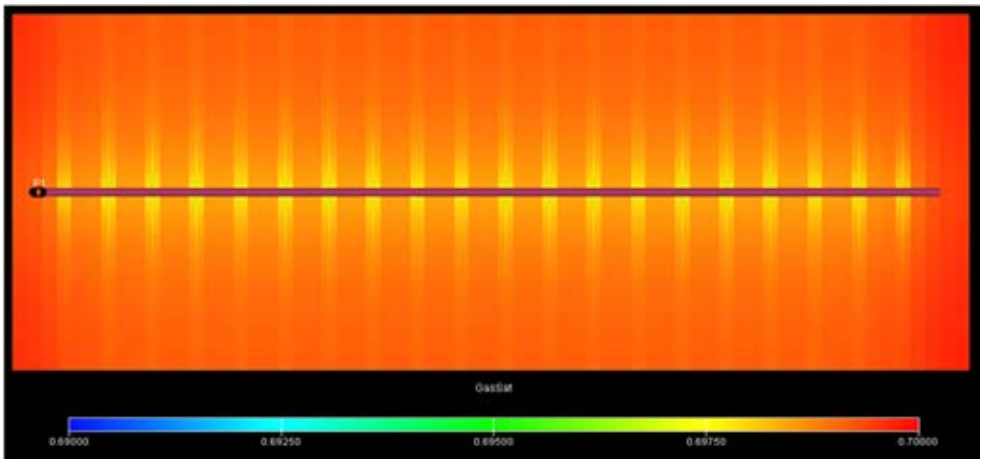

E-4 Gas saturation profile for Design B-1

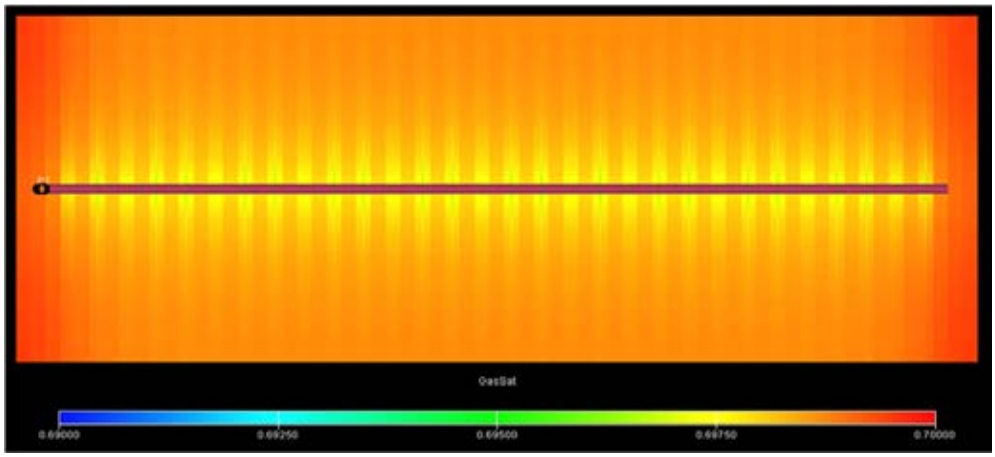

E-5 Gas saturation profile for Design C-1

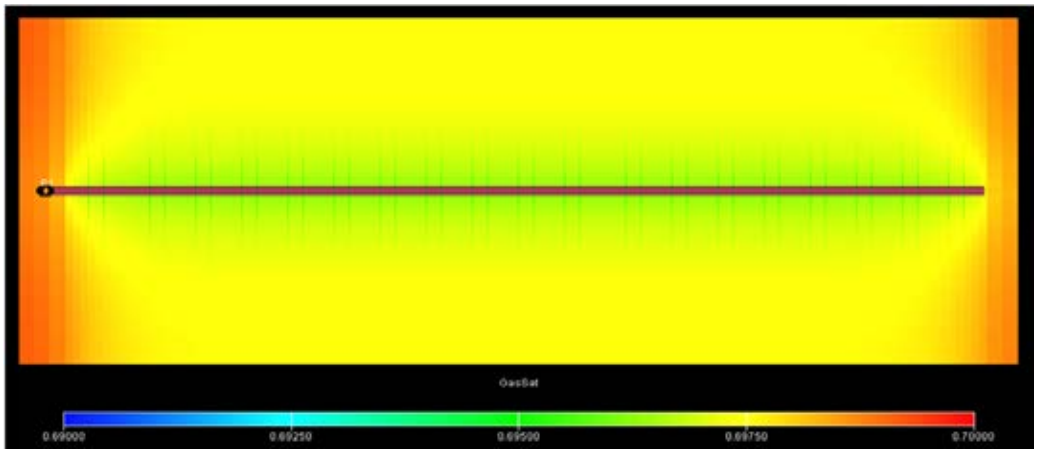

E-6 Gas saturation profile for Design D-1

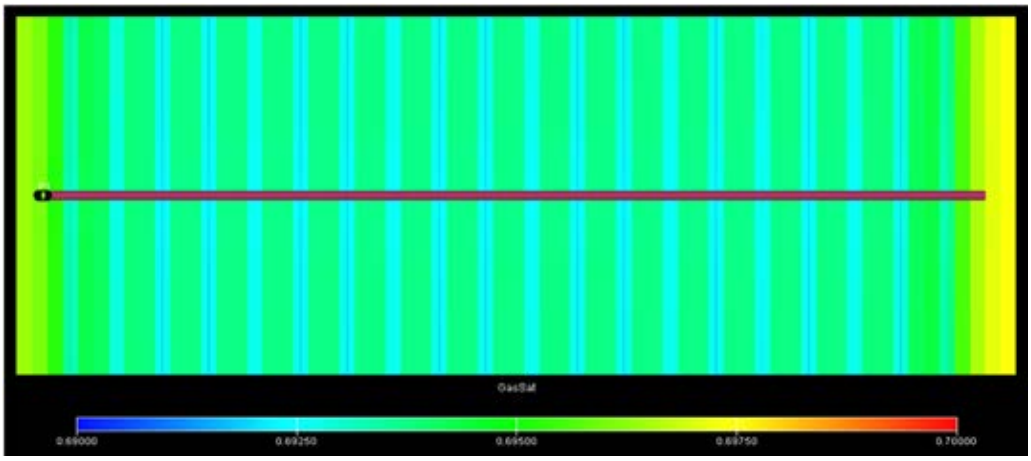

E-7 Gas saturation profile for Design B-2

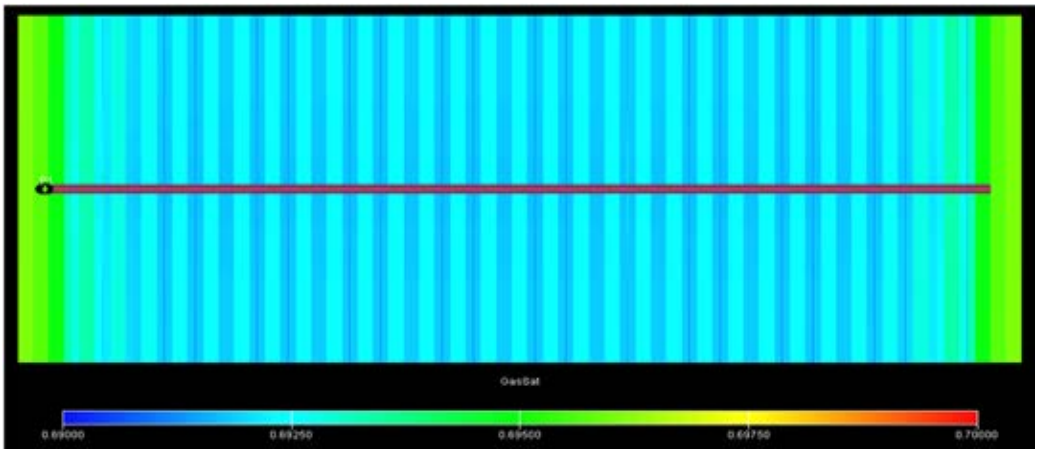

E-8 Gas saturation profile for Design C-2

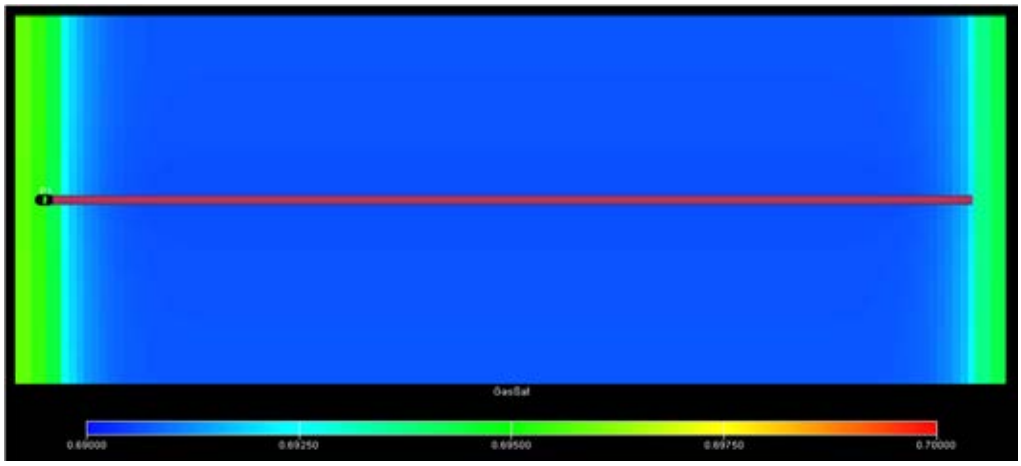

E-9 Gas saturation profile for Design D-2

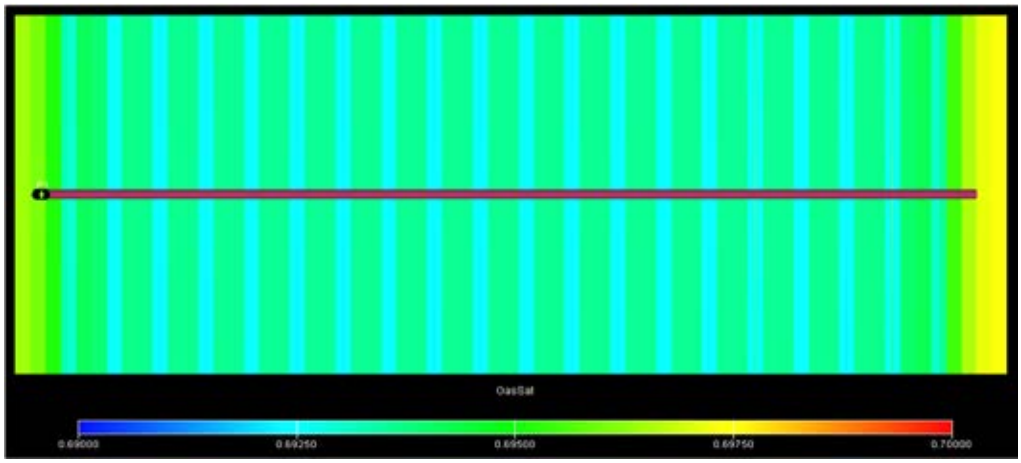

E-10 Gas saturation profile for Design B-3

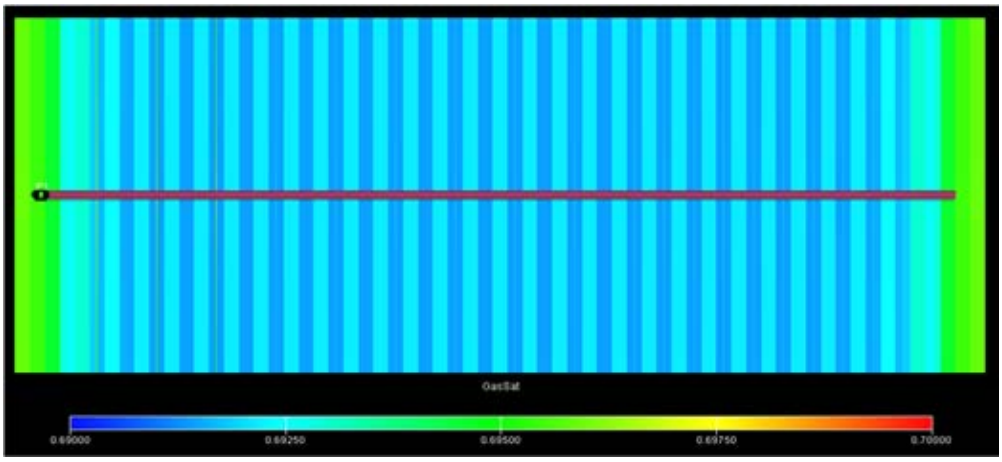

E-11 Gas saturation profile for Design C-3

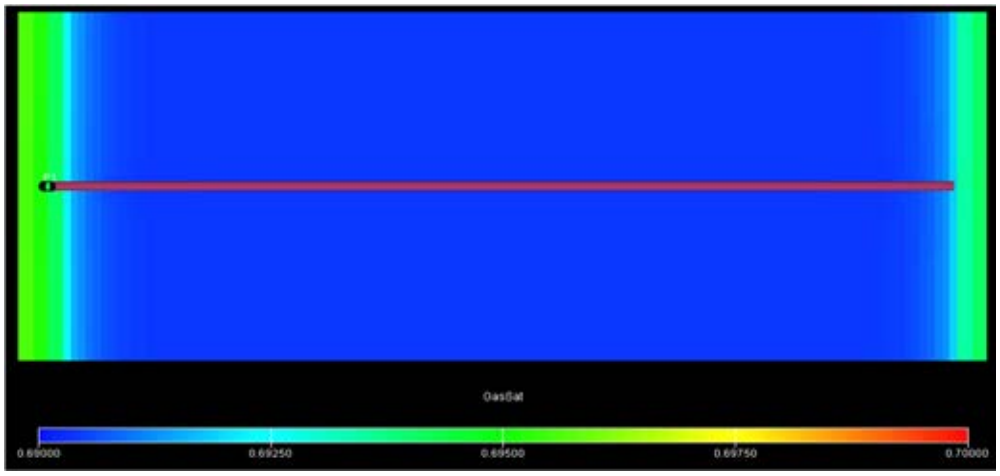

E-12 Gas saturation profile for Design D-3

Vitae

Ms. Duangkamon Jordnork was born on March 16th, 1986 in Nakhon Ratchasima Province, Thailand. She received her Bachelor Degree in Geotechnology from the Faculty of Engineering, Suranaree University of Technology in 2008. Then, she joined NOV downhole as a Drilling Solution Engineer based in Bangkok, Thailand for 4.5 years while also continued her study in Master Degree of Petroleum Engineering at graduate school of the Department of Mining and Petroleum Engineering, Chulalongkorn University since 2010. Presently, she is working for NOV downhole as a Sales Engineer.